THE UNIVERSITY OF CHICAGO

ENGINEERING THE INNATE IMMUNE RESPONSE USING NOVEL CONJUGATES AND BIOMATERIALS

A DISSERTATION SUBMITTED TO

THE FACULTY OF THE PRITZKER SCHOOL OF MOLECULAR ENGINEERING

IN CANDIDACY FOR THE DEGREE OF

DOCTOR OF PHILOSOPHY

BY

JAINU AJIT

CHICAGO, ILLINOIS

MARCH 2022

Table of Contents

List of tables

List of Figures

Acknowledgments

I would first like to thank my Ph.D. advisor, Professor Aaron Esser-Kahn. I thoroughly enjoyed all the scientific discussions we had from my very first day in the lab. Thank you for supporting me and my ideas throughout my time here. I sincerely appreciate your guidance in encouraging me to pursue my passion.

To my committee members, Prof. Nicolas Chevrier and Prof. Luis Barreiro, thank you so much for all the support and feedback. Thanks to Prof. Melody Swartz for all the constructive feedback during the early stages of my projects.

I would like to thank my incredible mentors- Dr. Brittany Moser and Dr. Flora Kimani. Thanks for teaching me a lot and supporting me through everything- from lab techniques and projects to proposal writing and presentations. I have learned a lot from both of you. I would like to especially thank Britteny, Jorge, Nihesh, and Yoseline for always being there for me. Graduate school would not have been the same without you guys. To my dear Jingjing, thank you for all the help (and yummy scones) you gave me throughout my time here. Thanks to my undergrad Sophia Tang for all the help with various projects. I worked with amazing collaborators in the Esser-Kahn lab- Tyler, Will, Adam, Qing, and Riley, thanks for all your help and scientific enthusiasm. Thank you Seong-Min, Jun, Brad, and Matt, for being awesome labmates and friends.

I would like to thank Namitha, Shany, and Mishel for always keeping me sane through the last ten years. A big thank you to my constants, Naveen, Pratheeksha, Sajesh, Firoz and Rohit, for all your love and support forever.

A big thank you to my family for always being there for me. Amma, Appa, and Achacha, I cannot thank you enough for all your love and support. It means the world to me. Thanks to my chechy

and Zeyu for bringing me so much joy. I could not imagine getting to this point without all of you.

Thank you!

Abstract

Vaccines are one of the most significant scientific discoveries allowing reduction and almost complete eradication of deadly diseases such as smallpox and polio. As diseases continue to emerge, we must develop ways to produce effective vaccines faster. The quality and magnitude of most vaccines can be modulated by targeting the innate immune system. To do this, we need a better understanding of the pathways regulating innate immunity. My work focuses on improving the innate immune system through two ways: the design of novel conjugates targeting multiple innate immune receptors and the design of novel biomaterials to control innate immune memory or trained immunity.

Vaccines use adjuvants to improve the immune response towards the antigen of interest. Adjuvants targeting multiple innate immune receptors produce distinct responses capable of modulating downstream adaptive immunity. However, there is a gap in mechanistic understanding of multi-TLR agonists, limiting their use as adjuvants. In chapter 2, I will discuss the mechanism of action of novel covalently linked TLR agonist dimers. Similarly, antigen-adjuvant conjugates offer promising ways to ensure co-delivery and effective innate immune cell activation leading to better downstream adaptive immune responses. In chapter 3, I describe the design of a novel antigen-adjuvant conjugate with improved $CD8^+$ T-cell responses in mice.

An alternate method of targeting innate immunity to improve overall disease resistance involves inducing non-specific memory referred to as trained immunity. Existing training methods do not offer temporal control, potentially leading to uncontrolled inflammation in certain populations. In chapter 4, I discuss the design and application of a novel biomaterial for the temporal control of trained immunity using a sustained release mechanism. Finally, in chapter 5, I discuss our recent findings on the impact of trained immunity in improving antigen-specific antibody responses.

Taken together, these chapters demonstrate two new avenues that make trained immunity an exciting tool for developing novel prophylactics for overall disease resistance and improved responses to vaccinations.

1. Introduction

1.1 Introduction

Vaccines are one of the most significant scientific discoveries allowing reduction and almost complete eradication of deadly diseases such as smallpox and polio.[1] Vaccination involves the safe introduction of antigenic material into the body. Immune cells respond to the introduced antigen and retain memory of the disease-causing agent.[2] This fundamental property of the immune system's memory makes vaccines very effective. However, several diseases, such as tuberculosis and HIV, still exist against which effective vaccines have not been developed.[3] This is primarily due to the empirical method of development of vaccines with little or no mechanistic understanding by which they introduce protection.[4] This lack of knowledge hinders the development of effective vaccines against existing and emerging diseases.

Vaccines are composed of two essential components -an antigen, which the vaccine elicits protection against, and an adjuvant, which enhances the magnitude of immune reaction.[5] Adjuvants are immunostimulatory compounds added to vaccines to enhance the immune response against the antigen. Adjuvants are also capable of biasing the immune response in distinct ways and can be tailored for effective disease control. Therefore, developing novel adjuvants is very important in vaccine design.[6] A single adjuvant alone is often incapable of generating a sufficient immune response. Combining multiple adjuvants can increase response by inducing immune synergies. However, current methods to incorporate adjuvants lack spatial and temporal control of agonist presentation and activation.[7] Chemical conjugation of multiple adjuvants using linkers of defined lengths can help us better understand and optimize vaccine design. Similar design and covalent linking strategies can also be used to co-deliver antigens and adjuvants. Such co-delivery

systems can potentially improve antigen uptake and processing mechanisms leading to enhanced T and B-cell responses.

Many whole-cell vaccines have now been understood to protect against unrelated pathogens.[8] The mechanism responsible for this nonspecific protection is called trained immunity and is mediated by the innate immune system.[9] Trained immunity helps strengthen our first line of defense against a diverse range of pathogens and can be potentially developed as a novel prophylactic against emerging infectious diseases. However, the exact duration of protection from these vaccines is not fully understood, or less controllable.[10] Over-activation of the innate immune system can lead to adverse effects due to uncontrolled inflammation. This lack of temporal control diminishes the utility of trained immunity for safe and effective disease prevention. Delivery platforms that exhibit sustained release can solve this problem by offering enhanced kinetic control over trained immunity. Finally, since innate immunity ultimately shapes the magnitude and duration of adaptive immune responses, trained immunity can also be used to improve the effects of existing vaccines.

1.2 The Innate and Adaptive Immune System

The vertebrate immune system is composed of two parts: the innate immune system and the adaptive immune system.[11] The innate arm forms the first line of defense that detects and responds to the pathogen that evades physical barriers such as the skin. The primary effector cells include monocytes, macrophages, neutrophils, basophils, eosinophils, natural killer cells, macrophages, and dendritic cells. These cells have specialized receptors on them that enable the detection of various pathogenic components. Once pathogenic material binds to these receptors, downstream signaling leads to the production of proteins called cytokines and chemokines to both kill and alert

neighboring immune cells. This response is generated almost immediately after the attack to contain the infection.

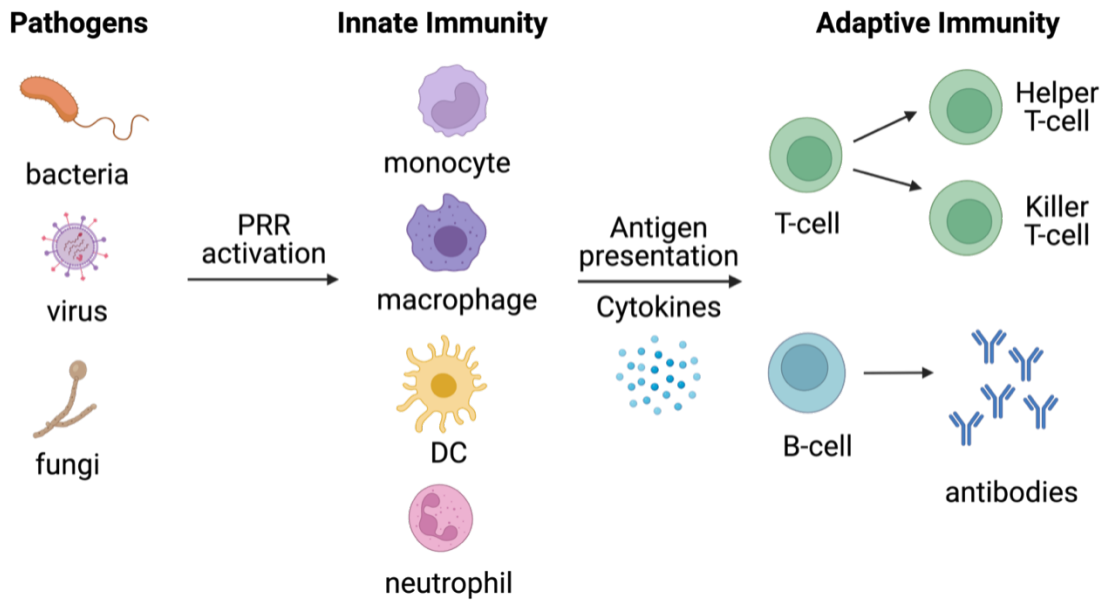

Figure 1.1: Overview of immune activation by pathogens

Pathogens like bacteria, fungi, and viruses activate pattern recognition receptors (PRRs) present on innate immune cells. Innate immune cells produce inflammatory cytokines and chemokines to control the infection. Meanwhile, antigen-presenting cells, like macrophages and dendritic cells, activate T-cells in the draining lymph nodes. Naive T-cells can develop into helper T-cells or killer T-cells. B-cell activation generates antibodies that confer long-lasting immunity. (created with BioRender)

During this time, antigen-presenting cells (APCs) like dendritic cells and macrophages take up antigenic material and drain to the nearest lymph node. At lymph nodes, they present the antigenic peptides on major histocompatibility (MHC) proteins to naïve T-cells to initiate adaptive immune responses.[12] T-cell receptors recognize antigen-MHC complexes present on APCs. Additionally, APCs express costimulatory molecules like CD86, CD80, and CD40, providing additional T-cell activation and expansion signals. $CD8^+$ T cells are cytotoxic and can directly kill infected cells and recruit other immune cells by secreting cytokines. $CD4^+$ helper T cells activate B-cells to produce

antibodies towards the pathogen.[13] (**Figure 1.1**) This adaptive immune arm is slow to develop, taking around 4-5 days after infection. However, their unique memory feature confers prolonged protection against future attacks. Coordination between the innate and adaptive immune arms ensures the efficient clearance of pathogen and memory to tackle future infections.

1.3 Innate immune activation through Pattern Recognition Receptors

Innate immune cells form the first line of defense and are critical in the early detection and clearance of pathogens. The innate immune system express germline-encoded pattern recognition receptors (PRRs) that bind to distinct pathogen-associated molecular patterns (PAMPs).[14] PRR activation results in a downstream signaling cascade that culminate in the secretion of inflammatory cytokines, chemokines, and other signals that constitute the early host response to infections.[15]

Among the various PRRs identified to date, toll-like receptors (TLRs) are the most well-studied.[16] They are expressed either on the cell membrane or within the endosome. Cell surface TLRs recognize microbial cell surface patterns, such as lipopolysaccharide (LPS) of gram-negative bacteria (TLR4) and lipoteichoic acids (LTA) of gram-positive and flagellin (TLR5). Endosomal TLRs, on the other hand, mainly detect microbial nucleic acids, such as dsRNA (TLR3), ssRNA (TLR7), and dsDNA (TLR9).[17] TLRs binding to ligands induces interactions with adaptor proteins like MyD88 and TRIF that lead to the production of inflammatory cytokines or interferons.

Other PRRs include C-type lectin receptors (CLRs), NOD-like receptors (NLRs), and Retinoic acid-inducible gene (RIG)-I-like receptors (RLRs).[18] Dectin-1 is a transmembrane CLR that is important in mediating anti-fungal immune responses.[19] Yeast cell wall component β-glucan binds to the Dectin-1 receptor, predominantly expressed on myeloid cells such as monocytes, macrophages, neutrophils, and dendritic cells. Dectin-1 activation leads to phagocytosis,

respiratory burst, inflammasome activation, and inflammatory cytokine and chemokine production.[19] Apart from the canonical activation, β-glucan can also metabolically and epigenetically rewire myeloid cells enabling them to respond strongly to subsequent infections through a mechanism called trained immunity. Other PRRs like NLRs have also been identified as key players in generating trained immunity by binding to bacterial peptidoglycan component muramyl dipeptide (MDP).[20]

1.4 Toll-like receptor activation

TLRs consist of an ectodomain with several leucine-rich repeat units (LRRs) that recognizes and binds to PAMPs and DAMPs. The binding of ligands induces homo/heterodimerization of two TLRs that recruit Toll/IL-1 receptor (TIR) domain-containing adaptor proteins. The type of TLR activated dictates the adaptor protein involved in further signaling. TLR 1, 2, 4-9 signal through the MyD88-dependent pathway, whereas TLR 3 and 4 signal the TRIF-dependent pathway. TLR 4 activates both MyD88 and TRIF-dependent pathways.[21] These signaling pathways culminate in the activation of transcription factors NF-κB, IRFs, or MAP kinases. They prime the transcription of cytokines, chemokines, and interferons for adequate protection against infections.

Innate immune cells like macrophages and dendritic cells secrete cytokines and increase costimulatory markers in response to TLR activation. They drain to the lymph nodes and activate T-cells. B-cells also express TLRs and function as antigen-presenting cells. The type of cytokines produced due to TLR activation programs the differentiation of naive CD4+ T cells into TH1, TH2, TH17, or regulatory T (Treg) cells. Activation through TLR 3,7 and 9 increases cross-presentation and induces differentiation of CD8 T cells into cytotoxic T cells (CTLs). In summary, both the quality and magnitude of T and B-cell responses are shaped by the initial TLR-activation on innate immune cells.

1.5 Vaccine adjuvants

Vaccines derived from whole-cell inactivated pathogens effectively generate long-lasting immune responses. However, this method is not ideal, leading to unwanted inflammatory reactions in certain populations. Additionally, not all natural infections yield a protective response, for example, influenza.[22,23,24] To combat these problems, antigenic portions can be synthesized and used instead as subunit vaccines. Since these molecules by themselves are less immunogenic, they are combined with molecules called adjuvants to improve the magnitude of response. Adjuvants help increase vaccine potency, reducing the amount of antigen needed, modulating the phenotype of T-cells, and thereby broadening the repertoire of B-cell responses.[25]

Currently, very few adjuvants have been licensed for use in humans. Among the licensed ones are aluminium-containing adjuvants and other oil-in-water emulsions like MF59.[26] Since TLRs are important pathogen sensors, adjuvants containing them can improve the effectiveness of vaccines.[27] For example, the yellow fever vaccine activates multiple TLRs, including TLR 2, 7, 8, and 9 making it one of the most effective vaccines developed.[28] Therefore, combinations of TLR agonists can make promising vaccine adjuvants by eliciting distinct immune responses.[24]

1.6 Chemical conjugation strategies for spatial control of TLR activation

Multiple PRR agonists are presented to innate immune cells at specific spatial orientations in natural infections. Therefore, combining multiple PRR agonists is an effective strategy in adjuvant design to yield unique immune responses.[29,30] However, most studies to elucidate multi-PRR synergies have utilized mixtures of agonists and therefore lack spatial information.[31] For example, the herpes simplex virus activates multiple TLRs, including TLR 2, 3, 7, and 9 via specific inter-agonist spacing.[32] Studies using unlinked combinations of agonists targeting these different TLRs do not recapitulate the original infection and therefore lack spatial information.

Chemical conjugation strategies offer an attractive solution to this problem. It is now possible to understand and design novel multi-TLR agonists as adjuvants by introducing chemical linkers of defined lengths and flexibility. Previous work showed that linked combinations of TLR agonists could serve as a unique alternative to traditional vaccines through spatially constrained multi-TLR activation. Unlike commercially available linked TLR agonists (CL413 ™, CL429 ™), our chemical constructs are immunomodulatory, allowing further control over activation.

1.7 Co-delivery of antigen and adjuvant

Optimal vaccine design requires co-delivery of antigen and adjuvants to generate effective adaptive immune responses. Adjuvants delivered separately can diffuse away from the injection site and degrade faster.[33] They can also activate cells that do not take up antigen, leading to autoimmunity.[34] However, co-delivery of antigen and adjuvant ensures the colocalization to the same endosome, which improves antigen presentation by DCs and efficient T-cell activation.[35] This also decreases off-target effects.

Oligodeoxynucleotides, such as unmethylated CpG, activate the innate immune system by binding endosomal toll-like receptor 9 (TLR9) to enhance the cross-presentation of antigenic components. TLR9 agonists conjugated to ovalbumin (OVA) improved both cross-presentation and antigen-specific CD8+ T-cell production.[36] However, existing methods to produce these conjugates often induce unwanted aggregation and loss of site-specific conjugation sites. Cell-free protein synthesis offers a unique alternative to generate scalable amounts of antigen with precise site-specific modifications. Antigens with site-specific modifications generated using cell-free protein synthesis can be used to link to desired adjuvants to generate improved immune responses.

1.8 Innate Immune Memory or Trained Immunity

Immunological memory was regarded as a hallmark of the adaptive immune system. However, recent work has shown that innate immune cells possess a memory feature.[37] This innate immune memory feature protects plants and invertebrates from re-infection because they lack an adaptive immune system.[38,9,39] Similarly, in humans, certain attenuated whole-cell vaccines such as BCG protect against unrelated infections in an innate immune-dependent mechanism called trained immunity.[40]

Trained immunity is induced by metabolic and epigenetic rewiring of innate immune cells. This heightened state of activation in trained cells allows faster transcription of inflammatory cytokines when later challenged by a pathogen. Various DAMPs and PAMPs can induce trained immunity by activating PRRs on innate immune cells. A cascade of changes follows this activation leading to changes in the cell. Histone modifications, such as methylation and acetylation, increase to favor rapid transcription and translation of inflammatory genes.[40] To fuel these cellular activities, the trained cell switches from oxidative phosphorylation to aerobic glycolysis as its primary energy source. Apart from producing higher energy, the metabolites generated from this switch, including acetylcholine, lactate, and succinate, play essential roles in further modifying chromatin architecture and histone modifications.

Trained immunity induced by whole-cell vaccines like BCG last for up to a year. Less immunogenic PAMPs, like β-glucan and MDP, also generate trained immunity.[41] The protective effects of these molecules are short-term and only last a week in mice. Recent work has also demonstrated inter and transgenerational inheritance of trained immunity in mice challenged sub-lethally with *Candida albicans*.[42] Progeny of trained mice showed increased resistance to infections. The variability in the duration of protection conferred by various stimuli may be due to

the differential induction of central vs. peripheral training.[43] Central mediators of trained immunity involve bone-marrow progenitor cells and provide long-term protection. Peripheral training relies on monocytes and macrophages, whose lifespan ranges between 4-7 days.

Trained immunity is beneficial for improved disease resistance and can be used as a prophylactic against emerging diseases. However, BCG and other whole-cell vaccines induce adverse effects due to over inflammation in certain populations. It is also hypothesized that the increased innate immune function arising from trained immunity could lead to tissue damage, including atherosclerotic plaques. Therefore while prolonging trained immunity-induced protection is valuable, methods to avoid uncontrolled inflammation are crucial to fully exploit the benefits of trained immunity. Novel delivery platforms can be utilized to achieve this controlled trained immunity. Additionally, the molecular architecture of these delivery platforms can be further fine-tuned to achieve advanced temporal control.

1.9 Trained immunity in disease resistance

The vaccine developed against tuberculosis – bacillus Calmette Guerin (BCG) is the most studied training stimuli and induces protection against unrelated neonatal infections.[44] BCG vaccine is effective against viral infections, including influenza and herpes simplex virus.[45,46] Similarly, other whole-cell vaccines, including polio and measles vaccines, also induce heterologous protection.[47] β-glucan-induced trained immunity protects against a broad spectrum of bacterial and viral diseases.[48,49] Pre-treatment of mice with β-glucan also reduced tumor growth.[50] Trained immunity inducing nano biologics targeting the bone marrow was also reported to significantly improve tumor resistance in combination with checkpoint therapies.[51]

1.10 Influence of trained immunity on adaptive immune responses

Innate immune cells shape adaptive responses through cytokines and costimulatory molecule expression. Trained immunity induces epigenetic and metabolic reprogramming of innate immune cells, including DCs and macrophages, facilitating higher inflammatory cytokines production following a secondary pathogenic challenge. These cytokines mainly include IL-1, IL-6, and TNF-α that can polarize and differentiate naive CD4-T cells. BCG and adenovirus increase the expression of costimulatory markers- MHCII, CD40, and CD80 in macrophages.[52,53] BCG vaccine has also been shown to induce heterologous TH1/TH17 activation in humans.[54] These key signals play essential roles in polarizing T-cell responses. However, the effects of trained immunity on adaptive immune responses are not yet fully understood. Here, we report the enhanced antibody responses generated as a result of training mice with β-glucan a week ahead of vaccination.

1.11 Conclusion

Innate immune cell activation shapes the magnitude and duration of subsequent adaptive immunity. Targeting multiple PRRs on innate immune cells using chemical conjugation can improve our understanding of signaling mechanisms and inform rational design of novel adjuvants. Similar chemical linking strategies can be used to attach an antigen of interest to the adjuvant to enhance uptake and cross-presentation for improved T-cell responses. Moreover, targeting the potential of innate immune cells to generate memory responses through trained immunity offers another exciting avenue for improving disease resistance. A cumulative understanding of these mechanisms can guide the development of novel prophylactics and adjuvants in the future.

1.12 References

1. Greenwood, B. The contribution of vaccination to global health: past, present and future. *Philos Trans R Soc Lond B Biol Sci* **369**, 20130433 (2014).

2. Pollard, A. J. & Bijker, E. M. A guide to vaccinology: from basic principles to new developments. *Nat Rev Immunol* **21**, 83–100 (2021).

3. Pulendran, B. & Ahmed, R. Translating Innate Immunity into Immunological Memory: Implications for Vaccine Development. *Cell* **124**, 849–863 (2006).

4. Pulendran, B. & Ahmed, R. Immunological mechanisms of vaccination. *Nat Immunol* **12**, 509–517 (2011).

5. Fox, C. B., Kramer, R. M., Barnes V, L., Dowling, Q. M. & Vedvick, T. S. Working together: interactions between vaccine antigens and adjuvants. *Ther Adv Vaccines* **1**, 7–20 (2013).

6. Marciani, D. J. Vaccine adjuvants: role and mechanisms of action in vaccine immunogenicity. *Drug Discovery Today* **8**, 934–943 (2003).

7. Tom, J. K. *et al.* Applications of Immunomodulatory Immune Synergies to Adjuvant Discovery and Vaccine Development. *Trends in Biotechnology* **37**, 373–388 (2019).

8. Netea, M. G. Training innate immunity: the changing concept of immunological memory in innate host defence. *European Journal of Clinical Investigation* **43**, 881–884 (2013).

9. Gourbal, B. *et al.* Innate immune memory: An evolutionary perspective. *Immunological Reviews* **283**, 21–40 (2018).

10. Garcia-Valtanen, P., Guzman-Genuino, R. M., Williams, D. L., Hayball, J. D. & Diener, K. R. Evaluation of trained immunity by β-1, 3 (d)-glucan on murine monocytes in vitro and duration of response in vivo. *Immunol Cell Biol* **95**, 601–610 (2017).

11. Clem, A. S. Fundamentals of Vaccine Immunology. *J Glob Infect Dis* **3**, 73–78 (2011).

12. Guermonprez, P., Valladeau, J., Zitvogel, L., Théry, C. & Amigorena, S. Antigen presentation and T cell stimulation by dendritic cells. *Annu Rev Immunol* **20**, 621–667 (2002).

13. Parker, D. C. T cell-dependent B cell activation. *Annu Rev Immunol* **11**, 331–360 (1993).

14. Janeway, C. A. Approaching the Asymptote? Evolution and Revolution in Immunology. *Cold Spring Harb Symp Quant Biol* **54**, 1–13 (1989).

15. Mogensen, T. H. Pathogen Recognition and Inflammatory Signaling in Innate Immune Defenses. *Clin Microbiol Rev* **22**, 240–273 (2009).

16. Medzhitov, R., Preston-Hurlburt, P. & Janeway, C. A. A human homologue of the Drosophila Toll protein signals activation of adaptive immunity. *Nature* **388**, 394–397 (1997).

17. Iwasaki, A. & Medzhitov, R. Regulation of adaptive immunity by the innate immune system. *Science* **327**, 291–295 (2010).

18. Takeuchi, O. & Akira, S. Pattern Recognition Receptors and Inflammation. *Cell* **140**, 805–820 (2010).

19. Herre, J., Gordon, S. & Brown, G. D. Dectin-1 and its role in the recognition of β-glucans by macrophages. *Molecular Immunology* **40**, 869–876 (2004).

20. Mourits, V. P. *et al.* BCG-Induced Trained Immunity in Healthy Individuals: The Effect of Plasma Muramyl Dipeptide Concentrations. *J Immunol Res* **2020**, 5812743 (2020).

21. Kawai, T. & Akira, S. TLR signaling. *Cell Death Differ* **13**, 816–825 (2006).

22. Pulendran, B., S. Arunachalam, P. & O'Hagan, D. T. Emerging concepts in the science of vaccine adjuvants. *Nat Rev Drug Discov* **20**, 454–475 (2021).

23. O'Hagan, D. T. & Valiante, N. M. Recent advances in the discovery and delivery of vaccine adjuvants. *Nat Rev Drug Discov* **2**, 727–735 (2003).

24. Coffman, R. L., Sher, A. & Seder, R. A. Vaccine Adjuvants: Putting Innate Immunity to Work. *Immunity* **33**, 492–503 (2010).

25. Ulmer, J. Vaccine Adjuvants: Mode of Action. *Frontiers in Immunology* **4**, 214 (2013).

26. Kool, M., Fierens, K. & Lambrecht, B. N. Alum adjuvant: some of the tricks of the oldest adjuvant. *Journal of Medical Microbiology* **61**, 927–934 (2012).

27. Ignacio, B. J., Albin, T. J., Esser-Kahn, A. P. & Verdoes, M. Toll-like Receptor Agonist Conjugation: A Chemical Perspective. *Bioconjugate Chem.* **29**, 587–603 (2018).

28. Querec, T. *et al.* Yellow fever vaccine YF-17D activates multiple dendritic cell subsets via TLR2, 7, 8, and 9 to stimulate polyvalent immunity. *Journal of Experimental Medicine* **203**, 413–424 (2006).

29. Moyer, T. J., Zmolek, A. C. & Irvine, D. J. Beyond antigens and adjuvants: formulating future vaccines. *J Clin Invest* **126**, 799–808 (2016).

30. Tom, J. K. *et al.* Applications of Immunomodulatory Immune Synergies to Adjuvant Discovery and Vaccine Development. *Trends in Biotechnology* **37**, 373–388 (2019).

31. Madan-Lala, R., Pradhan, P. & Roy, K. Combinatorial Delivery of Dual and Triple TLR Agonists via Polymeric Pathogen-like Particles Synergistically Enhances Innate and Adaptive Immune Responses. *Sci Rep* **7**, 2530 (2017).

32. Xagorari, A. & Chlichlia, K. Toll-Like Receptors and Viruses: Induction of Innate Antiviral Immune Responses. *Open Microbiol J* **2**, 49–59 (2008).

33. Wang, Z.-B. & Xu, J. Better Adjuvants for Better Vaccines: Progress in Adjuvant Delivery Systems, Modifications, and Adjuvant–Antigen Codelivery. *Vaccines (Basel)* **8**, 128 (2020).

34. Kreutz, M. *et al.* Antibody-Antigen-Adjuvant Conjugates Enable Co-Delivery of Antigen and Adjuvant to Dendritic Cells in Cis but Only Have Partial Targeting Specificity. *PLOS ONE* **7**, e40208 (2012).

35. Xu, Z. & Moyle, P. M. Bioconjugation Approaches to Producing Subunit Vaccines Composed of Protein or Peptide Antigens and Covalently Attached Toll-Like Receptor Ligands. *Bioconjugate Chem.* **29**, 572–586 (2018).

36. Kramer, K., Young, S. L. & Walker, G. F. Comparative Study of 5′- and 3′-Linked CpG–Antigen Conjugates for the Induction of Cellular Immune Responses. *ACS Omega* **2**, 227–235 (2017).

37. Netea, M. G. *et al.* Defining trained immunity and its role in health and disease. *Nat Rev Immunol* **20**, 375–388 (2020).

38. Reimer-Michalski, E.-M. & Conrath, U. Innate immune memory in plants. *Seminars in Immunology* **28**, 319–327 (2016).

39. Conrath, U., Beckers, G. J. M., Langenbach, C. J. G. & Jaskiewicz, M. R. Priming for enhanced defense. *Annu Rev Phytopathol* **53**, 97–119 (2015).

40. Netea, M. G., Quintin, J. & van der Meer, J. W. M. Trained immunity: a memory for innate host defense. *Cell Host Microbe* **9**, 355–361 (2011).

41. Kaufmann, E. *et al.* BCG Educates Hematopoietic Stem Cells to Generate Protective Innate Immunity against Tuberculosis. *Cell* **172**, 176-190.e19 (2018).

42. Katzmarski, N. *et al.* Transmission of trained immunity and heterologous resistance to infections across generations. *Nat Immunol* **22**, 1382–1390 (2021).

43. Netea, M. G. *et al.* Defining trained immunity and its role in health and disease. *Nat Rev Immunol* **20**, 375–388 (2020).

44. Benn, C. S., Netea, M. G., Selin, L. K. & Aaby, P. A small jab – a big effect: nonspecific immunomodulation by vaccines. *Trends in Immunology* **34**, 431–439 (2013).

45. Mukherjee, S. *et al.* Boosting efferocytosis in alveolar space using BCG vaccine to protect host against influenza pneumonia. *PLoS One* **12**, e0180143 (2017).

46. Floc'h, F. & Werner, G. H. Increased resistance to virus infections of mice inoculated with BCG (Bacillus calmette-guérin). *Ann Immunol (Paris)* **127**, 173–186 (1976).

47. Goodridge, H. S. *et al.* Harnessing the beneficial heterologous effects of vaccination. *Nat Rev Immunol* **16**, 392–400 (2016).

48. Moorlag, S. J. C. F. M. *et al.* β-Glucan Induces Protective Trained Immunity against Mycobacterium tuberculosis Infection: A Key Role for IL-1. *Cell Rep* **31**, 107634 (2020).

49. Ciarlo, E. *et al.* Trained Immunity Confers Broad-Spectrum Protection Against Bacterial Infections. *The Journal of Infectious Diseases* **222**, 1869–1881 (2020).

50. Kalafati, L. *et al.* Innate Immune Training of Granulopoiesis Promotes Anti-tumor Activity. *Cell* **183**, 771-785.e12 (2020).

51. Priem, B. *et al.* Trained Immunity-Promoting Nanobiologic Therapy Suppresses Tumor Growth and Potentiates Checkpoint Inhibition. *Cell* **183**, 786-801.e19 (2020).

52. Yao, Y. *et al.* Induction of Autonomous Memory Alveolar Macrophages Requires T Cell Help and Is Critical to Trained Immunity. *Cell* **175**, 1634-1650.e17 (2018).

53. Jeljeli, M. *et al.* Trained immunity modulates inflammation-induced fibrosis. *Nat Commun* **10**, 5670 (2019).

54. Kleinnijenhuis, J. *et al.* Long-Lasting Effects of BCG Vaccination on Both Heterologous Th1/Th17 Responses and Innate Trained Immunity. *Journal of Innate Immunity* **6**, 152 (2014).

2. Understanding the mechanism of action of linked TLR agonists

This chapter has been published in ACS Chemical Biology 16 (2): 380–88, 2021.

2.1 Summary

Toll-like receptors (TLRs) are among the most studied pattern recognition receptors (PRRs) presnt on immune cells that sense a variety of pathogens. Upon activation, they initiate a downstream signaling cascade that produces cytokines, chemokines, and costimulatory molecules. Targeting multiple TLRs through covalent conjugation of ligands has been known to produce synergistic, additive, and subtractive effects, which can uniquely tailor the downstream adaptive immune responses. In our continued efforts to move toward rational development of immune agonists that mimic their spatial distribution in a pathogen, we sought to investigate the mechanism of action of spatially controlled, covalently linked dual TLR agonists.

We report a mechanistic study comparing the immune activation of conjugated TLR agonists and their unlinked mixtures. Herein, we synthesized a set of 6 linked dual agonists with different ligands, molecular structures, receptor location, and biophysical characteristics. We ran a series of *in-vitro* cell-based assays with these dimers, comparing initial and overall NF-κB (nuclear factor kappa-light-chain-enhancer of activated B cells) activation, cytokine expression profiles, and as time-resolved TNF-α (Tumor Necrosis Factor-alpha) expression. We show that initial activation kinetics, ligand specificity, and the dose of the agonist influence the activity of these linked TLR systems. These results can help improve vaccine design by showing how linked TLR agonists can enhance potency with the appropriate selection of key criteria.

2.2 Introduction

Whole-cell vaccines produce potent and prolonged immune responses against pathogens. The efficacy of whole vaccines is due to the simultaneous presentation of multiple pathogen-associated

molecular patterns (PAMPs) to innate immune cells, often leading to a robust response and overall protection.[1,2] Innate immune cells are activated by the recognition and binding of specific PAMPs to receptors such as Toll-like receptors (TLRs).[3] This causes a complex signaling cascade that results in the production of inflammatory cytokines, chemokines, and costimulatory molecules which then modulate the magnitude and duration of antigen-specific adaptive responses.[4,5,6] In previous work, we have shown that linked combinations of TLR agonists can serve as a unique alternative to the traditional whole-cell vaccines through spatially constrained multi-TLR presentation and activation. Additionally, such constructs are immunomodulatory, allowing for fine-tuned responses against pathogens of interest.[7–9] Multi-TLR agonists are therefore promising candidates for application as immunostimulants (adjuvants) in subunit vaccines and are currently included in several pre-clinical trials.[10,11] We also found that covalently linked agonists induces synergistic responses by increasing inflammatory cytokines and promoting a T_H1-biased response compared to the unlinked agonist mixtures. We observed spatial inductions that change the cytokine and antibody profile as well as epitope affinity.[7,12,13] Others have shown that immune cell response to dual stimulation by a mixture of unlinked agonists and cytokines leads to distinct ligand and dose-dependent NF-κB dynamics.[14,15] Simultaneous activation of TLR 2 and 4 in a cell population using a mixture of Pam_3CSK_4 and LPS resulted in each cell's NF-κB dynamics resembling the response to one or the other ligand and not a combination of both.[14] In contrast, a mixture of TNF-α and LPS led to a combinatory response of NF-κB dynamics.[15] These results taken together suggest that cells have a complex system of integrating and processing multi TLR signals that may be dependent on upstream events in the NF-κB activation pathway.

Most mechanistic studies of synergistic induction by multiple stimuli have been conducted using mixtures of agonists or cytokines. In our continued efforts to move toward rational development

of immune agonists that mimic their spatial distribution in a pathogen, we sought to investigate the mechanism of action of spatially controlled, covalently linked dual TLR agonists. To achieve this, we synthesized a small library of six combinations of linked agonists—varying the size of the agonist, signaling adaptor involved and the location of the TLR. With these six dimers we ran a series of *in vitro* experiments on murine macrophages to define the structural and molecular mechanisms that influence immune responses of linked dual TLR ligands.

2.3 Results and discussion

2.3.1 Design and synthesis of TLR agonist heterodimers

TLRs recognize a varied set of PAMPs and can be further classified based on the ligands that activate the TLRs; TLR 1,2 and 6 recognize lipids, TLR 3,7,8 and 9 recognize nucleic acids, and TLR 4 recognizes diverse structural elements.[3] To investigate the mechanism of action of the linked TLR agonists, we needed to synthesize a set of molecules sufficient to test (1) molecular variation, (2) receptor location variation, and (3) differences in biophysical characteristics of the ligand.

While the TLR system is limited in the available ligands, we selected five molecules of varying size and receptor identity to form six combinations. The six combinations were made up of synthetic lipopeptides Pam_2CSK_4 (TLR 2/6) and Pam_3CSK_4 (TLR 2/1),[16-18] synthetic oligonucleotides CPG_ODN 1826 (TLR 9)[19], pyrimido[5,4-b]indole (TLR 4)[20,21] and imidazoquinoline (TLR 7/8)[22]. To covalently link the agonists, we synthesized derivatives with orthogonal conjugatable handles and used a heterotelechelic polyethylene glycol (PEG) discrete linker. We installed azide groups on the lipopeptides and used amine-derivatized indole[25] and imidazoquinoline[27] and CPG for conjugation. With these agonists we made the following pairs: 2/6_peg13_4, 2/6_peg13_7/8, 2/1_peg13_4, 2/1_peg13_7/8, 2/6_peg13_9 and 2/1_peg13_9

(**Figure 2.1**). Based on previous work done by us and others[23], we did not synthesize homodimers (e.g. 4_4 or 9_9) as we were interested in inducing dual TLR stimuli. Similarly, 2/6 and 2/1 both target TLR2-containing receptor complexes rendering dimers of the two as possible antagonists of one or both pathways. Additionally, 7/8_9, dimer targeting endosomal receptors, never showed altered responses in our hands, and we have not reported on these molecules further. These rules left us with these six combinations to examine.

The synthesized dimers were purified by chromatographic techniques and spectroscopically characterized. Synthetic lipopeptides have been shown to self-assemble into micelle structures when studied at a concentration of 0.5 wt%.[24] In this mechanistic study, we sought to rule out self-assembly of the dimers and the influence of secondary structure to immune response. We characterized the dimers by dynamic light scattering in PBS pH 7.4 at experimentally relevant concentrations to investigate possible particle formation and aggregation. At concentrations of 250 nM and above, we observed that the lipopeptide-small molecule dimers formed larger particles than of the parent lipopeptides (**Figure A4**). 2/1_peg13_4, 2/1_peg13_7/8 dimers showed evidence of aggregation with no uniform distribution of particles. However, we did not observe particle formation by DLS at the lower concentrations that we used for *in vitro* analyses.

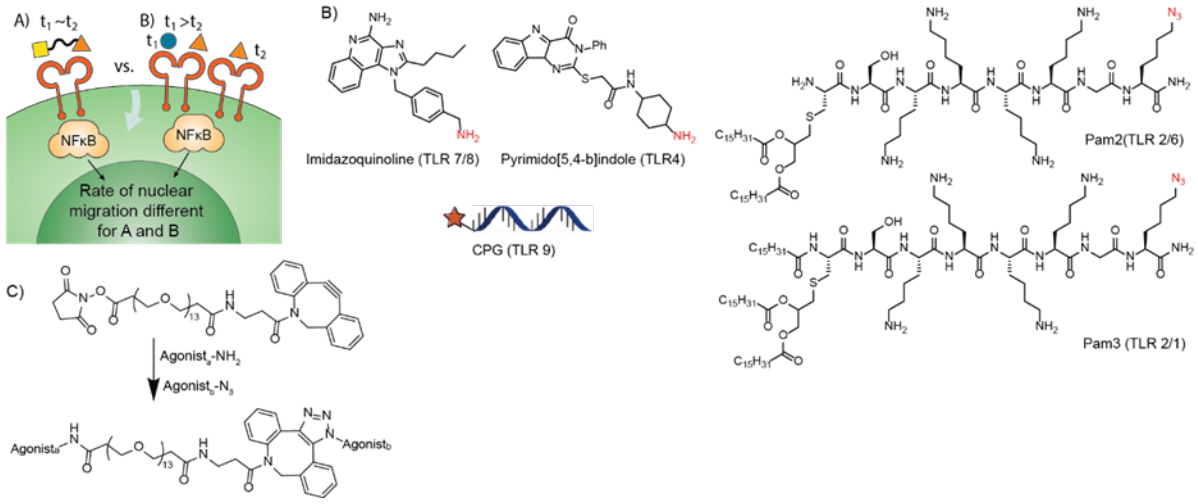

Figure 2.1: Conceptual illustration of immune activation by linked TLR agonists

A)Comparing mechanism of NF-κB migration and subsequent immune response after activation with linked agonist and unlinked agonist mixture. B) Molecular structures of agonist selected in this study. C) Covalent site-specific linking strategy for synthesis of linked TLR agonist dimers.

2.3.2 NF-κB activity of TLR dimers

Initially, we sought to ascertain the differences in activity between these compounds. TLR activation by ligands or agonists activates MyD88 and TRIF pathways where the downstream effect is activation of transcription factors NF-κB and AP-1 (Activator Protein 1).[25] Using the RAW 264.7 macrophage reporter cell line, RAW-Blue™, we profiled the overall transcriptional activity of the linked agonists by measuring the level of secreted embryonic alkaline phosphatase (SEAP) induced by both NF-κB and AP-1. The lipopeptide-CPG dimers, 2/1_peg13_9 and 2/6_peg13_9 showed significantly higher activity than the corresponding equimolar agonist mixtures (**Figure 2.2**). 2/6_peg13_9 was slightly higher compared to the agonist mixtures and the monomers while 2/1_peg13_9 showed an additive response at 10 nM concentration. Surprisingly, the small molecule derived dimers of Pam_2CSK_4, 2/6_peg13_4 and 2/6_peg13_7/8 2/1_peg13_4 and 2/1_peg13_7/8 showed a subtractive response when compared to the individual and unlinked mixture of agonists. Reduction in activity for conjugated small molecule agonists such as the

indole and the imidazoquinoline has been reported and could be attributed to a disruption in the receptor-agonist interactions.[8] In some cases, the activity is either restored due to synergistic effects after conjugation or the dimer retains the activity of the more potent monomer. In this case, the small molecules conjugated onto the lipopeptide agonists did not increase the cellular response. However, the decrease in activity was not expected indicating a possible molecular change in the cellular immune response. The set of 6 dimers were representative of additive, subtractive and unaltered effects, which made it an ideal toolset to study.

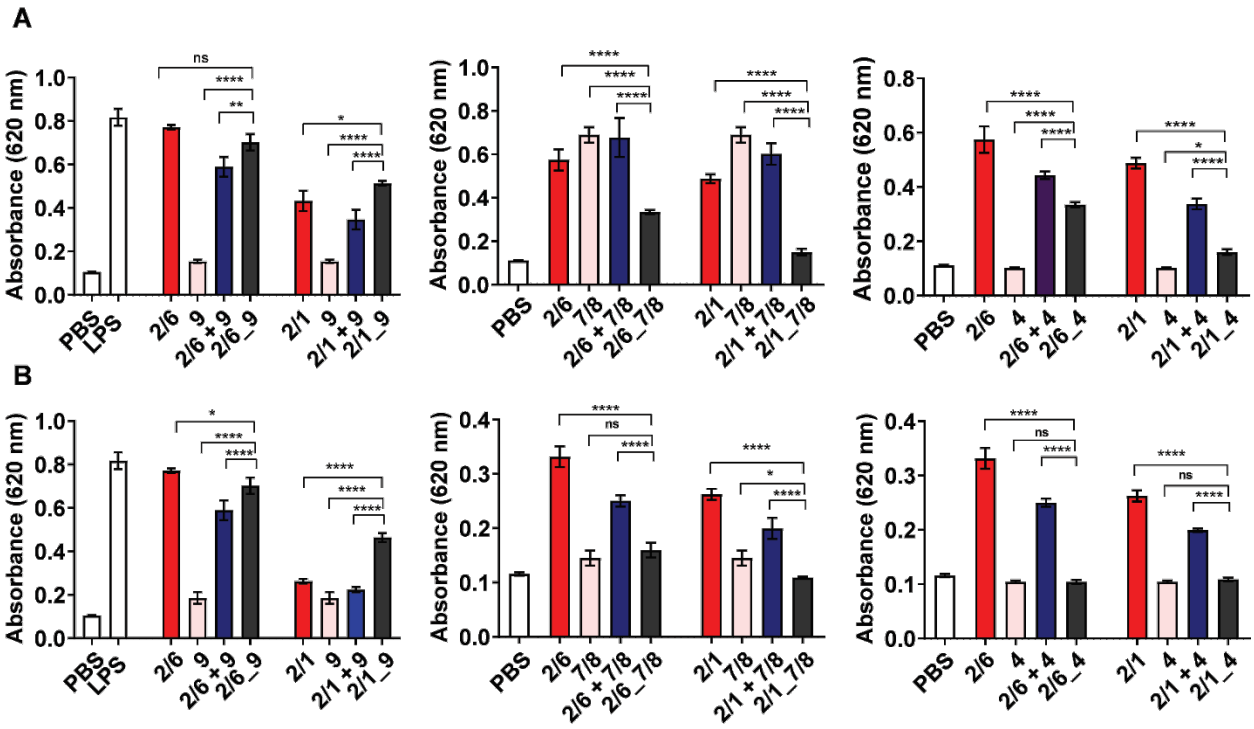

Figure 2.2: Immune activation of linked TLR agonists

Immune activation of Pam_2CSK_4 (2/6), Pam_3CSK_4 (2/1), CpG_1826 (9) indole (4) and imidazoquinoline (7/8), corresponding equimolar mixtures and linked agonists measured by RAW-Blue activation via NF-κB stimulation after 24 h incubation at 37 °C. A) 50 nM, B) 10 nM. Samples run in triplicate. Statistical significance is between the single, unlinked mixtures vs linked agonists, compared by the one-way ANOVA *$p \leq 0.05$, **** $p \leq 0.0001$.

2.3.3 Comparing cytokine secretion profiles of linked and unlinked agonists.

After analysis of overall immune activation using RAW-Blue™ assay, we compared the cytokine profile of cells treated with linked and unlinked equimolar heterodimer agonists. Equimolar mixtures of agonists and ligands resulted in either synergistic or inhibitory cytokine responses. The downstream effects are governed by the interaction of the MyD88 and TRIF pathways. Upon recognition of PAMPs, TLRs initiate downstream signaling with the help of adaptor proteins, mainly MyD88 and TIR-domain-containing adapter-inducing interferon-β (TRIF). While all TLRs except TLR 3 activate MyD88, TRIF is only activated by TLR 3 and 4. MyD88 signaling leads to the activation of NF-κB thereby producing pro-inflammatory cytokines such as IL-6 and TNF-α. Signaling through the TRIF pathway results in the production of inflammatory cytokines and type 1 interferons. TLR4 activates both MyD88 and TRIF pathways.[5] Inhibitory responses are caused by tolerance induced by sequential activation of multiple pathways.[26-28] By conjugating the agonists, we had more spatial and temporal control on the simultaneous activation of dual TLR receptors on a single cell. We incubated bone marrow-derived dendritic cells (BMDCs) with 25 nM linked agonists and the corresponding equimolar single agonist. We measured the secreted cytokines after 24 h using an inflammatory panel cytokine bead array assay for IL-6, IL-10, MCP-1, IFN-γ, TNF-α, and IL-12p70. We detected measurable levels of TNF-α, MCP-1 and IL-6 levels at this concentration. We observed no significant differences in cytokine production between the lipopeptide-CPG dimers and the corresponding monomers and unlinked mixtures. Most lipopeptide derived indole dimers showed lower levels of TNF-α, IL-6 and MCP-1—except 2/6_peg13_4 which had higher levels of TNF-α (**Figure** 2.**3**). This cytokine secretion profile correlated results from the RAW-Blue™ assay, indicating that for these dimers, the level of activation of NF-κB was linked to the amount of cytokine secreted. On the other hand, we did not

observe any synergistic or additive secretion of cytokines in cells treated with the 2/1_peg13_9 dimer which had shown higher immune response in the RAW-Blue™ assay. In addition, the 2/6_peg13_7/8 dimer induced similar cytokine secretion levels in contrast to the lower immune activity as shown by the RAW-Blue assay at the same concentration.

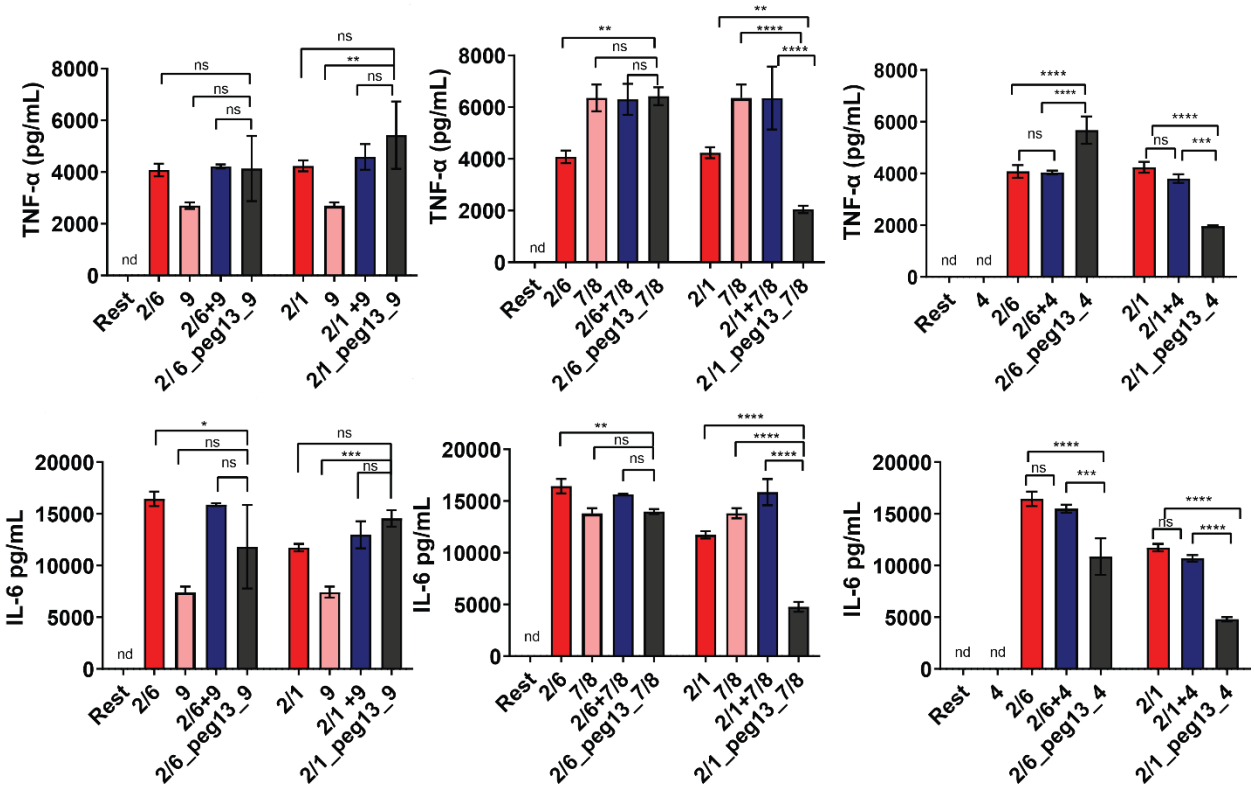

Figure 2.3: *In-vitro* cytokine production from BMDC cells measured by cytokine bead array assay. Cells were incubated with 25 nM of Pam_2CSK_4 (2/6), Pam_3CSK_4 (2/1), CpG_1826 (9) indole (4) and imidazoquinoline (7/8), corresponding equimolar mixtures and linked agonists for 24 h at 37 °C, 5% CO_2. Samples run in triplicate. Statistical significance is between the single, unlinked mixtures vs linked agonists, compared by the one-way ANOVA *p ≤ 0.05, **** p ≤ 0.0001

2.3.4 Effect of dose on TNF-α secretion over time.

After observing the differences in cytokines, we became curious as to why these differences appeared to contrast so much between different compounds and different agonist sets. In these experiments, we noted that, while TNF-α levels appeared similar after 24 h, at earlier time

points there were distinct differences, implying that kinetics of synergistic interactions are related to early time points. We decided to explore these kinetic differences further, as they seemed to show a potential explanation for clear distinctions between the agonists. Investigating TNF-α secretion could explain the differences observed in the other cytokines and provide a standard basis for comparison, as most agonist sets resulted in similar levels at 24 h. In previous reports, we have also observed that lowering agonist concentration can sometimes alter the synergistic response, so we conducted our kinetic screen with varying concentrations. Using RAW 264.7 macrophages, we measured the secretion of TNF-α from 0-24 hr at 2 and 4 h intervals after stimulating the cells with agonists at concentrations of 10, 25, and 50 nM. We observed dose- and time-dependent activity for the different agonist combinations. At lower concentrations (10 nM), treatment with 2/1_peg13_4, 2/6_peg13_4 and 2/1_peg13_7/8 dimers consistently produced lower cytokine secretion over 24 h. As the dose was increased, these dimers activated RAW 264.7 cells at comparable levels as the unlinked equimolar mixtures (**Figure 2.4**). This data suggests that activation of TLRs was modulated by the rate of receptor-agonist interactions for these dimers, which increased as the dimer concentration increased. However, for the 2/1_peg13_9 dimer, we observed a significant increase in TNF-α secretion at lower concentrations, but this effect was not observed at higher concentrations. This correlated with the overall immune activity data measured by RAW-Blue™ assay (**Figure 2.2**) suggesting that a synergistic activation involving these specific 2/1 and 9 agonists is facilitated by conjugation.

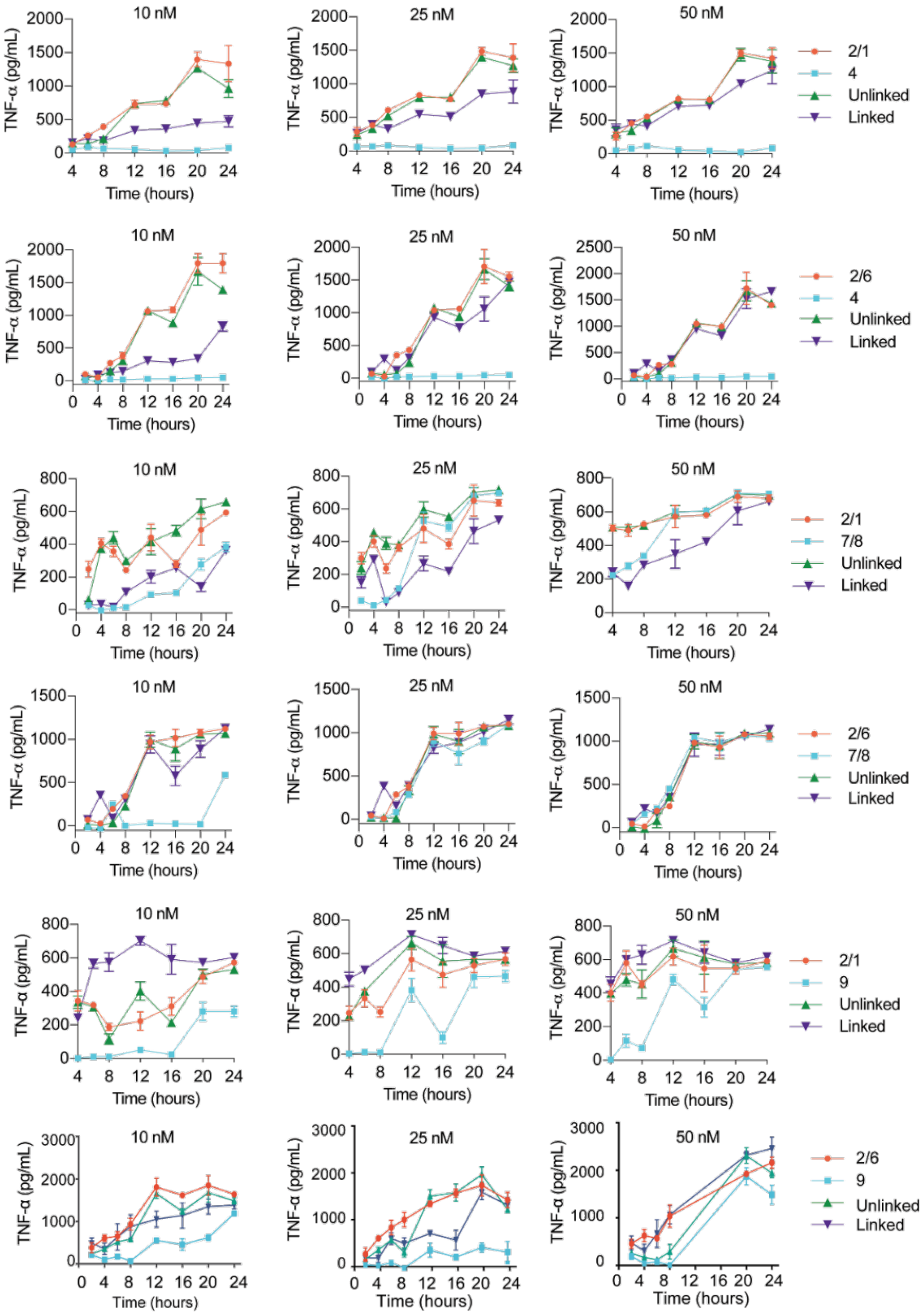

Figure 2.4: Kinetic profiling of cytokine TNF-α secretion

Figure 2.4 continued
RAW macrophages were incubated with of Pam_2CSK_4 (2/6), Pam_3CSK_4 (2/1), CpG_1826 (9) indole (4) and imidazoquinoline (7/8), corresponding equimolar mixtures and linked agonists at 10, 25 and 50 nM concentrations. Secreted TNF-α in the supernatant was measured at defined time intervals for 24 hours. The supernatant was incubated with HEK-Blue TNF-α reporter cell line for 20 to 24 h and quantified using TNF-α standards by measuring secreted SEAP levels.

2.3.5 NF-κB translocation kinetics

Upon observing the differences in cytokine production that did not uniformly correlate with the overall immune activity measured by RAW-Blue™ assay 24 h after activation, we hypothesized that initial transcription kinetics would give insight into the differences in activity. This hypothesis is based on mounting evidence that NF-κB activation and translocation from cytoplasm to the nucleus is a rapid response to TLR activation and the first step towards transcription of immune genes.[29] We expected that a synergistic response would correlate to higher rate of transcription and, conversely, that an inhibitory response would correlate to a lower rate of transcription. Using an engineered RAW 264.7 cell line with a stably expressed GFP-tagged fusion of the RelA NF-κB protein, we quantified and compared the rate of NF-κB translocation of the linked agonists and unlinked mixtures.[30] After treating the cells with the linked agonists and the corresponding single and unlinked mixtures, we used confocal microscopy to track GFP-tagged NF-κB translocation from cytoplasm to nucleus. A nuclear stain allowed us to calculate the ratio of nuclear to cytoplasmic NF-κB in each cell using CellProfiler. Using this technique, we resolved single-cell-level differences in NF-κB response dynamics. Comparing distributions of single-cell activation we observed distinct patterns of activation of the cells when treated with the dimers, equimolar mixtures or single agonists. The activation profiles of most of the unlinked mixtures resembled that of the monomers. Most of the dimers seemed to follow this trend and resemble the unlinked mixtures and the monomers in the activation profiles. In contrast the 2/1_peg13_4 dimer profile matched the TLR 4 agonist with the unlinked mixture resembling the TLR 2/1 agonist

(**Figure 2.5**). Interestingly, this data correlates closely with the difference we had observed in the RAW-Blue™ assay (**Figure 2.2**) where we saw significant differences in activity for the indole (TLR 4) activating dimers. These distinct profile patterns indicate that the linked agonists' activation of NFκB is determined by specific ligand interactions.

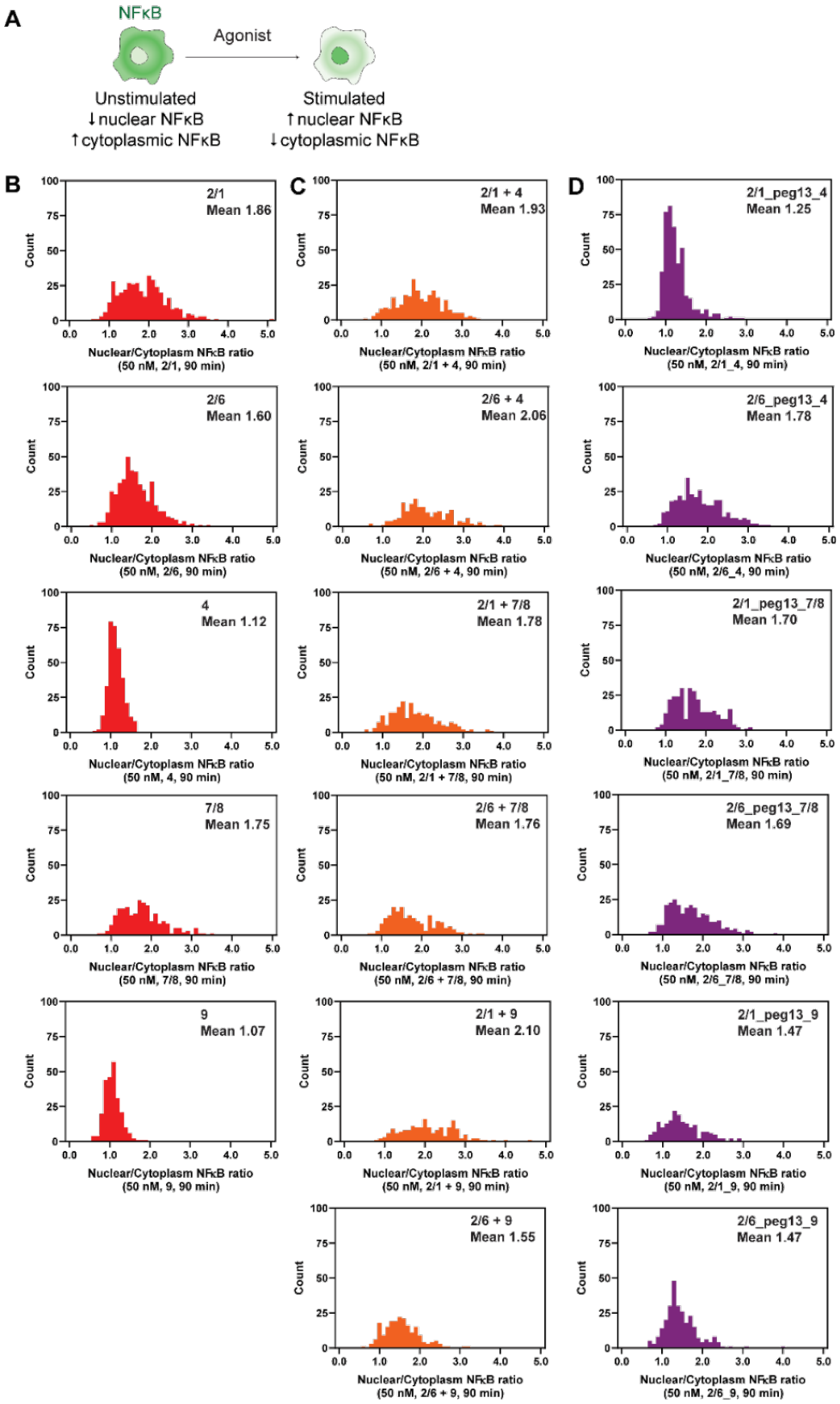

Figure 2.5: Single-cell analysis NF-κB migration studies.

Figure 2.5 continued

A) GFP- NF-κB migration from the cytoplasm to the nucleus. RAW-G9 cells containing NF-κB-GFP are imaged and the kinetics of NF-κB migration into the nucleus are quantified after 90 minutes of stimulation with 50 nM B) Pam_2CSK_4 (2/6), Pam_3CSK_4 (2/1), CPG (9) indole (4) and imidazoquinoline (7/8), C) corresponding equimolar mixtures and D) linked agonists. Each image contains a distribution the ratios for all cells in the field of view for multiple images. Mean values were calculated from all available data.

When we investigated the effect of dose on the NF-κB activation profiles we observed a change in the activation profile of the 2/1_peg13_4 dimer. At this lower concentration (10 nM) the dimer activated more cells to >2 nuclear/cytoplasm ratio. The profile also seemed to resemble the activation profile of the lipopeptide and the mixture of agonists (2/1 and 2/1 +4). However, the lipopeptide-CPG dimers had a similar NF-κB activation profile was similar to the lipopeptides and the agonist mixtures at both concentrations (**Figure 2.6**).

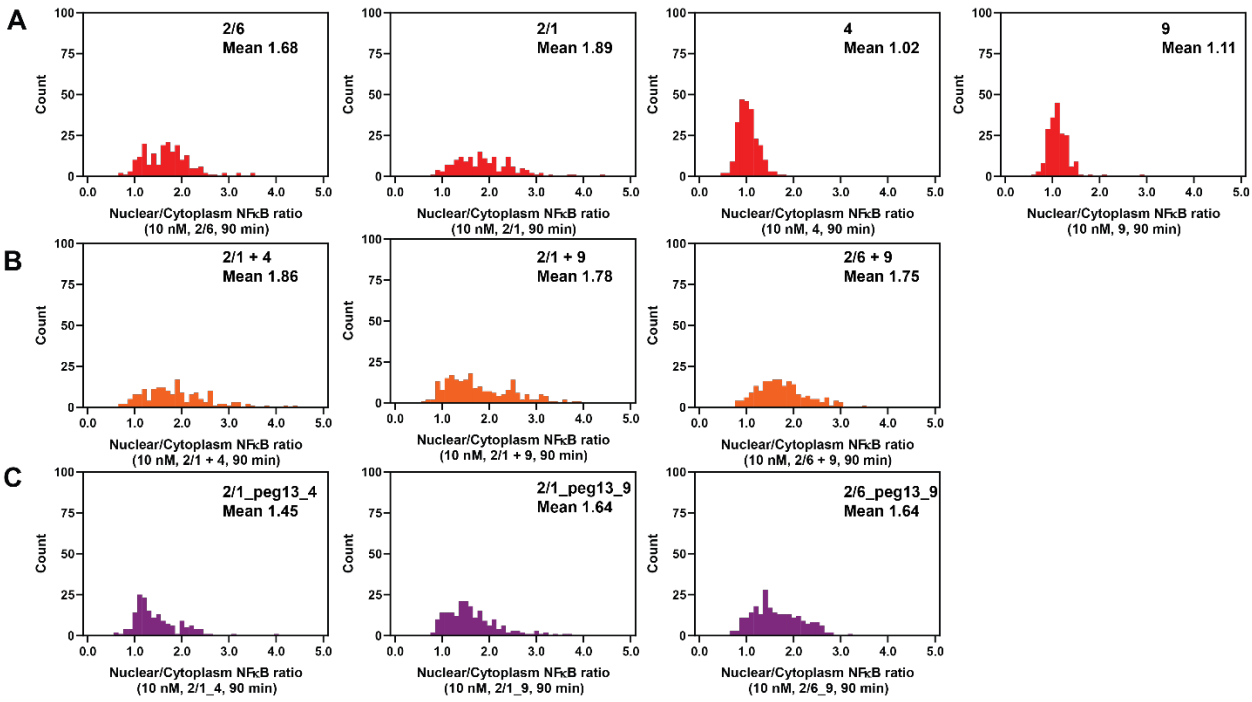

Figure 2.6 : Effect of dose on NF-κB migration.

RAW-G9 cells containing NF-κB-GFP are imaged and the kinetics of NF-κB migration into the nucleus are quantified after 90 min. of stimulation with 10 nM A) Pam_2CSK_4 (2/6), Pam_3CSK_4

Figure 2.6 continued
(2/1), CPG (9) and indole (4) B) corresponding equimolar mixtures and C) linked agonists. Each image contains a distribution the ratios for all cells in the field of view for multiple images. Mean values were calculated from all available data.

2.4 Conclusion

Linked TLR agonists elicit unique responses in both *in vitro* and *in vivo* systems. Understanding how these multi-activating systems works is key in the rational development of vaccine adjuvants. Combinatory responses to multiple stimuli by unlinked agonist mixtures is correlated to synergistic immune responses and distinct NF-κB activation profiles. Previous work has shown that cellular integration and processing of these multiple stimuli is specific to the type of NF-κB activating stimuli and processing capacity.[14,15] Our study on the mechanism of activation of linked dual TLR agonists suggests that ligand-receptor interactions influence initial transcriptional kinetics and thus downstream cytokine secretion profiles. The immune response is also dictated by specific single ligand interactions which can be attributed to the physical characteristics of the dimer constituents, the potency of the agonist pair, or the pathway (MyD88 and TRIF) that is activated by the agonist pair.

Overall NF-κB activity measured by RAW 264.7 cells showed significant differences in immune response when comparing between linked and unlinked agonists. These differences in activity were dose- and agonist-dependent with unaltered, additive, and inhibitory outcomes. Synthetic lipopeptides Pam_3CSK_4 and Pam_2CSK_4 both stimulate cell surface, membrane-bound TLR2 complexes. However, the dimers derived by conjugating these two agonists to small-molecule agonists—indole (TLR4) and imidazoquinoline (TLR7/8)—had different immune activity and cytokine secretion profiles. The dimers showed inhibitory NF-κB immune activity with lower downstream cytokine secretion compared to treatment with the lipopeptides and agonist

mixtures. The lipopeptide-CPG dimers showed an increase in immune activity that was more pronounced at lower concentrations.

By evaluating single-cell NF-κB dynamics we observed that 2/1_peg13_4 had a similar profile as the cells stimulated with indole (TLR 4) suggesting that this dimer preferentially activates through TLR 4. The low potency of the TLR4 activating indole could explain the decrease in the immune activity of this dimer especially if the dimer preferentially activates through the TLR 4 receptor. This agonist biasing effect was not observed with the 2/1_peg13_7/8, 2/6_peg13_4, and the 2/6_peg13_7/8 which had a similar profile as the corresponding unlinked mixture and the single agonists. Additionally, the time course of TNF-α cytokine secretion over time further illustrates the dose and agonist specificity of the linked agonists. Ligand-receptor interactions depend on the dose of the agonist with the high immune response being attributed to increased interactions. In the TNF-α secretion data set, we observe that increase in the dose of 2/1_peg13_7/8 and 2/1_peg13_4 dimers from 10 nM to 50 nM led to similar levels of cytokine production as the unlinked agonist and the corresponding mixtures. However, in the case of 2/1_peg13_9 we observe synergy in the overall immune response as well as in TNF-α secretion in lower concentrations but not at higher concentrations, indicating that for this dimer the synergistic interaction is derived from the altered kinetics of NF- κB signaling. While we have not definitively concluded what physical phenomenon results in the altered kinetics, by contrasting TLR 2/1and TLR 2/6 systems, we can conjecture that the difference may stem either from specific receptor pairings enhanced by linkage or by strong lipid interactions of the tri-palmitoylation of the TLR 2/1 agonist.

In this study, we show that the activity of dual linked agonists is both ligand- and dose-dependent. By observing the initial kinetics of activation, we observed distinct NF-κB dynamics

that can be attributed to how the immune cells integrate and process two activation signals, which further informs the downstream immune response. Using this set of dimers, we show ligand-dependent immune response with synergy being induced with only specific sets of dimers. We also observe a dependence of dose on the magnitude of the immune response, which indicates that kinetics of receptor activation by the ligands play a role in the mechanism of activation in linked systems.

2.5 Materials and methods

Unless otherwise noted, all reagents were purchased from commercial sources and used as received. DBCO-NHCO-PEG_{13}-NHS ester was purchased from BroadPharm. CPG ODN 1826 was purchased from Integrated DNA technologies. Azido acetic acid was purchased from Sigma Aldrich. Peptide reagents were purchased from CEM corporation. Nα-Fmoc-Nε-azide-L-Lysine was purchased from Chem-Impex. Automated solid-phase peptide synthesis was performed using Liberty Blue™ automated peptide synthesizer. Analytical reversed-phase HPLC was performed using Agilent Zorbax SB-C18 or C8 column (50 mm X 4.6 mm) with a flow rate of 1.0 mL/min on an Agilent 1260 Infinity LC system. Preparative reversed-phase HPLC purification was carried using Phenomenex Luna C18 or C8 Prep (150 X 21.2250 mm, 5 μm particle size) column with a flow rate of 21.2 mL/min on a Gilson 333/334 pump system and GX-271 liquid handler system. UV detection (214 nm, 254 nm, and 260 nm) was used for analytical and preparative HPLC. Size exclusion chromatography was performed on a GE superdex G75 in DPBS, pH 7.4 at a flow rate of 1mL/min with a UV/Vis detector set to monitor at 495 nm and 260 nm. Gel electrophoresis was carried out using Any KD Mini-PROTEAN TGX precast protein gels in a Mini-PROTEAN tetra cell (BIO-RAD). Gel electrophoresis samples were analyzed using Azure biosystems imager. UV-Vis was measured on Thermo Scientific Nano Drop. Mass spectrum was obtained using Agilent

LC/MSD. MALDI was obtained using Bruker Ultraflextreme MALDI-TOF/TOF. Cytometric bead array data was acquired on a NovoCyte Benchtop Flow Cytometer. Data was analyzed using student T-test or one-way ANOVA in Graph Pad Prism software. All values were reported as mean ± SD.

Synthetic Procedures

2/6_peg$_{13}$_9

Synthesis of $Pam_2CSK_4GN_3$: Rink amide resin (100-200 mesh, 0.55 mmole/g, 0.05 mg) was weighed out into a solid-phase peptide synthesizer reaction vessel. The peptide was constructed by coupling Fmoc-Cys((RS)-2,3-di(palmitoyloxy)-propyl)-OH, Fmoc-Ser(tBu)-OH, Fmoc-Lys-OH, Fmoc-Gly-OH, Nα-Fmoc-Nε-azide-L-Lysine (0.2 M in DMF) from the C terminus to the N terminus. Deprotection was done using 20% piperidine in DMF. Coupling was done after activation with diisopropylcarbodiimide (DIC) (0.5 M in DMF) in the presence of Ethyl cyanohydroxyiminoacetate (oxyma) (1M in DMF). Fmoc-Cys((RS)-2,3-di(palmitoyloxy)-propyl)-OH was coupled at 90˚C for 10 min. All other couplings were done at 90˚C for 5 min. All reactions and subsequent washes were performed in DMF. After the synthesis was completed, the resin was transferred into a Bio-Rad Poly-Prep chromatography column.

Deprotection and Purification: Global deprotection was done by agitating the resin in trifluoroacetic acid (TFA)/thioanisole/anisole/H_2O (8.5:0.5:0.5:0.5) for 2 hours. The peptide was precipitated by adding the cleavage cocktail filtrate to 30 mL diethyl ether in a 50 mL centrifuge tube pre-cooled to -78˚C. The precipitate was collected by centrifuge (4000 XG for 5 min). The precipitate was dissolved in 20% CH_3CN in 0.1%TFA) and filtered through a 0.45 µm syringe filter. Purification was performed using reverse-phase HPLC C8 column (gradient elution with

30–90% CH_3CN /0.1% TFA over 15 min). Pure fractions were pooled together and the peptide was recovered through lyophilization. MALDI-TOF MS (m/z) 1482.38 $[M+H]^+$

Synthesis of 2/6_peg$_{13}$_9

5'-FAM-tccatgacgttcctgacgtt-3'-NH2 (2.2 mg, 0.32 µmol) in 3 mL PBS pH 8 was incubated with DBCO-NHCO-PEG_{13}-NHS ester (7 mg, 6.70 µmols, 0.75 mg/ml in DMSO) overnight at 37˚C with vigorous stirring while protected from light. The reaction mixture was purified with a centrifugal filter unit with a 3 kDa cutoff, washing (X6) with pH 7.4 PBS to remove unreacted DBCO-NHCO-PEG13-NHS ester. The resulting reaction mixture was diluted to 3 mL PBS pH 8 and incubated with Pam_2CSK_4GK-Azide (3.0 mg, 2.0 µmols, 5 equiv.) overnight at 37˚C with vigorous stirring. The reaction mixture was first purified using a centrifugal filter unit with a 3 kDa cutoff washing (X6) with pH 7.4 PBS then purified passed through a 0.2 µm filter and directly purified by fast protein liquid chromatography (Superdex G75, DPBS, 0.2 mL/min). Elution of the heterodimer was confirmed by monitoring the elution absorbance at 495 nm. The dimers were quantified by UV/Vis and quantified via the local Abs_{max} at 495 nm using a standard curve generated by known concentrations of Fam-CPG (**Figure S1**) before serial dilutions in PBS to relevant assay concentrations.

2/1_peg$_{13}$_9

Synthesis of $Pam_3CSK_4GN_3$: Rink amide resin (100-200 mesh, 0.55 mmole/g, 0.05 mg) was weighed out into a solid-phase peptide synthesizer reaction vessel. The peptide was constructed by coupling Palmitic acid, Fmoc-Cys((RS)-2,3-di(palmitoyloxy)-propyl)-OH, Fmoc-Ser(tBu)-OH, Fmoc-Lys-OH, Fmoc-Gly-OH, Fmoc-Lys-azide-OH (0.2M in DMF) from the C terminus to the N terminus. Deprotection was done using 20% piperidine in DMF. Coupling was done after

activation with diisopropylcarbodiimide (DIC) (0.5M in DMF) in the presence of Ethyl cyanohydroxyiminoacetate (oxyma) (1M in DMF). Palmitic acid and Fmoc-Cys((RS)-2,3-di(palmitoyloxy)-propyl)-OH were coupled at 90°C for 10 min. All other couplings were done at 90°C for 5 min. All reactions and subsequent washes were performed in DMF. After the synthesis was completed, the resin was transferred into a Bio-Rad Poly-Prep chromatography column.

Deprotection and Purification

Global deprotection was achieved by agitating the resin in trifluoroacetic acid (TFA)/thioanisole/anisole/H_2O (8.5:0.5:0.5:0.5) for 2 hours. The peptide was precipitated by adding the cleavage cocktail filtrate to 30 mL diethyl ether in a 50 mL centrifuge tube pre-cooled to -78°C. The precipitate was collected by centrifuge (4000 XG for 5 min). The precipitate was dissolved in 20% CH_3CN in 0.1%TFA) and filtered through a 0.45 µm syringe filter. Purification was performed using reversed-phase HPLC C8 column (gradient elution with 30–90% Methanol /0.1% TFA over 15 min). Pure fractions were pooled together and the peptide was recovered through lyophilization. MALDI-TOF MS (m/z) 1719.28 $[M+H]^+$

Synthesis of 2/1_peg_{13}_9

5'-FAM-tccatgacgttcctgacgtt-3'-NH2 (2.2 mg, 0.32 µmols) in 3 mL PBS pH 8 was incubated with DBCO-NHCO-PEG_{13}-NHS ester (7 mg, 6.70 µmols, 0.75 mg/ml in DMSO) overnight at 37°C with vigorous stirring. The reaction mixture was purified with a centrifugal filter unit with a 3 kDa cutoff washing X6 with pH 7.4 PBS to remove unreacted DBCO-NHCO-PEG13-NHS ester. The resulting reaction mixture was divided into 3 equal fractions, diluted to 2 mL with PBS (pH 8.0) and incubated with Pam_3CSK_4GK-Azide (1.0 mg, 0.67 µmols, 5 equiv.,10 mg/ml, DMSO) overnight at 37°C with vigorous stirring. The reaction mixture was first purified using a centrifugal

filter unit with a 3 kDa cutoff washing X6 with pH 7.4 PBS then purified passed through a 0.2 µm filter and directly purified by fast protein liquid chromatography (Superdex G75, DPBS, 0.2 mL/min). Elution of the heterodimer was confirmed by monitoring the elution absorbance at 475 nm. The dimers were quantified by UV/Vis and quantified via the local Abs_{max} at 495 nm using a standard curve generated by known concentrations of Fam-CPG (**Figure SI.1**) before serial dilutions in PBS to relevant assay concentrations.

2/6_peg_{13}_4

Cyclohexyl amine derivatized TLR 4 activating indole was synthesized as described in previous publications.[8]

To the indole (10 mg, 0.023 mmols) in 2 mL DMSO was added triethylamine (4.5 mg, 0.046 mmoles, 2 equiv.) and DBCO-NHCO-PEG_{13}-NHS ester (10 mg, 0.01 mmoles, 0.5 equiv.) and the mixture stirred at RT overnight. The reaction mixture was purified using reversed-phase HPLC C8 column (gradient elution with 30–90% CH_3CN /0.1% TFA over 15 min). Pure fractions were pooled together and lyophilized to obtain the product as a white powder. (6.2 mg, 40%) MALDI-TOF MS (m/z) 1400.85 $[M+Na]^+$

Synthesis of 2/6_peg_{13}_4

$Pam_2CSK_4GN_3$ (3.2 mg, 0.0021 mmols) and DBCO derivatized indole (3.6 mg, 0.0026 mmols) was incubated with agitation at 37°C for 12 hours. The reaction mixture was purified using reversed-phase HPLC C8 column (gradient elution with 30–90% CH_3CN /0.1% TFA over 15 min). Pure fractions were pooled together and lyophilized to obtain the product as a white powder. (5 mg, 67%) MALDI-TOF MS (m/z) 2860.55 $[M+H]^+$

2/1_peg$_{13}$_4

$Pam_3CSK_4GN_3$ (2.0 mg, 0.0015 mmols) and DBCO derivatized indole (2.8 mg, 0.002 mmols) was incubated with agitation at 37˚C for 12 hours. The reaction mixture was purified using reversed-phase HPLC C8 column (gradient elution with 30–90% MeOH /0.1% TFA over 10 min). Pure fractions were pooled together and lyophilized to obtain the product as a white powder. (1.7 mg, 37%) MALDI-TOF MS (m/z) 3100.19 $[M+H]^+$

2/6_peg$_{13}$_7/8

Benzyl amine derivatized TLR 7/8 activating imidazoquinoline was synthesized as described in previous publications.[7]

To the imidazoquinoline (10 mg, 0.027 mmols) in 2 mL DMSO was added triethylamine (4.5 mg, 0.046 mmoles, 2 equiv.) and DBCO-NHCO-PEG_{13}-NHS ester (10 mg, 0.01 mmoles, 0.5 equiv.) and the mixture stirred at RT overnight. The reaction mixture was purified using reversed-phase HPLC C8 column (gradient elution with 30–90% CH_3CN /0.1% TFA over 15 min). Pure fractions were pooled together and lyophilized to obtain the product as a white powder. (7.3 mg, 43%) MALDI-TOF MS (m/z) 1312.34 $[M+Na]^+$

Synthesis of 2/6_peg$_{13}$_7/8

$Pam_2CSK_4GN_3$ (2.0 mg, 0.0013 mmols) and DBCO derivatized imidazoquinoline (2.0 mg, 0.0016 mmols) was incubated with agitation at 37˚C for 12 hours. The reaction mixture was purified using reversed-phase HPLC C8 column (gradient elution with 30–90% MeOH /0.1% TFA over 10 min). Pure fractions were pooled together and lyophilized to obtain the product as a white powder. (1.3 mg %, 37%) MALDI-TOF MS (m/z) 2772.68 $[M+H]^+$

2/1_peg$_{13}$_7/8

$Pam_3CSK_4GN_3$ (2.0 mg, 0.0011 mmols) and DBCO derivatized imidazoquinoline (2.0 mg, 0.0016 mmols), in 2 mL DMSO was incubated with agitation at 37°C for 12 h. The reaction mixture was purified using reversed-phase HPLC C8 column (gradient elution with 30–90% MeOH /0.1% TFA over 10 min). Pure fractions were pooled together and lyophilized to obtain the product as a white powder. (1.1 mg, 32%) MALDI-TOF MS (m/z) 3011.68 $[M+H]^+$

Biological Procedures

Raw Blue NF-κB reporter assay

RAW-Blue cells were passaged and plated in a 96 well plate at a density of 100,000 cells/well in 180 μL DMEM containing 10% heat-inactivated FBS (HI-FBS) and selective antibiotics. The cells were stimulated with the conjugates and unlinked controls for 20 to 24 h at 37 °C and 5% CO_2. NF-κB activity was measured by a QUANTI-Blue (InvivoGen) assay and the absorbance was measured at 620 nm using a Multiskan FC plate reader (Thermo Scientific).

Measurement of cytokine levels secreted by RAW macrophages and BMDCs stimulated with agonists or unlinked mixtures

RAW 264.7 macrophages or BMDCs were plated at a density of 100,000 cells/well in 180 μL DMEM containing 10% HIFBS. The cells were stimulated with the conjugates and unlinked controls and supernatants were collected at the desired time points between 2 h and 24 h post stimulation and stored at -20 °C until further analysis. The IL-6 and MCP-1 levels were quantified was performed using Mouse Inflammation Cytokine Bead Arrays (BD, Cat. 552364). The TNF- α levels were measured using HEK-blue TNF-α reporter cell line as described below.

HEK-Blue TNF-α reporter assay

Stimulation of HEK-Blue TNF-α cells with TNF-α triggers a signaling cascade leading to the activation of AP-1/NF-κB and the subsequent production of SEAP. HEK-Blue cells were passaged and plated in a 96 well plate at a density of 100,000 cells/well in 180 µL DMEM containing 10% HI-FBS and selective antibiotics. The cells were stimulated with 20 µL of the stored cell culture supernatants collected at various time points. A standard curve was generated using incubation with recombinant mouse TNF-α. The cells were incubated for 24 h at 37 °C and 5% CO_2. SEAP levels was measured by a QUANTI-Blue (InvivoGen) assay and the absorbance was measured at 620 nm using a Multiskan FC plate reader (Thermo Scientific).

NF-κB Imaging

RAW 264.7 G9 macrophages[30] were plated at a density of 50,000-100,000 per well in 8-well microscopy plates in 200µL DMEM with 10% FBS and 1% antibiotic-antimycotic and incubated overnight in an incubator at 37 °C and 5% CO_2. The medium was then replaced with 180 µL DMEM with 10% HI-FBS and incubated for an additional 2 hours. The cells were then stimulated with 20 µL of the conjugates or unlinked controls for the desired time after which the media was removed and the cells were fixed with 200 µL cold 3% formaldehyde in PBS for 10 min at room temperature, washed three times with PBS, and stained with HOECHST nuclear stain (0.5 µg/mL, 200 µL) for 20 mins at room temperature in the dark. The cells were then washed three times before imaging.

The cells were imaged on an Olympus spinning disc confocal microscope using a 40x water objective. Images captured included GFP NF-κB stain at 480 nm excitation, nuclear HOECHST stain at 405 nm excitation, and a brightfield image. The overlap of the GFP signal and HOECHST signal (indicating nuclear translocation of NF-κB) was determined using CellProfiler. Briefly, each nucleus in the HOECHST stain was outlined, and then the outlines were slightly shrunken

and expanded. In the GFP image, the area between the expanded and original outlines was taken to be cytoplasmic GFP signal, and the area inside the shrunken outline was taken to be nuclear GFP signal. The ratios of these numbers determined cellular activation for each cell. The activation state of each cell was then plotted as a histogram in R.

Dynamic light scattering

Dynamic light scattering (DLS) measurements were performed by a Wyatt Mobius DLS instrument. Measurements were performed at 25^{o}C using a laser wavelength of 532 nm. Scattered light was collected at a fixed angle of 163.5^{o} . The size distribution plots were obtained using the installed software from the instrument.

Endotoxin test

Endotoxin concentrations were determined with ToxinSensor™ Single Test Kit (GenScript) according to the manufacturer's instructions. No gelation occurred with any of the synthesized dimers which confirmed the absence of endotoxin.

2.6 References

1. Pulendran, B. & Ahmed, R. Immunological mechanisms of vaccination. *Nat Immunol* **12**, 509–517 (2011).

2. Ahmed, R. & Pulendran, B. Learning vaccinology from viral infections. *Journal of Experimental Medicine* **208**, 2347–2349 (2011).

3. Akira, S., Uematsu, S. & Takeuchi, O. Pathogen recognition and innate immunity. *Cell* **124**, 783–801 (2006).

4. Parker, L. C., Prince, L. R. & Sabroe, I. Translational Mini-Review Series on Toll-like Receptors: Networks regulated by Toll-like receptors mediate innate and adaptive immunity. *Clin Exp Immunol* **147**, 199–207 (2007).

5. Kawasaki, T. & Kawai, T. Toll-Like Receptor Signaling Pathways. *Frontiers in Immunology* **5**, (2014).

6. Tipping, P. G. Toll-Like Receptors: The Interface between Innate and Adaptive Immunity. *JASN* **17**, 1769–1771 (2006).

7. Tom, J. K. *et al.* Modulation of Innate Immune Responses via Covalently Linked TLR Agonists. *ACS Cent. Sci.* **1**, 439–448 (2015).

8. Albin, T. J. *et al.* Linked Toll-Like Receptor Triagonists Stimulate Distinct, Combination-Dependent Innate Immune Responses. *ACS Cent. Sci.* **5**, 1137–1145 (2019).

9. Gilkes, A. P. *et al.* Tuning Subunit Vaccines with Novel TLR Triagonist Adjuvants to Generate Protective Immune Responses against Coxiella burnetii. *J Immunol* **204**, 611–621 (2020).

10. Madan-Lala, R., Pradhan, P. & Roy, K. Combinatorial Delivery of Dual and Triple TLR Agonists via Polymeric Pathogen-like Particles Synergistically Enhances Innate and Adaptive Immune Responses. *Sci Rep* **7**, 2530 (2017).

11. Orr, M. T. *et al.* A Dual TLR Agonist Adjuvant Enhances the Immunogenicity and Protective Efficacy of the Tuberculosis Vaccine Antigen ID93. *PLOS ONE* **9**, e83884 (2014).

12. Mancini, R. J., Tom, J. K. & Esser-Kahn, A. P. Covalently coupled immunostimulant heterodimers. *Angew Chem Int Ed Engl* **53**, 189–192 (2014).

13. Ryu, K. A., Slowinska, K., Moore, T. & Esser-Kahn, A. Immune Response Modulation of Conjugated Agonists with Changing Linker Length. *ACS Chem Biol* **11**, 3347–3352 (2016).

14. Kellogg, R. A., Tian, C., Etzrodt, M. & Tay, S. Cellular Decision Making by Non-Integrative Processing of TLR Inputs. *Cell Reports* **19**, 125–135 (2017).

15. Gutschow, M. V. *et al.* Combinatorial processing of bacterial and host-derived innate immune stimuli at the single-cell level. *MBoC* **30**, 282–292 (2019).

16. Takeuchi, O. *et al.* Discrimination of bacterial lipoproteins by Toll-like receptor 6. *Int Immunol* **13**, 933–940 (2001).

17. Buwitt-Beckmann, U. *et al.* Toll-like receptor 6-independent signaling by diacylated lipopeptides. *Eur J Immunol* **35**, 282–289 (2005).

18. Aliprantis, A. O. *et al.* Cell activation and apoptosis by bacterial lipoproteins through toll-like receptor-2. *Science* **285**, 736–739 (1999).

19. Krieg, A. M. *et al.* CpG motifs in bacterial DNA trigger direct B-cell activation. *Nature* **374**, 546–549 (1995).

20. Chan, M. *et al.* Identification of substituted pyrimido[5,4-b]indoles as selective Toll-like receptor 4 ligands. *J Med Chem* **56**, 4206–4223 (2013).

21. Shukla, N. M., Malladi, S. S., Mutz, C. A., Balakrishna, R. & David, S. A. Structure-activity relationships in human toll-like receptor 7-active imidazoquinoline analogues. *J Med Chem* **53**, 4450–4465 (2010).

23. Shukla, N. M. *et al.* Toll-Like Receptor (TLR)-7 and -8 Modulatory Activities of Dimeric Imidazoquinolines. *J. Med. Chem.* **55**, 1106–1116 (2012).

24. Hamley, I. W. *et al.* Toll-like receptor agonist lipopeptides self-assemble into distinct nanostructures. *Chem. Commun.* **50**, 15948–15951 (2014).

25. Takeda, K. & Akira, S. TLR signaling pathways. *Semin Immunol* **16**, 3–9 (2004).

26. Napolitani, G., Rinaldi, A., Bertoni, F., Sallusto, F. & Lanzavecchia, A. Selected Toll-like receptor agonist combinations synergistically trigger a T helper type 1-polarizing program in dendritic cells. *Nat Immunol* **6**, 769–776 (2005).

27. Trinchieri, G. & Sher, A. Cooperation of Toll-like receptor signals in innate immune defence. *Nat Rev Immunol* **7**, 179–190 (2007).

28. Liu, Q. & Ding, J. L. The molecular mechanisms of TLR-signaling cooperation in cytokine regulation. *Immunol Cell Biol* **94**, 538–542 (2016).

29. Karin, M. & Ben-Neriah, Y. Phosphorylation meets ubiquitination: the control of NF-[kappa]B activity. *Annu Rev Immunol* **18**, 621–663 (2000).

30. Ernst, O., Vayttaden, S. J. & Fraser, I. D. C. Measurement of NF-κB Activation in TLR-Activated Macrophages. *Methods Mol Biol* **1714**, 67–78 (2018).

3. Site-specific antigen-adjuvant conjugation using cell-free protein synthesis enhances antigen presentation and $CD8^+$ T-cell response

This chapter has been published in Scientific Reports 11 (1): 6267, 2021.

3.1 Summary

Vaccines consist of antigens combined with adjuvants to elicit a strong immune response. If delivered separately, adjuvants diffuse away leading to decrease in local concentration thereby creating less effective responses. Co-delivery ensures that both the antigen and adjuvant activate the same innate immune cell by colocalizing within the same endosome. This method ensures efficient APC activation and antigen-specific T-cell production. Among co-delivery methods, covalent conjugation of antigen to an adjuvant of interest has been demonstrated to improve cross presentation and CD8 T cell activation.

Currently, there are no scalable methods to generate site-specific conjugation for clinical translation of this technique. We report the use of the cell-free protein synthesis (CFPS) platform as a rapid method to produce large quantities (> 100 mg/L) of a model antigen, ovalbumin (OVA), with site-specific incorporation of *p*-azidomethyl-L-phenylalanine (pAMF) at two solvent-exposed sites away from immunodominant epitopes. Using copper-free click chemistry, we conjugated CpG oligodeoxynucleotide toll-like receptor 9 (TLR9) agonists to the pAMF sites on the mutant OVA protein. The OVA-CpG conjugates demonstrate enhanced antigen presentation *in-vitro* and increased antigen-specific $CD8^+$ T-cell production *in-vivo*. Moreover, OVA-CpG conjugation reduced the dose of CpG needed to invoke antigen-specific T-cell production tenfold. These results highlight how site-specific conjugation and CFPS technology can be implemented to produce large quantities of covalently-linked antigen-adjuvant conjugates for use in clinical vaccines.

3.2 Introduction

Synthetic subunit vaccines that invoke potent cellular immune responses are desirable for the safe and scalable prevention of disease. Early vaccines were composed of whole pathogens attenuated by heat inactivation or chemical modification. Traditional attenuated vaccines are highly potent, and their administration has led to reductions in morbidity from many diseases.[1] Despite their potency, attenuated vaccines pose a safety risk resulting from the presence of live pathogens, limiting use in elderly or immunocompromised individuals. Furthermore, attenuated vaccines can contain harmful pathogenic material, undergo spontaneous mutations to revert to their infectious form, and risk infecting the host if incompletely inactivated.[2] Thus, there is interest in designing synthetic alternatives to attenuated vaccines.

Subunit vaccines comprising a protein antigen do not contain live pathogenic material and therefore serve as desirable alternatives to attenuated vaccines. Subunit vaccines are composed of poorly immunogenic protein antigens co-administered with one or more adjuvants which bind pattern-recognition receptors (PRRs) to activate innate immunity.[2-5] Innate immune activation is critical for cross-presentation of proteolyzed antigen on MHC by antigen-presenting cells (APCs) and recognition by antigen-specific T-cells, resulting in protective adaptive immune responses.[4] FDA-approved subunit vaccines containing synthetic adjuvants have been developed for hepatitis B and shingles, among others.[6-7]

Despite the success of subunit vaccines, they have been limited by weak immunogenicity of the antigen, necessitating co-administration of large doses of adjuvant. Synthetic PRR agonists often generate adverse inflammatory profiles when used as adjuvants, resulting in poor translation to clinical use.[8] One method to reduce the dose of agonist is through co-delivery of antigen and adjuvant to the same APC.[9] Co-delivery allows adjuvant-mediated activation of the APC along

with concurrent antigen processing and presentation, resulting in efficient T-cell responses and dose sparing.[10] Precise control over the amount of adjuvant administered with the antigen can prevent adverse responses and improve efficiency of subunit vaccines.

Co-delivery of antigen and adjuvant through conjugation can facilitate efficient activation of APCs and enhanced antigen exposure using a single construct, enhancing proliferation of antigen-specific T-cells.[9,14-15] Oligodeoxynucleotides, such as unmethylated CpG, activate the innate immune system by binding endosomal toll-like receptor 9 (TLR9) to enhance cross-presentation of antigenic components.[16] TLR9 agonists conjugated to ovalbumin (OVA) were shown to enhance both cross-presentation and antigen-specific $CD8^+$ T-cell production.[9,11] However, these systems were limited by poor control over the modification site and aggregation resulting from over-conjugation of ODN adjuvants. To overcome this limitation, we hypothesized that cell-free protein synthesis would allow scalable production of dose controlled, site-specific antigen-adjuvant conjugates that would not affect protein folding or disrupt major epitopes.

Cell-free protein synthesis (CFPS) is an efficient, *E.coli*-derived platform to express and purify unglycosylated proteins containing non-native amino acids (nnAA) in their natively-folded state. The translational machinery provided by the cellular lysate supplemented with energy sources and plasmid DNA facilitates *in-vitro* synthesis of proteins that are unnatural, insoluble, or toxic to living systems.[17] Historically, CFPS systems were limited by feedback inhibition caused by byproducts resulting from use of ATP as an energy source.[18] Recently, the XpressCF^{+TM} CFPS system (Vaxcyte, Inc.) has overcome these limitations by using pyruvate as an alternative energy source to allow scalable production of complex proteins.[18-19] By using an orthogonal tRNA and aminoacyl synthetase pairing, this technology allows site-specific incorporation of nnAAs with reactive side chains into the folded protein.[19-21] Using this system, we aimed to test if scalable

production of site-specific antigen-adjuvant conjugates could induce production of a $CD8^+$ killer T cell response in a vaccination model.

Herein, we describe a novel strategy to generate a model antigen-adjuvant conjugate subunit vaccine using CFPS. OVA-2pAMF, an unglycosylated OVA mutant containing two site-specific *p*-azidomethyl-L-phenylalanine (pAMF) mutations at K20 and K370, was synthesized using XpressCF^{+TM} on a 14 mg scale. A TLR9 agonist, CpG1018, was conjugated to the pAMF sites using azide-alkyne click chemistry to generate the conjugate vaccine, OVA-CpG. Functionally, the conjugate vaccine enhanced antigen cross-presentation and APC activation *in-vitro* and promoted $CD8^+$ T-cell responses *in-vivo* without showing aggregation or cytotoxicity. Most importantly, these studies demonstrate that large quantities of mutant proteins containing nnAAs at specific sites in the folded protein can be prepared using CFPS and that conjugating a CpG oligonucleotide TLR agonist to these sites can enhance antigen-specific $CD8^+$ T-cell production in a vaccination model.

3.3 Results and discussion

3.3.1 Synthesis of OVA-CpG Conjugates Using CFPS

CFPS is a versatile approach to synthesize protein antigens with site-specific mutations for antigen-adjuvant conjugation. To demonstrate the applicability of CFPS and to provide an appropriate comparison to previous antigen-adjuvant co-localization experiments,[9-15] we used a model antigen, OVA. Noting that a pioneering study of non-specific conjugation of CpG to OVA at a ≥2:1 ratio induced aggregation and reduced antigen presentation,[11] we introduced two site-specific conjugatable handles on one OVA protein to overcome this limitation of non-specific conjugation. We selected the human-mouse cross-reactive CpG1018 as a clinically relevant TLR9 agonist and appended a commercially available 5'-thiol handle for conjugation.[6]

In selecting the conjugation sites, we considered the structure of OVA with a focus on its immunodominant MHC epitopes, SIINFEKL ($OVA_{257-264}$) and ISQAVHAAHAEINEAGR ($OVA_{323-339}$). We hypothesized that epitope blocking and aggregation could be mitigated by introducing spatially-isolated and solvent-exposed away from the immunodominant epitopes. K20 and K370 were therefore selected as optimal conjugation sites (**Figure 3.1 A-B**). The handles were introduced by replacing lysine codons with amber codons in the coding sequence for OVA. Using an orthogonal tRNA and synthetase pair, we selectively incorporated *p*-azidomethyl-L-phenylalanine (pAMF) at these sites to generate one protein with two azide reactive sites, OVA-2pAMF. A TEV protease cleavage site coupled to a poly-Histidine tag was expressed at the C terminus to facilitate purification of the protein by sequential combination of affinity and size-exclusion chromatography. Protein expression conditions were optimized to a temperature of 25°C (**Figure 3.1 C**) and the purity of the purified protein was confirmed by SDS-PAGE (**Figure 3.1 D and Figure B1**). The protein was further characterized by Q-TOF MS and MALS (**Figure 3.1 D-F**). CFPS was subsequently scaled up to generate 14 mg of the purified protein. After purification, endotoxin was removed using Triton X-114 to a level <1.5 EU/mL.[22] A recovery yield of 78% for the endotoxin purification step was achieved (**Figure B2**), permitting use of milligram-scale OVA-2pAMF in later biological experiments.

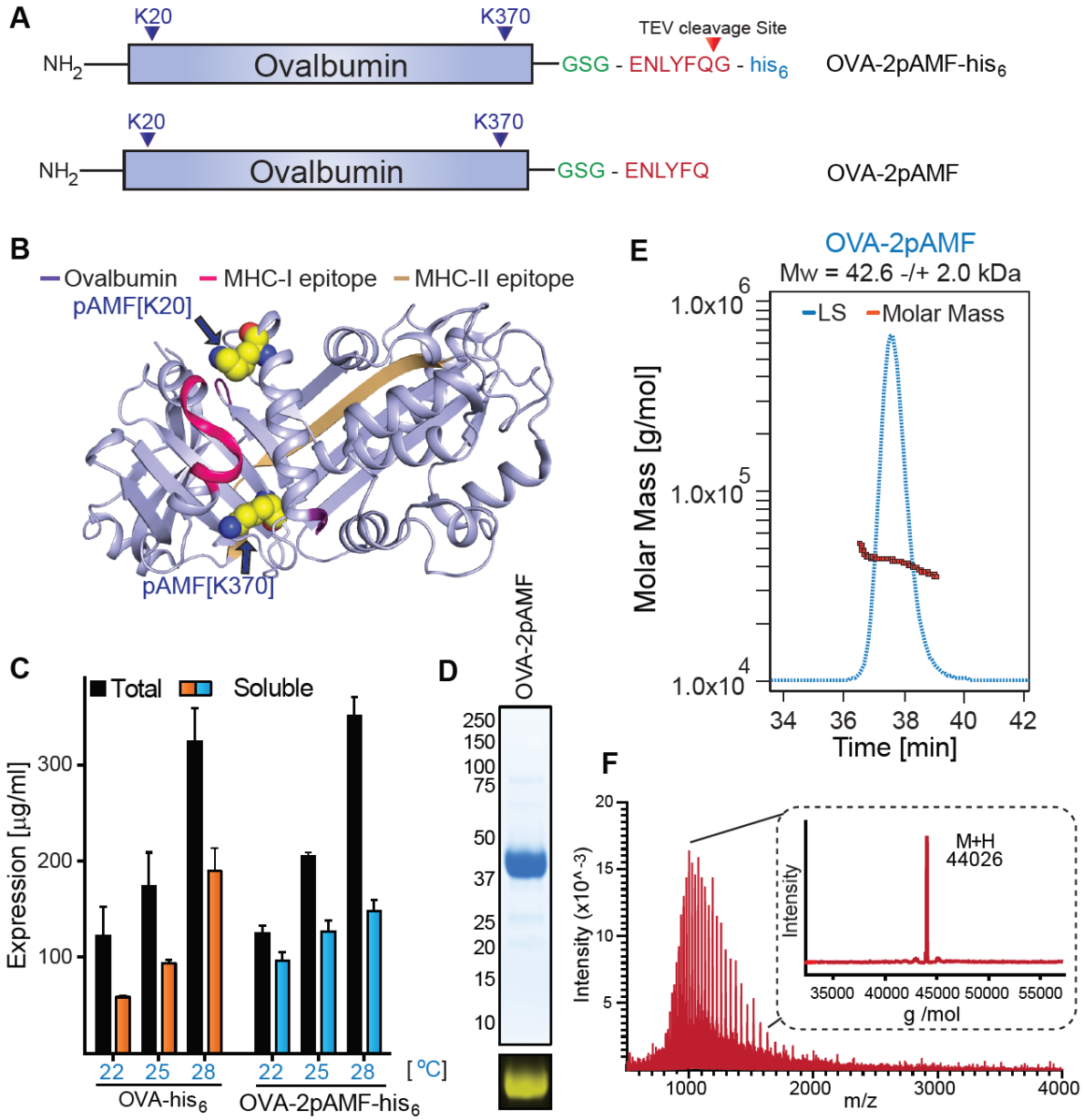

Figure 3.1: Expression, purification, and characterization of OVA-2pAMF.

A) Modular architecture and expression construct design of OVA-2pAMF with B) the K20 and K370 pAMF conjugation sites noted. C) Optimization of OVA-2pAMF expression conditions. D) SDS-PAGE demonstrates > 95% purity, and DBCO-TAMRA labeling confirms pAMF incorporation. Biophysical characterization of purified OVA-2pAMF using E) SEC-MALS indicates a monodisperse protein preparation and F) Q-TOF ESI-MS (deconvoluted in inset) indicates close agreement with the expected mass, 44,026 Da.

After synthesizing and purifying OVA-2pAMF, we conjugated the 5'-thiol modified CpG1018 through a DBCO-Maleimide linker (**Figure 3.2 A-B and Figure B3**). Copper-free click chemistry was employed to facilitate this reaction under aqueous conditions. Unreacted CpG-DBCO was removed by centrifugal filtration, and the OVA-CpG conjugates were characterized using SDS-PAGE gel chromatography. Three batches of OVA-CpG were prepared, and loading densities of 1.2, 1.5, and 1.3 CpGs/OVA were obtained (**Figure 3.2 C and Figure B4**). It should be noted that SDS-PAGE revealed two distinct peaks for the 1 CpG/OVA component; while both components were included in the densitometry analysis, we believe these species correspond to different charge states of the K20 or K370 conjugation sites after reaction with CpG which may have resulted in minor electrostatic variations during electrophoresis. We also attempted to improve loading by increasing reaction temperature, but these efforts resulted in degradation of OVA-2pAMF observed through the presence of large, low molecular weight bands ≤ 37 kDa in SDS-PAGE gels of the crude product (not shown). Addition of excess CpG-DBCO or prolonging the reaction were also found to be insufficient to drive the reaction to completion; we believe that the negative charge of CpG could shield the pAMF sites during later stages of the reaction to result in this effect. Unreacted CpG was found to be sufficiently removed using size-exclusion HPLC of the purified product (**Figure B5**). Preparative anion exchange chromatography using a 0-1 M NaCl gradient in a method previously described by the Chertok group was shown to remove unreacted OVA-2pAMF from the reaction mixture; however, components containing one and two CpG/OVA eluted together (**Figure B6**).[11] With the limited benefit to this purification strategy, we opted to use the unpurified heterogeneous mixtures in future studies; thus, site-specific OVA-CpG conjugates containing 1.2-1.5 CpG/OVA were achieved for use in subsequent experimentation.

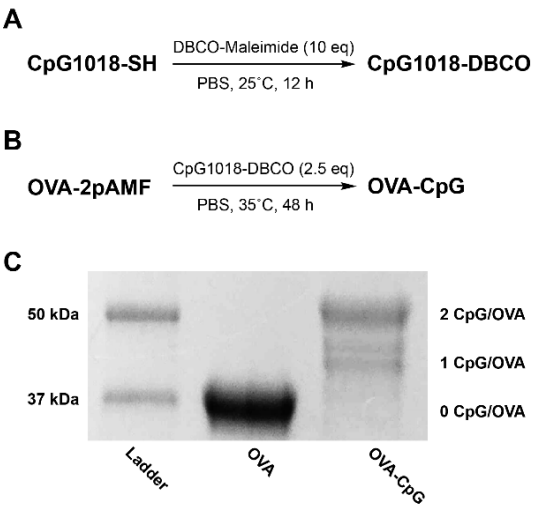

Figure 3.2: Synthesis and characterization of OVA-CpG conjugate

A) Synthesis of CpG-DBCO and B) conjugation of CpG-DBCO to OVA-2pAMF. C) SDS-PAGE gel of OVA-CpG conjugates visualized using One-Step Blue protein gel staining demonstrates loading of 1.5 OVA/CpG in batch one of the OVA-CpG conjugate.

3.3.2 *in-vitro* Immunostimulatory Activity of Conjugates

Having successfully synthesized OVA-CpG, we validated its *in-vitro* immune activity of our linked systems relative to unlinked controls using RAW-Blue and HEK mTLR9 reporter cell lines. Conjugation of PRR agonists to a macromolecule can alter receptor binding, and it is therefore important to validate activity after conjugation. We first tested activity using HEK mTLR9 reporter cells. OVA-CpG conjugates exhibited enhanced mTLR9 activation relative to unlinked OVA + CpG (**Figure 3.3A**). For all in-vitro studies, the dose of OVA and CpG used in the OVA+CpG treatment was designed to match that of the linked OVA-CpG conjugate. Native EndoFit™ Ovalbumin (InvivoGen) was used for all *in-vitro* and *in-vivo* experiments as a non-immunogenic control; though OVA-2pAMF is not expected to induce an immune response, such controls could prevent aberrant activation in control groups from non-specific immunostimulatory activity of OVA-2pAMF. We then used the RAW-Blue NF-κB reporter cells to test downstream signaling of

the TLR9 receptor. Again, signaling induced by OVA-CpG was increased relative to unlinked controls (**Figure 3.3 B**). These results validated that conjugation of CpG to OVA-2pAMF enhanced TLR9 signaling. TLR9 is expressed in the endocytic compartment; thus, the divalency of the OVA-CpG construct both facilitates enhanced endosomal uptake through conjugation and increases TLR activation in the endosome to facilitate activation of APCs. Indeed, linked antigen-adjuvant formulations have been shown previously to enhance APC activation *in-vitro*.[15]

After confirming activity of our conjugates, we tested their capability relative to unlinked controls to induce cross-presentation and activate dendritic cells *in-vitro*. The DC2.4 dendritic cell line was used as APCs, and cross-presentation was quantified by co-culturing with B3Z hybridoma T-cells. These T-cells specifically recognize the OVA MHC-I epitope motif, SIINFEKL, presented on H-2K^b. Upon recognition, β-galactosidase is produced which is quantified using a colorimetric substrate, CPRG. At concentrations ≥ 10 μg/mL, linked OVA-CpG incubated with the DC2.4 cells for 5 h invoked greater cross-presentation than unlinked controls (**Figure 3.3 C**). Indeed, the unlinked OVA + CpG was unable to induce cross-presentation even at the highest dose tested; we believe that this unexpected result might occur due to changes in the kinetics of OVA-CpG uptake relative to soluble CpG at the 5 h timepoint as well as enhanced TLR9 binding resulting from co-localization of OVA and CpG in a single endosome. These results highlight the importance of enhanced uptake and high endosomal adjuvant concentrations in facilitating cross-presentation.

To further demonstrate that TLR9 signaling is at the basis of the enhanced CD8$^+$ T cell activation, we then evaluated dendritic cell activation resulting from treatment with our conjugates. CD80 and CD86 are common cell surface markers which would serve as a viable proxy of activation. OVA-CpG or unlinked controls were incubated with DC2.4 cells at 50 μg/mL for 20 h, and cells were subsequently stained and analyzed using flow cytometry. The DC2.4 cells showed enhanced

cell surface expression of CD80, but not CD86, when treated with OVA-CpG relative to unlinked controls (**Figure 3.3 D-E and Figure B7**). Previous studies have shown that both mature and immature DC2.4 cells highly express CD86, but not CD80, which could explain differences in their expression patterns in this model.[23] Moreover, a distinct activated DC population marked by an increase in granularity was observed by flow cytometry after treating the cells with linked conjugates relative to their unlinked controls, further validating the activated phenotype (**Figure 3F and S8**). Higher cross-presentation and activation efficiency at lower CpG concentration demonstrates effectiveness of our conjugation strategy.

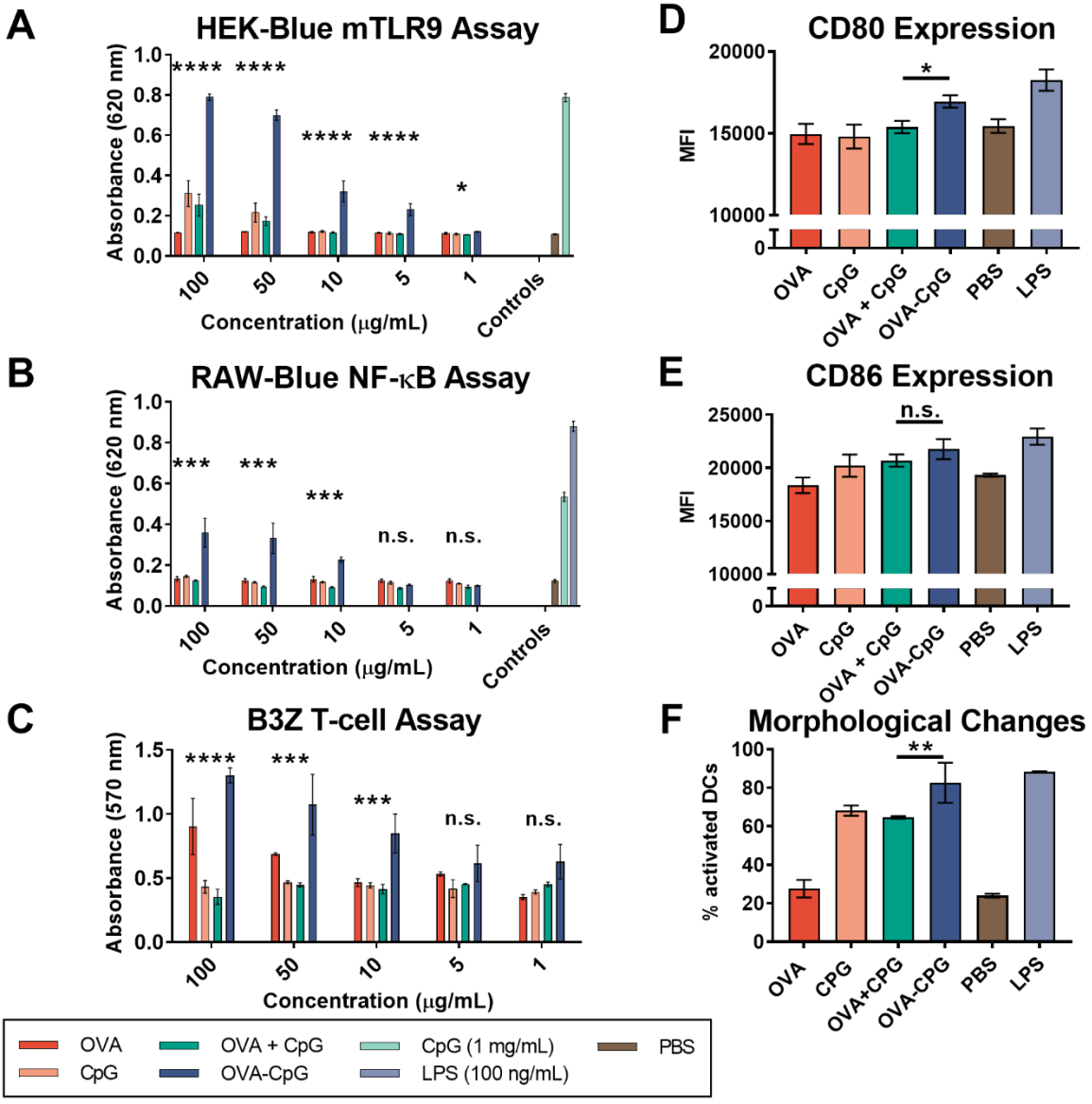

Figure 3.3: Immune activity of OVA-CpG conjugates *in-vitro*

In-vitro TLR9 activity of OVA-CpG conjugates in A) HEK mTLR9 and B) RAW-Blue NF-κB reporter cell activity was enhanced in OVA-CpG conjugates relative to unlinked controls. C) Cross-presentation of OVA-CpG on DC2.4 cells was enhanced relative to unlinked controls as measured using the B3Z T-cell hybridoma model. Flow cytometry evaluating mean fluorescent intensity of D) CD80 and E) CD86 as well as F) morphological changes associated with activation after stimulation with 50 μg/mL OVA-CpG or unlinked controls. Statistics were conducted using one- or two-way ANOVA with multiple comparisons testing to evaluate OVA-CpG relative to OVA + CpG.

3.3.3 *in-vivo* vaccination experiments

After characterizing our conjugates *in-vitro*, we designed an *in-vivo* experiment to assay cellular and humoral immune responses to the conjugate OVA-CpG systems. Previous experience in our laboratory indicated that 10-50 μg of OVA and 25-50 μg of CpG are optimal for murine vaccination; however, given the linked nature of our conjugates, these doses were infeasible. We therefore implemented a dose of 1 nmol of the OVA-CpG conjugate (44 μg OVA + 12 μg CpG for a loading of 1.5 CpG/OVA) and corresponding amount of unlinked controls (44 μg EndoFit™ Ovalbumin + 12 μg uncapped CpG-SH). 1 nmol of unadjuvanted OVA and PBS were used as controls. A boost was administered 14 d after initial intramuscular injection, and humoral and cellular immune responses were assayed after 21 and 28 d, respectively.

In response to the vaccination schedule (described **in Figure B9 A**), no changes in body weight were observed, although OVA-CpG conjugates induced increased IFN-γ and MCP-1 production 24 h after injection (**Figure B9**). This could result from greater TLR9 stimulation in the draining lymph nodes facilitated by conjugation to OVA, as observed with other nanoparticulate constructs.[5] After 21 d, no differences in total or IgG1/IgG2c antibody titers were observed between the linked and unlinked groups (**Figure B10-B11**), indicating that the conjugates did not improve humoral immunity or induce Th1/Th2 bias in the immune response. The ability of antigen-adjuvant conjugates to enhance antibody production is disputed in the literature.[9,11,16] Our result suggests that OVA-TLR9 agonist linkage enhances the efficiency of endosomal uptake and TLR activation rather than global antigen recognition, providing little advantage for humoral immunity. After 28 d, spleens were harvested, cultured, and stained using antigen-specific MHC tetramers to assay the cellular response. The conjugates showed >3x enhancement in antigen-specific T-cell production (**Figure B11**) indicating enhanced *in-vivo* cellular immune

responses.Given these results, we reduced the dose of our linked vaccine system, running additional experiments at 1.0, 0.1, and 0.01 nmol (10 µg, 1.0 µg and 0.1 µg CpG for a loading of 1.2 CpG/OVA) using batch 2 of the OVA-CpG conjugates (as well as unlinked controls as described above) to observe the efficiency of our linked systems in generating cellular immunity (**Figure 3.4 A**). Again, serum anti-OVA antibody titers showed no differences after 21 d (**Figure 3.4B**), while splenic antigen-specific $CD8^+$ T-cell production was enhanced relative to unlinked controls at the 1.0 nmol dose. Intriguingly, a modest antigen-specific $CD8^+$ T-cell response was also observed using the reduced 0.1 nmol OVA-CpG amount, which is less than one tenth of the CpG commonly used as an adjuvant. In contrast, minimal antigen-specific $CD8^+$ T-cell production was observed using 1.0 or 0.1 nmol of unlinked control **(Figure 3.4 C-D**). Based on these results, we conclude CFPS is a scalable platform for generating antigens with site-specific nnAAs for conjugation to adjuvants. Our OVA-CpG conjugates reduced the quantity of adjuvant needed to invoke antigen-specific $CD8^+$ T-cell production in our vaccine model.

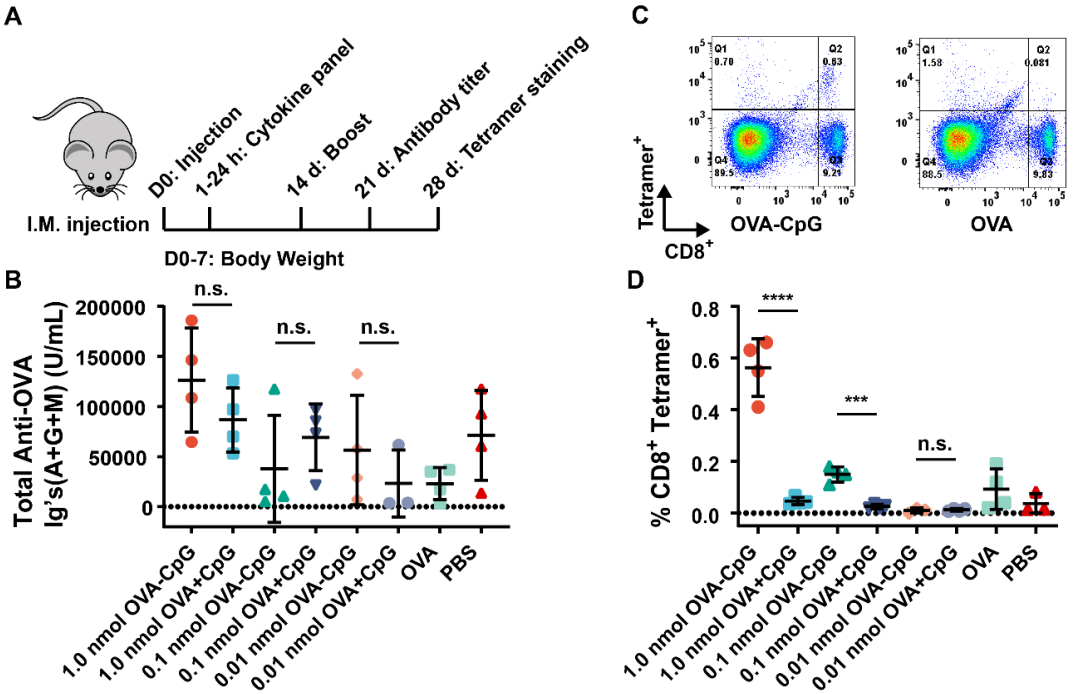

Figure 3.4: Effect of OVA-CpG conjugates on T-cell and antibody responses

Figure 3.4 continued

A) Second *in-vivo* experiment overview. B) No significant differences in anti-OVA total antibody titers were observed 21 d after injection ($p > 0.05$). C) Representative flow cytometry gating for evaluation of antigen specific CD8+ T-cell production. D) Summary statistics for all flow cytometry gated as shown in (C) demonstrating enhanced antigen specific CD8+ T-cell production of OVA-CpG conjugates relative to unlinked controls. Statistics were conducted using student's t-test to evaluate OVA-CpG relative to OVA + CpG.

3.4 Conclusion

We demonstrate herein that CFPS is a facile technique to synthesize large quantities of protein containing site-specific nnAAs for antigen-adjuvant conjugation without disrupting protein folding or epitope recognition. Our OVA-CpG conjugates enhanced cross-presentation compared to unlinked controls *in-vitro*, corresponding to increased antigen-specific $CD8^+$ T-cell production *in-vivo*. Moreover, our OVA-CpG conjugates reduced the dose of CpG needed to invoke antigen-specific $CD8^+$ T-cell production tenfold. Our results suggest that CFPS can be used as a reliable method to produce antigenic proteins with efficient, site-specific conjugation of adjuvants. Given the need to generate potent $CD8^+$ T-cell responses in both prophylactic and protective vaccines, future work using the antigen-adjuvant conjugation strategy described herein will focus on translating this model system to clinically relevant vaccines against disease. In particular, the antigen-adjuvant conjugation strategy holds promise to enhance responses at reduced doses in vaccines protecting against viral infections, such as influenza, where $CD8^+$ T-cell responses are critical but inflammation limits the use of synthetic TLR agonists at efficacious doses. This strategy also holds promise to improve robustness of protective responses in bacterial polysaccharide conjugate vaccines, such as those targeted against pneumococcal or streptococcal bacteria, which suffer from poor immunogenicity. This method can overcome the limitations of conventional antigen-adjuvant conjugation and will be another useful approach for the treatment and prevention of disease.

3.5 Materials and methods

Mice and Materials

All chemical reagents unless noted were obtained from Sigma Aldrich. 5'ThioMC6-capped CpG1018 was obtained from IDT Tech. DBCO-Maleimide (Catalog# A108) was obtained from Click Chemistry Tools. RAW-Blue NF-κB, HEK mTLR9 SEAP-reporter cells, and EndoFit™ Ovalbumin (Catalog# vac-pova) used for control assays were obtained from InvivoGen. DC 2.4 cells were obtained from EMD Millipore. B3Z T-cell hybridomas were obtained as a gift from N. Shastri (UC Berkeley). All cell culture reagents were obtained from Thermo Fisher Scientific. Anti-CD16/32 (clone 2.4G2), FITC anti-CD86 (clone PO3), and APC anti-CD80 (clone 16-10A1) were obtained from BioLegend. DC2.4 cells were cultured in RPMI-1640 supplemented with 10% FBS, 10 mM HEPES, 100 μM non-essential amino acids and 50 μM β-mercaptoethanol. B3Z cells were cultured in RPMI-1640 supplemented with 10% FBS and 50 μM β-mercaptoethanol. RAW-Blue and HEK mTLR9 cells were cultured in DMEM supplemented with 10% FBS and selective antibiotics. Cells were maintained at 37°C and 5% CO_2. C57Bl/6J mice were obtained from Jackson Laboratories and acclimatized for 1 week prior to experimentation. All experiments were conducted with approval of the University of Chicago Institutional Animals Care and Use Committee, and animals were maintained in accordance with guidelines and regulations defined by the National Institutes of Health. All statistical analyses were performed using GraphPad Prism.

Cloning, Expression, and Purification of OVA-2pAMF

Ex

The codon-optimized gene for the expression of OVA containing two non-native amino acid, *p*-azidomethyl phenylalanine (pAMF) sites, K20pAMF and K370pAMF, was synthesized at ATUM (Menlo Park, CA) and subcloned with an N-terminal methionine into a proprietary vector. The

final gene for OVA-[K20pAMF/K370pAMF]-TEV-his_6 contains a C-terminal TEV protease site (ENLYFQG) followed by a his_6-affinity tag for purification. *In-vitro* protein expression using cell free protein synthesis was performed as described elsewhere.[19] For titer estimates, expression of native or pAMF-containing OVA genes was monitored by incorporation of ^{14}C-leucine (GE Life Sciences, Piscataway, NJ). Autoradiography (Storm 840 PhosphoImager) was used to estimate total and soluble fractions of each protein. For large scale expression of OVA [K20/K370-pAMF]-TEV-his_6, the DASbox Mini Bioreactor System (Eppendorf AG) was used. Expression was performed at 25°C and pH 7.2 for 10 h with stirring at 650 rpm while sparging 30% oxygen in air through the reaction. After 10 h, the reaction mixtures were ultracentrifugated at 15,000 G at 4°C for 30 min and filtered using a 0.45 μm filter. The crude filtrate was loaded onto a 5 ml HisTrap column and equilibrated in 10 mM imidazole in Buffer A (50 mM Tris, 10% Glycerol, 150 mM NaCl). The protein was eluted using a step gradient of 10-500 mM imidazole in Buffer A. The eluent was pooled, concentrated, and incubated with his_6-tagged TEV protease overnight under dialysis against Buffer A. The dialyzed cleavage reaction was loaded onto a second pre-equilibrated, 5 ml HisTrap column and untagged OVA-2pAMF was collected. The crude OVA-2pAMF was concentrated and purified on a size exclusion column (Superdex 200 26/60 and Superdex 75 26/60 columns connected in tandem) pre-equilibrated with Buffer A. Finally, OVA-2pAMF containing fractions were pooled, 3x diluted in Buffer B (50 mM Tris, 10% Glycerol, pH 8.0), and loaded onto Capto Q ImpRes anion exchange column pre-equilibrated with Buffer B. The bound protein was eluted using a linear gradient of 0-1 M NaCl in Buffer B. The eluent containing purified OVA-2pAMF was pooled and frozen at -80°C for further use.

Multi-Angle Light Scattering (MALS) Analysis

The SEC MALS UV-RI setup consists of an Agilent HPLC 1100 degasser, temperature-controlled auto-sampler (4°C), column compartment (25°C), and UV-VIS diode array detector (Agilent, Santa Clara, CA) in line with a DAWN-HELEOS multi-angle laser light scattering detector and Optilab T-rEX differential refractive interferometer (Wyatt Technology, Santa Barbara, CA) coupled to three TOSOH columns in series: TSKgel Guard PWXL 6.0 mm ID x 4.0 cm long, 12 µm particle; TOSOH TSKgel 6000 PWXL 7.8 mm ID x 30 cm long, 13 µm particle; and a TSKgel 3000 PWXL 7.8 mm ID x 30 cm long, 7µm particle. A mobile phase consisting of 0.2 µm filtered PBS was used at a 0.5 mL/min flow rate and 50-100 µg sample was injected for analysis. Agilent Open Lab software was used to control the HPLC, and Wyatt Astra 7 software was used for data collection and molecular weight analysis.

pAMF site confirmation using DBCO-TAMRA labeling

Purified OVA-2pAMF (50 µM) was incubated with excess of Dibenzocyclooctyne-PEG4-tetramethylrhodamine (DBCO-TAMRA) dye (5 mM) for 1 h to label azide moieties. Thereafter, the reactions were analyzed using SDS-PAGE gel and fluorescence readout was recorded using a Syngene G-box gel imager.

Mass spectrometry of OVA-2pAMF

Positive mode analysis of proteins was performed on a Waters Xevo G2 XS Q-TOF mass analyzer. A 5 min gradient from 0% B to 97% B was used to elute the protein off a Waters BEH phenyl 300 Å stationary phase at 0.2 ml/min. Mobile buffers were prepared gravimetrically; phase A consisted

of 0.1% formic acid in water while phase B was 0.1% formic acid in acetonitrile. Waters Masslynx MaxEnt1 software was used to deconvolute the charge-state ladder into a deconvoluted mass.

Synthesis of CpG-DBCO

To remove the 5' thiol cap, MC6-capped CpG1018 (CpG-S-S-$(CH_2)_6$-OH) was shaken at 1500 rpm overnight with 100 mM tris(2-carboxyethyl)phosphine hydrochloride (TCEP-HCl) in PBS adjusted to pH 8.5 with 1 M NaOH. The oligonucleotide product was precipitated with ethanol, resuspended in PBS, and characterized by ESI-MS. Positive mode analysis of oligonucleotide conjugates was performed on a Waters Xevo G2 XS Q-TOF mass analyzer. A 5 min run in 50 mM pH 7.4 ammonium acetate was used to elute each sample off a Waters BEH 200 Å 150 mm SEC stationary phase at 0.1 mL/min. The concentration of DNA was verified by UV-VIS spectroscopy, and presence of thiol was confirmed by Ellman's assay. A cyclooctyne handle was then introduced using DBCO-Maleimide to react with the free thiol. DBCO-Maleimide was dissolved at 10 mg/mL in DMSO, and 10 eq of this stock solution was added to 1 mL of CpG-SH in PBS. The reaction mixture was shaken at 25°C overnight. Unreacted DBCO-Maleimide and trace DMSO was removed by passing the crude thrice through a 3k MWCO Amicon centrifugal filter, and the product was characterized by ESI-MS. Complete reaction of the thiol was confirmed by Ellman's assay, and concentration of DNA in the product solution was verified by UV-VIS spectroscopy on a Nanodrop 2000 instrument. CpG-DBCO was stored in PBS (1 mg/mL) at -20°C for later use.

OVA-CpG Synthesis

The OVA-CpG conjugate was prepared using azide-alkyne click chemistry. To a 1 mg/mL solution of OVA-2pAMF was added 2.5 eq CpG-DBCO (from the 1 mg/mL stock) at 35°C for 48 h. Unreacted CpG-DBCO was removed by passing the crude thrice through a 30k MWCO Amicon

centrifugal filter. The purified product was characterized by SDS-PAGE gel electrophoresis. Samples were treated with 2.5% β-mercaptoethanol, heated to 90°C, and separated by SDS-PAGE gel. Gels were stained with One-Step Blue Protein Gel Stain (Biotium), and imaged with an Azure c600 Imager (Azure Biosystems). Reaction extent was determined using ImageJ.

Endotoxin Removal

Endotoxin removal was conducted as previously reported with minor alterations. Briefly, a 5% Triton X-114 solution in PBS was cooled in an ice bath, and 100 µL of this solution was added to 400 µL protein solution. The solution was shaken for 40 min at 4°C, warmed to 37°C for 10 min, and ultracentrifugated at 37°C for 10 min at 12,000 G. The top layer containing protein was collected, and the lower layer discarded. This procedure was repeated three times, and protein solution was incubated with SM2 Bio-Beads (Bio Rad) overnight to remove residual Triton X-114. Endotoxin removal <1.5 EU/mL was validated by diluting 2 µL protein solution with 198 µL LAL Reagent Water and performing 0.015 EU/mL ToxinSensor Single Test Assay Kit (GenScript) according to the manufacturer's procedure. Protein concentration before and after endotoxin removal was determined by Pierce BCA Assay Kit (Thermo Scientific).

Size-exclusion HPLC

Aggregate and sample purity analysis using size-exclusion HPLC was conducted on an Agilent 1260 Infinity system equipped with a Yarra 3 µm SEC-2000 300 x 4.6 mm LC Column. A 15 min isocratic elution in 100 mM pH 6.8 phosphate buffer was used to separate samples, and samples were monitored at 254 and 280 nm to resolve peaks.

Anion Exchange Chromatography

Separation of OVA-CpG components was conducted using a HiTrap Q FF 1 mL anion exchange column (Cytiva). Briefly, the column was flushed with 5 mL PBS (pH = 6.8). Then, the OVA-CpG mixture was loaded onto the column, and the column was washed with 5 mL PBS. A stepwise elution was subsequently conducted by eluting 5 mL of 0.3, 0.4, 0.5, and 1.0 M NaCl in PBS (pH = 6.8). The fractions were collected and concentrated using 30k MWCO Amicon centrifugal filters. The concentrated fractions were the characterized by SDS-PAGE gel electrophoresis. Fractions were treated with 2.5% β-mercaptoethanol, heated to 90°C, and separated by SDS-PAGE gel. Gels were stained with One-Step Blue Protein Gel Stain (Biotium), and imaged with an Azure c600 Imager (Azure Biosystems). Reaction extent was determined using ImageJ.

RAW-Blue Assay

RAW-Blue cells were passaged and plated in a 96 well plate at 50,000 cells/well in 180 µL DMEM containing 10% HI-FBS and selective antibiotics. The cells were stimulated with the conjugates and unlinked controls for 20 h at 37°C and 5% CO_2. NF-κB activity was measured by a QUANTI-Blue (Invivogen) assay and the absorbance was measured at 620 nm using a Multiskan FC plate reader (Thermo Scientific).

HEK mTLR9 Assay

HEK mTLR9 cells were passaged and plated in a 96 well plate at 100,000 cells/well in 180 µL DMEM containing 10% HI-FBS and selective antibiotics. The cells were stimulated with the conjugates or unlinked controls for 20 h at 37°C and 5% CO_2. TLR9 binding was measured by a QUANTI-Blue (Invivogen) assay and the absorbance was measured at 620 nm using a Multiskan FC plate reader (Thermo Scientific).

In-vitro Cross Presentation Assay

The cross-presentation efficiency of conjugates was measured as described previously with minor changes.[11] DC2.4 cells (100,000 cells/well) were plated in 96-well plates and stimulated with linked OVA-CpG conjugates or unlinked controls for 5 h at 37°C and 5% CO_2. Subsequently, the media was replaced and DC2.4 cells were co-cultured with B3Z T-cell hybridomas (100,000 cells/well) for 18 h. The cells were centrifugated at 500 G for 5 min and the supernatant was removed. The cells were washed twice with 100 µL PBS. 0.15 mM CPRG reagent was prepared in lysis buffer (0.5% (v/v) NP-40 in PBS), 100 µL of the prepared reagent was added to each well, and cells were incubated at 37°C for 12-16 h in the dark. β-gal activity was quantified by measuring absorbance at 570 nm using a Multiskan FC plate reader (Thermo Scientific).

In-vitro DC Activation Assay

DC2.4s (2 million cells/well) were incubated in untreated 24-well plates and treated with OVA-CpG conjugates or unlinked controls in 0.5 mL culture media for 20 h at 37°C and 5% CO_2. The cells were mechanically released from the plate and centrifuged at 2500 RPM at 4°C for 10 min. The cell pellet was resuspended in 100 µL cold FACS buffer (10% FBS + 0.1% NaN_3 in PBS) and incubated with anti-CD16/32 (Fc receptor blocking antibody) (1.0 µg/million cells) on ice for 10 min. The cell suspension was pelleted and the supernatant was removed. The cell pellet was then resuspended in cold FACS buffer and incubated with FITC anti-CD86 (1.0µg/million cells) and APC anti-CD80 (0.5 µg/million cells) on ice in darkness for 30 min. Cells were washed twice with 300 µL cold FACS buffer, and then resuspended in FACS buffer (150 µL) and kept on ice until analysis. DC activation was assayed using an ACEA Novocyte flow cytometer and data were processed using the NovoExpress software.

In-vivo Characterization

Mice were injected intramuscularly in each flank with 50 μL OVA-CpG conjugates, OVA + CpG, OVA, or PBS (n=4/group). Body weight was measured prior to injection and daily for one week. Mice were bled via facial vein 1 and 24 h after injection, and serum cytokine production was assayed using LEGENDPlex Mouse Inflammation Panel 13plex (BD Biosciences). After 14 d, the same formulation was administered as a boost. After 21 d, serum was collected and antibody production was assayed using mouse Anti-Ovalbumin Ig's total (A+G+M) (Alpha Diagnostic International), Anti-Ovalbumin IgG1 (Alpha Diagnostic International), and Anti-Ovalbumin IgG2c (Chondrex) ELISA kits. After 28 d, mice were sacrificed and spleens were collected for tetramer staining. Spleens were homogenized, and cells were filtered through a 70 μm strainer. Red blood cells were lysed by incubating with ACK Lysing Buffer for 5 min at 25°C. Splenocytes (2 million cells) were plated in a 96-well plate and incubated with anti-CD16/32 (Fc receptor blocking antibody) (1.0 μg/million cells) for 15 min at 4 °C. Splenocytes were washed with FACS buffer (PBS with 2% FBS), resuspended, and stained with APC MHC Class I tetramers (Tetramer Shop) at 37°C in the dark. After 15 mins, FITC anti-CD8 (BD Biosciences) was added and incubated for 30 min longer. Splenocytes were washed and resuspended in FACS buffer. Antigen-specific T-cell production was assayed using an ACEA Novocyte flow cytometer, and data were processed using FlowJo.

3.6 References

1. Lauring, A. S.; Jones, J. O.; Andino, R., Rationalizing the development of live attenuated virus vaccines. *Nat Biotechnol* **2010**, 28 (6), 573-9.

2. Moyle, P. M.; Toth, I., Modern subunit vaccines: development, components, and research opportunities. *ChemMedChem* **2013**, 8 (3), 360-76.

3. Fearon, D. T.; Locksley, R. M., The instructive role of innate immunity in the acquired immune response. *Science* **1996**, 272 (5258), 50-3.

4. Schulz, O.; Diebold, S. S.; Chen, M.; Näslund, T. I.; Nolte, M. A.; Alexopoulou, L.; Azuma, Y.T.; Flavell, R.A.; Lindström, P.; Reis e Sousa, C., Toll-like receptor 3 promotes cross-priming to virus-infected cells. *Nature* **2005**, 433 (7028), 887-892.

5. Tom, J. K.; Albin, T. J.; Manna, S.; Moser, B. A.; Steinhardt, R. C.; Esser-Kahn, A. P., Applications of Immunomodulatory Immune Synergies to Adjuvant Discovery and Vaccine Development. *Trends Biotechnol* **2018**, 37 (4), 373-388.

6. Jackson, S.; Lentino, J.; Kopp, J.; Murray, L.; Ellison, W.; Rhee, M.; Shockey, G.; Akella, L.; Erby, K.; Heyward, W. L.; Janssen, R. S.; Immunogenicity of a two-dose investigational hepatitis B vaccine, HBsAg-1018, using a toll-like receptor 9 agonist adjuvant compared with a licensed hepatitis B vaccine in adults. *Vaccine* **2018**, 36 (5), 668-674.

7. Heineman, T. C.; Cunningham, A.; Levin, M., Understanding the immunology of Shingrix, a recombinant glycoprotein E adjuvanted herpes zoster vaccine. *Curr Opin Immunol* **2019**, 59, 42-48.

8. Di Pasquale, A.; Bonanni, P.; Garcon, N.; Stanberry, L. R.; El-Hodhod, M.; Tavares Da Silva, F., Vaccine safety evaluation: Practical aspects in assessing benefits and risks. *Vaccine* **2016**, 34 (52), 6672-6680.

9. Cho, H. J.; Takabayashi, K.; Cheng, P. M.; Nguyen, M. D.; Corr, M.; Tuck, S.; Raz, E., Immunostimulatory DNA-based vaccines induce cytotoxic lymphocyte activity by a T-helper cell-independent mechanism. *Nat Biotechnol* **2000**, 18 (5), 509-14.

10. Nierkens, S.; den Brok, M. H.; Sutmuller, R. P.; Grauer, O. M.; Bennink, E.; Morgan, M. E.; Figdor, C. G.; Ruers, T. J.; Adema, G. J., In-vivo colocalization of antigen and CpG within dendritic cells is associated with the efficacy of cancer immunotherapy. *Cancer Res* **2008**, 68 (13), 5390-6.

11. Clauson, R. M.; Berg, B.; , B., The Content of CpG-DNA in Antigen-CpG Conjugate Vaccines Determines Their Cross-Presentation Activity. *Bioconjug Chem* **2019**, 30 (3), 561-567.

12. Heit, A.; Schmitz, F.; O'Keeffe, M.; Staib, C.; Busch, D. H.; Wagner, H.; Huster, K. M., Protective CD8 T-cell immunity triggered by CpG-protein conjugates competes with the efficacy of live vaccines. *J Immunol* **2005**, 174 (7), 4373-80.

13.Fischer, N. O.; Rasley, A.; Corzett, M.; Hwang, M. H.; Hoeprich, P. D.; Blanchette, C. D., Colocalized delivery of adjuvant and antigen using nanolipoprotein particles enhances the immune response to recombinant antigens. *J Am Chem Soc* **2013**, 135 (6), 2044-7.

14. Wille-Reece, U.; Flynn, B. J.; Lore, K.; Koup, R. A.; Kedl, R. M.; Mattapallil, J. J.; Weiss, W. R.; Roederer, M.; Seder, R. A., HIV Gag protein conjugated to a Toll-like receptor 7/8 agonist improves the magnitude and quality of Th1 and CD8+ T-cell responses in nonhuman primates. *Proc Natl Acad Sci* **2005**, 102 (42), 15190-4.

15. Irie, H.; Morita, K.; Koizumi, M.; Mochizuki, S., Immune Responses and Antitumor Effect through Delivering to Antigen Presenting Cells by Optimized Conjugates Consisting of CpG-DNA and Antigenic Peptide. *Bioconjug Chem* **2020**, 31, 2585-95.

16. Maurer, T.; Heit, A.; Hochrein, H.; Ampenberger, F.; O'Keeffe, M.; Bauer, S.; Lipford, G. B.; Vabulas, R. M.; Wagner, H., CpG-DNA aided cross-presentation of soluble antigens by dendritic cells. *Eur J Immunol* **2002**, 32 (8), 2356-64.

17. Carlson, E. D.; Gan, R.; Hodgman, C. E.; Jewett, M. C., Cell-free protein synthesis: applications come of age. *Biotechnol Adv* **2012**, 30 (5), 1185-94.

18. Zawada, J. F.; Yin, G.; Steiner, A. R.; Yang, J.; Naresh, A.; Roy, S. M.; Gold, D. S.; Heinsohn, H. G.; Murray, C. J., Microscale to manufacturing scale-up of cell-free cytokine production--a new approach for shortening protein production development timelines. *Biotechnol Bioeng* **2011**, 108 (7), 1570-8.

19. Kapoor, N.; Vanjak, I.; Rozzelle, J.; Berges, A.; Chan, W.; Yin, G.; Tran, C.; Sato, A. K.; Steiner, A. R.; Pham, T. P.; Birkett, A. J.; Long, C. A.; Fairman, J.; Miura, K., Malaria Derived Glycosylphosphatidylinositol Anchor Enhances Anti-Pfs25 Functional Antibodies That Block Malaria Transmission. *Biochemistry* **2018**, 57 (5), 516-519.

20. Wang, L.; Brock, A.; Herberich, B.; Schultz, P. G., Expanding the genetic code of Escherichia coli. *Science* **2001**, 292 (5516), 498-500.

21. Stafford, R. T.; Thanos, C.D.; Yang, W. Modified Amino Acids. 2017. US Patent 0260137.

22. Teodorowicz, M.; Perdijk, O.; Verhoek, I.; Govers, C.; Savelkoul, H. F.; Tang, Y.; Wichers, H.; Broersen, K., Optimized Triton X-114 assisted lipopolysaccharide (LPS) removal method reveals the immunomodulatory effect of food proteins. *PLoS One* **2017**, 12 (3), e0173778.

23. Hargadon, K. M.; Forrest, O. A.; Reddy, P. R., Suppression of the maturation and activation of the dendritic cell line DC2.4 by melanoma-derived factors. *Cell Immunol* **2012**, 272 (2), 275-282.

4. Temporal control of trained immunity via encapsulated release of β-glucan improves therapeutic applications

4.1 Summary

Nonspecific innate immune memory, called trained immunity, reprograms innate immune cells to resist invading pathogens. Many molecules, most notably β-glucan, induce trained immunity, but their effects are often short-lived and uncontrolled. Methods for temporal control over trained immunity can help inform rational design of novel prophylactics to potentially improve overall disease resistance. To achieve this, we engineered PLGA nanoparticles encapsulating β-glucan to attain sustained release over a month. We observed improved training, marked by increased systemic cytokines against an LPS challenge, in both a 7-day *in-vitro* assay and a 28-day *in-vivo* assay. Additionally, nanoparticle trained mice resisted the growth of B16.F10 tumors better than an equivalent amount of free β-glucan. To further fine-tune the duration of trained immunity, we synthesized nanoparticles composed of different molecular weights of PLGA to modulate the release kinetics. We report that sustained release methods using nanomaterials provide a novel platform for increased temporal control over the duration of trained immunity.

4.2 Introduction

Innate immune cells form the first line of defense against pathogens.[1] Recent work has revealed that innate immune cells experience nonspecific "memory," which allows modulation of responses against repeated pathogenic insult, which was previously not considered an innate function. This enhanced responsiveness conferred by innate cells, called trained immunity, can improve the first line of defense and subsequent adaptive immune responses by increasing antigen presentation and T-cell activation.[2] Certain pathogenic stimuli, such as whole-cell inactivated mycobacteria, induces epigenetic and metabolic changes that rewire innate immune cells.[3] This rewiring

improves pathogen detection and immune reactivity of the "trained" cells to better respond to a second attack by both the same or an unrelated pathogen.

Many whole-cell inactivated vaccines, such as *Bacillus* Calmette-Guérin (BCG)[4,5], polio[5], and measles[6], have been reported to induce trained immunity and protect against several unrelated viral and bacterial infections.[4,7,8] Less active trained immunity inducers, such as the yeast-derived β-glucan, are functional substitutes and protect mice against a diverse range of pathogens.[9,10,11,12] However, their protective effects are transient-lasting for only a few days.[13,14] Therefore, methods to control and extend trained immunity could help provide new tools in generating durable disease resistance. This paper demonstrates using conventional materials methods to control trained immunity responses over time and its application to a disease model.

Since macrophages and monocytes have a relatively short lifespan, methods to prolong trained immunity have thus far focused on targeting the bone marrow to generate trained myeloid precursors.[15,16] Priem et al. developed high-density lipoprotein (HDL) based nano-biologics encapsulating trained immunity inducing muramyl tripeptide (MTP) that suppressed tumor growth in mice.[17] However, bone marrow targeted nanomaterials do not provide precise temporal control over trained immunity and can potentially lead to unwanted side effects due to accumulation in the liver.[18] We sought to employ an efficient method of controlling the kinetics of trained immunity through the sustained release of trained immunity-inducing molecules from biodegradable nanoparticles. Poly (lactic-co-glycolic acid) (PLGA) is a widely used FDA-approved polymer that exhibits slow degradation via hydrolysis of ester bonds with broad applications.[19] PLGA nanoparticles can be easily formulated to deliver the encapsulated cargo to their intended target cells. Moreover, the release kinetics can be controlled by modulating the properties of PLGA.

[20,21] Therefore, to test the hypothesis of if sustained release would alter the temporal control of trained immunity - PLGA nanoparticles were an excellent test-bed.

We investigated if the sustained release of β-glucan from PLGA nanoparticle formulation would prolong trained immunity effects by controlling release kinetics (**Figure 4.1**). We synthesized and characterized PLGA nanoparticles varying the rate of release of β-glucan over 30 days. We observed enhanced pro-inflammatory cytokine production in nanoparticle trained bone-marrow-derived macrophages (BMDMs) challenged with lipopolysaccharide (LPS) in a 7 day *in vitro* assay. To better capture slow release and its effect on inducing trained immunity, we tested the synthesized nanoparticles in an *in vivo* model. While the standard dose of 1 mg of free β-glucan conferred trained immunity for more than a week, nanoparticle-trained mice demonstrated peak systemic effects extending over a month of training. This prolonged response enabled the nanoparticle-trained mice to resist tumor growth better than conventionally trained animals when challenged with B16.F10 melanoma three weeks after training. We demonstrated that different molecular weight PLGA could fine-tune the duration of training for various applications by controlling release kinetics. We report for the first time that sustained release from biodegradable polymer nanoparticles can be used for temporal control of trained immunity over a predictable window of a week to a month.

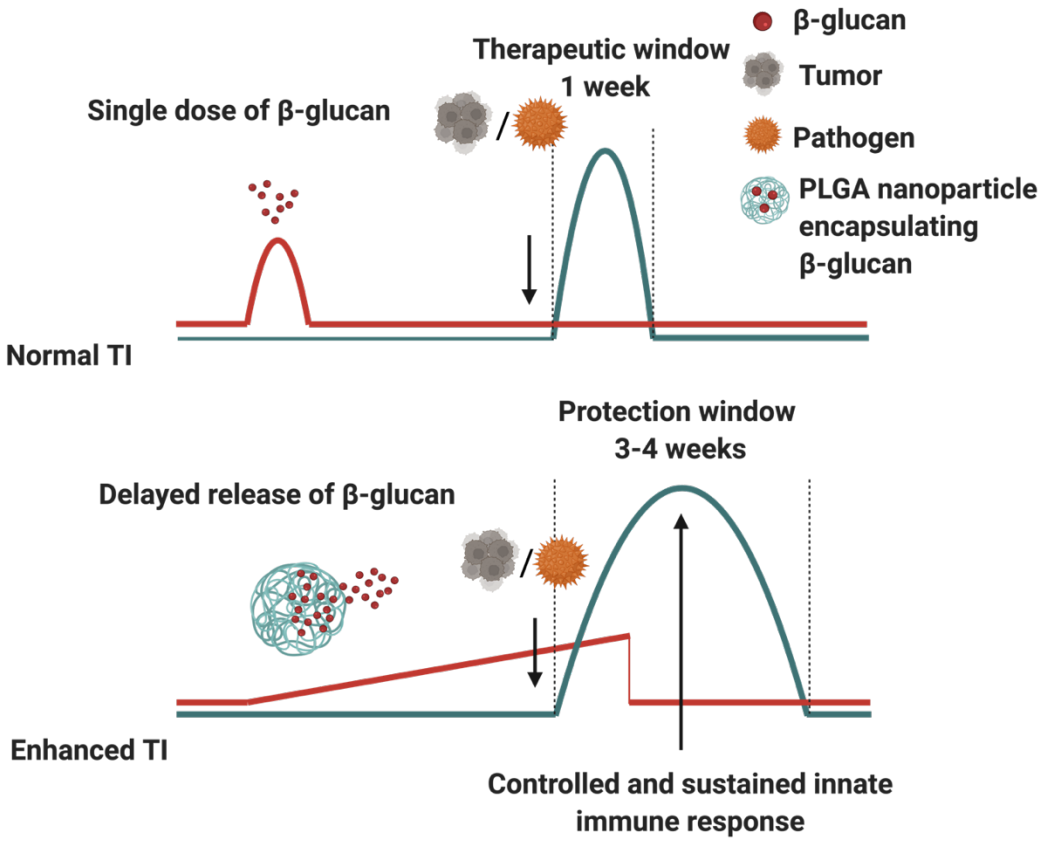

Figure 4.1: Schematic representation of the proposed mechanism of action of PLGA nanoparticles encapsulating β-glucan.

Trained immunity mediated by free β-glucan confers protective effects that last only one week. Sustained release of β-glucan from engineered PLGA nanoparticles enable prolonged trained immunity effects that can last up to four weeks depending on the release profile. (created with BioRender.com)

4.3 Results and discussion

4.3.1 Synthesis and characterization of PLGA nanoparticles encapsulating β-glucan

To test the hypothesis that sustained release can prolong trained immunity, we first synthesized nanoparticles composed of PLGA encapsulating β-glucan. Nanoparticles were synthesized using a modified version of a previously reported double emulsion technique,[22] owing to its ease and consistency in creating homogenous nanospheres that degrade in a controlled release fashion. In

brief, nanoparticles were synthesized by ultrasonication of an aqueous solution of β-glucan and PLGA dissolved in dichloromethane. The solution was ultrasonicated again after adding 5% PVA and left stirring for 6 hours in a 0.5% PVA stabilizing solution. The resulting precipitated nanoparticles were washed and lyophilized for characterization.

In examining the consistency of nanoparticles, scanning electron microscopy (SEM) images revealed nanosphere morphology of particles that were around 67 ± 20 nm in diameter (**Figure 4.2 A**). However, we detected larger radiuses under DLS measurements suggesting that the particles significantly aggregate in aqueous solutions (**Figure C1**). The amount of β-glucan encapsulated within the nanoparticles was quantified using a total carbohydrate assay.[23] Encapsulation efficiency was determined by the percentage of β-glucan as measured by the carbohydrate assay divided by the amount of β-glucan initially loaded in each formulation. Synthesized nanoparticles had a high encapsulation efficiency of 73%. We also evaluated the *in-vitro* release profile at pH 7.4, which showed a sustained release profile of β-glucan over the 4-week period of testing (**Figure 4.2 B**). We confirmed that the synthesized nanoparticles were devoid of endotoxin using a HEK-mTLR4 reporter assay (**Figure C3**). Concluding that the particles were loaded with β-glucan and devoid of any other immuno-stimulatory materials, we next tested them for their ability to train innate cells.

4.3.2 *in-vitro* TI assay

As previous work had shown that PLGA nanoparticles exhibit slow-release, we first tested if the synthesized nanoparticles encapsulating β-glucan improved trained immunity using a standard BMDM training model.[24] In this model, macrophages are trained with added material (e.g., β-glucan) and later challenged with a conventional secondary stimulant (e.g., LPS). If training occurs, the macrophages increase transcription of pro-inflammatory cytokines like IL-6 and TNF-

α. Following a standard 7-day training assay, murine BMDMs at a density of 100,000 cells per well were incubated for 24 h with a set of "training material." Each group of cells were trained for 24 h, rested for four days, and later challenged with 10 ng/mL of LPS in a total volume of 200 mL. We compared how the release of β-glucan affected training by using nanoparticles containing either β-glucan (100 μg/ml) or administering the free form of an equivalent amount of β-glucan (3.7 μg/mL). We included an untrained (or PBS trained) group as our negative control. We observed significantly higher IL-6 and TNF-α levels confirming that nanoparticles enhanced trained immunity *in-vitro* (**Figure 4.2 C**). In fact, encapsulating the β-glucan in nanoparticles resulted in an approximately 1.5-fold increase in both IL-6 and TNF-α produced by BMDMs in response to the same stimulus compared to the unencapsulated equivalent. In addition, we observed that nanoparticles with no β-glucan did not induce training (**Figure C3**). Together, these results suggested that encapsulation of the training material, β-glucan, could strongly enhance the training effect in preliminary in vitro assays.

While the initial *in-vitro* data was promising, one important consideration was if encapsulation affected the mechanism of action of trained immunity mediated by β-glucan. In previous experiments, others established that β-glucan induces epigenetic and metabolic changes via histone methylation and acetylation to control transcription of pro-inflammatory cytokines.[25] We tested if the nanoparticles activated similar pathways in trained immunity using our *in-vitro* assay. To do this, BMDMs were pre-treated with small-molecule epigenetic and metabolic inhibitors for 30 min before exposing them to each training material in the standard 7-day BMDM training assay used in the previous experiment.[24,26] All the epigenetic inhibitors reduced trained immunity induced by free β-glucan, as reported previously – validating the assays. Histone demethylase inhibitor-pargyline hydrochloride significantly reduced training by nanoparticles, whereas histone

methyltransferase inhibitor (methylthioadenosine or MTA) did not affect training. Histone acetyltransferase inhibitor (Epigallocatechin-3-gallate or EGCG) reduced nanoparticle-induced training *in vitro*; however, the difference was not significant ($p = 0.073$) (**Figure 4.2 D**). The results confirm that the nanoparticles induce training through an epigenetic mechanism. However, the results also suggest that nanoparticle-based training operates through a slightly different overall temporal process, perhaps owing to the timing and delivery of the β-glucan. This may bear further examination in fundamental studies in the future.

Apart from epigenetics, metabolic changes also contribute to β-glucan induced training. Dectin-1 activation by β-glucan results in phosphorylation of Akt, thereby activating the mammalian target of rapamycin (mTOR). Akt inhibitor- wortmannin reduced trained immunity mediated by free β-glucan but not by nanoparticles. Inhibiting mTOR by pre-treating cells with rapamycin significantly reduced training effects in both the free β-glucan equivalent and nanoparticle groups. Trained innate cells switch from oxidative phosphorylation to glycolysis to meet the energy demands to induce epigenetic changes for higher effector function, such as secretion of pro-inflammatory cytokines. This process also generates metabolites that further modulate their epigenetic profile.[27,28] To test the metabolic effects of training with nanoparticles, we depleted glucose by pre-treating cells with 2-deoxy D-glucose and observed reduced training effects by all training materials tested, confirming that glycolysis is a key to trained immunity effects by nanoparticles. (**Figure 4.2 E**). Taken together, these results demonstrate that nanoparticles mediate trained immunity through much the same pathways targeted by free β-glucan encompassing both metabolic and epigenetic reprogramming of BMDMs. However, they show distinctive differences in how the particles may alter the pathways, perhaps in the kinetics of the overall dose of β-glucan,

which may explain the resulting improvements in training observed in the preliminary *in vitro* results.

One potential explanation for these subtle mechanistic differences would be the kinetics and delivery of β-glucan to the cells. We reasoned that better uptake of nanoparticles by BMDMs might be one reason for better training *in-vitro* compared to an equivalent amount of free β-glucan. To test this hypothesis, we labeled β-glucan with fluorescein isothiocyanate (FITC) and monitored their uptake by BMDMs at the end of 24 h, mimicking the *in-vitro* training assay using flow cytometry. After 24 h of training, we observed higher levels of FITC+ cells in the nanoparticle trained groups than the free equivalent group (**Figure 4.2 E**, **Figure C4**). We performed the 7-day *in-vitro* assay by pre-treating BMDMs with known inhibitors targeting caveolae and clathrin-mediated endocytosis pathways to test if endocytosis is involved.[29] We observed a significant reduction in nanoparticle-mediated training with inhibitors of both caveolae-specific endocytosis (filipin) and both caveolae and clathrin-dependent endocytosis (dynasore). (**Figure 4.2 G**). Clathrin inhibitor (chlorpromazine) did not cause any change in nanoparticle-mediated training. These results strongly support that nanoparticle-induced trained immunity *in-vitro* proceeded through increased uptake by BMDMs.

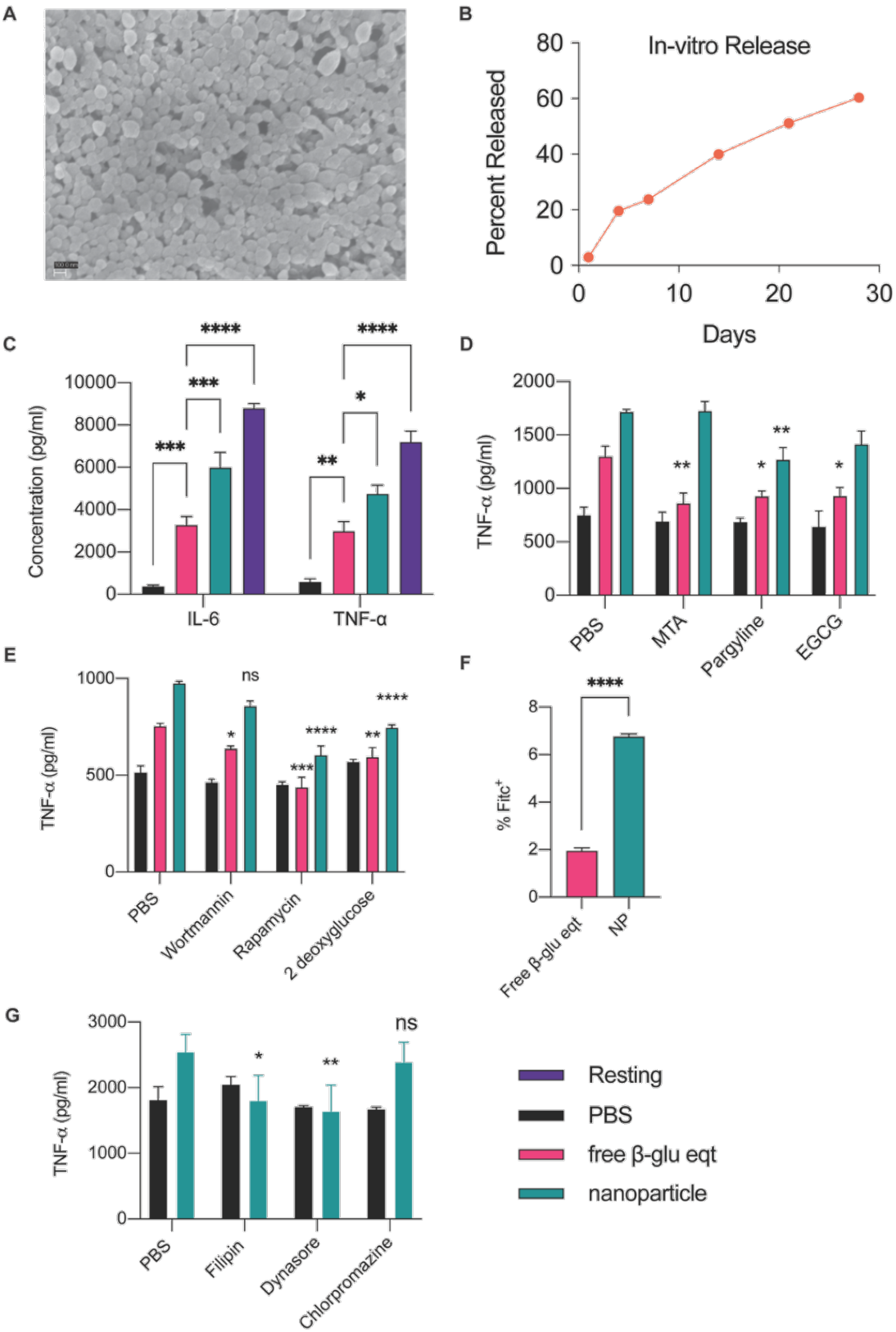

Figure 4.2: Nanoparticle characterization and *in vitro* TI assays

Figure 4.2 continued

A) Scanning electron microscopy image of PLGA nanoparticles synthesized by double emulsion technique. (scale bar = 100 nm)
B) 7-day *in vitro* release kinetics of encapsulated β-glucan from the synthesized PLGA nanoparticles at pH 7.4.
C) *in-vitro* trained immunity assay comparing cytokine levels in resting cells (purple bar) or following an LPS challenge in BMDMs trained with either PBS (black bar), the free equivalent amount of β-glucan (pink bar) or PLGA nanoparticles encapsulating β-glucan (green bar), n=3, significance compared with PBS.
D) Assay determining changes in epigenetic training response. BMDMs were pretreated for 30 min with inhibitors targeting epigenetic modifications, namely MTA (histone methyltransferase inhibitor), EGCG (histone demethylase inhibitor), or pargyline hydrochloride (histone acetyltransferase inhibitor). Cytokine levels were measured after an LPS challenge on day 5 with BMDMs trained with PBS (black bar), the free equivalent amount of β-glucan (pink bar), or PLGA nanoparticles (green bar) n=3, significance compared with PBS (no inhibitor) group.
E) Assay determining changes in metabolic training response. BMDMs were pretreated for 30 min with inhibitors targeting metabolic pathways, namely wortmannin (Akt inhibitor), metformin (AMPK activator), rapamycin or 2-deoxy D-glucose (glycolysis inhibitor). Cytokine levels were measured after an LPS challenge on day 5 with BMDMs trained with– PBS (black bar), the free equivalent amount of β-glucan (pink bar), or PLGA nanoparticles (green bar), n=3, significance compared with PBS (no inhibitor) group.
F) BMDMs were treated with either free FITC-labelled β-glucan (pink bars) or nanoparticles encapsulating FITC- β-glucan (green bars) for 24 h. BMDMs were analyzed by flow cytometry to measure the percentage of cells that were FITC+, n=3.
G) BMDMs were pre-treated for 30 min with inhibitors targeting endocytosis pathways, namely dynasore (caveolae and clathrin inhibitor), filipin (caveolae inhibitor), or chlorpromazine (clathrin inhibitor). IL-6 levels were measured after an LPS challenge on day 5 with BMDMs trained with– PBS (black bar), the free equivalent amount of β-glucan (pink bar), or PLGA nanoparticles (green bar), n=3, significance compared with PBS (no inhibitor) group.
$*P < 0.05$, $**P < 0.01$, and $***P < 0.001$. n.s., not significant.

4.3.3 *in-vivo* TI assay

To accurately test how controlled release might affect trained immunity in a prophylactic model, we tested the particles using an *in-vivo* model (**Figure 4.3 A**). Mice were trained twice with either nanoparticles or an equivalent amount of free β-glucan. To account for the potential effects of age and injection, we included an "untrained" (PBS) group. For comparison, we also included a conventional standard training regimen –1 mg of free β-glucan. To determine the increase in innate response from training, mice were then challenged intraperitoneally with a secondary stimulus-

LPS, at defined time points after the training regimen. In a standard training assay, LPS challenge results in systemic pro-inflammatory cytokines (IL-6 and TNF-α). Higher cytokine response indicates better trained mice. Since the synthesized nanoparticles exhibit slow release of the encapsulated β-glucan over thirty days, we hypothesized that the training response in the nanoparticle-trained group would coincide with its release profile, peaking after 30 days of training. To test this hypothesis, we analyzed systemic cytokines following an LPS challenge at two different time points– 7 and 28 days after the first training material was administered. In previous work, mice trained with standard 1 mg free β-glucan elicited peak systemic cytokines after 7 days of training.[30] At 7 days, for the β-glucan (1 mg) group, systemic cytokines following an LPS challenge were highest, matching previous work. The group trained with the free equivalent amount of β-glucan (35 mg/mouse) did not show any systemic responses. This result may be due to the very low dosage – only 3.5% of a responsive amount. Also, mice trained with nanoparticles at 7 days somewhat surprisingly showed no systemic response (**Figure 4.3 B**). However, when challenged 28 days after the first training, nanoparticle-trained mice showed higher peak systemic responses than mice trained with 1 mg of β-glucan or the nanoparticle-free equivalent dosage. Of note, the level was nearly as high as that of the standard training at day 7 with only 3.5 % as much β-glucan added. This result provided strong support for our initial hypothesis. Additionally, we observed no increase in cytokines in any category when mice were challenged with LPS 35 days after training (**Figure C5**)- indicating the transient nature of training. To rule out innate immune priming effects, we analyzed serum cytokines before the LPS challenge on day 28. We observed no significant differences between untrained and nanoparticle trained mice (**Figure C6**), indicating that the system was not actively responding to previous stimulation. Taken together, these results strongly support that the controlled release from

nanoparticles prolonged training, but only peak around 28 days. They did not extend training beyond a predictable time window- preventing potential uncontrolled inflammation.

A critical question remained: how long do the particles persist upon injection, and how does that timing impact the controlled training regimen? To assess the biodistribution of the synthesized nanoparticles, mice were injected intra-peritoneally with NIR-labelled PLGA nanoparticles with the same formulation of encapsulated β-glucan (See **Appendix C** for formulation). The injected nanoparticles localized to the peritoneal cavity 30 min after injection (**Figure 4.3C**). To confirm that nanoparticles exhibited sustained release, we monitored the fluorescence intensity emitted from the nanoparticles. Fluorescence intensity measurement was reduced to zero by three weeks post-training (**Figure 4.3 Cand 4.3 D**). After confirming the absence of residual nanoparticles, we challenged the mice with LPS and observed higher systemic cytokines from the nanoparticle-trained mice (**Figure C7**). These results add further support to our hypothesis that it is the sustained release of β-glucan from the nanoparticles which increases the effect of training. We also confirm that peak training effects induced in the nanoparticle-trained group occurred after the nanoparticles appeared fully dispersed.

After confirming that the nanoparticles localized at the peritoneal cavity, we examined if peritoneal macrophages contributed to the response of nanoparticle-induced training when peak systemic responses were induced at day 28. To test this hypothesis, we isolated peritoneal macrophages from mice that received training material four weeks earlier. The isolated trained peritoneal macrophages were challenged ex-vivo with LPS, and pro-inflammatory cytokines were quantified. We observed 77% higher IL-6 levels from peritoneal macrophages isolated from nanoparticle-trained mice than those isolated from unencapsulated free equivalent β-glucan trained mice (**Figure 4.3 E**). We performed an adoptive transfer experiment to determine if peritoneal

macrophages could act as a sole mediator of training. After 28 days of training in mice administered standard nanoparticles, the free-equivalents of β-glucan, or 1 mg of β-glucan, peritoneal macrophages were adoptively transferred to naïve mice. The recipient mice were challenged with LPS 1 day later, and systemic cytokines were quantified. Analogous to the *ex vivo* challenge experiment, we observed that peritoneal macrophages isolated from nanoparticle trained mice conferred naïve mice with improved training effects against LPS challenge compared to all other groups tested (**Figure 4.3 F**). Mice that received peritoneal macrophages from nanoparticle trained mice produced a 2-fold increase in IL-6 compared to the group with an unencapsulated amount of free β-glucan. This result provided evidence that peritoneal macrophages are one of the primary cellular mediators of training for nanoparticle-induced training and that sustained-release platforms can target macrophages to improve training effects.

We then explored if nanoparticle trained mice exhibit localized training effects, particularly at the administration site, i.e., the peritoneal cavity, at earlier times (one week after training). In previous work, inflammation in the peritoneal cavity was observed to induce the recruitment of monocyte-derived small peritoneal macrophages (SPMs).[9,31] Mice were trained with the same regiment of desired training materials, challenged with LPS after 7 days and their peritoneal cavity cells were harvested. We observed that mice trained with nanoparticles had much higher populations of SPMs (40 %) than the free β-glucan groups (**Figure 4.3 G, Figure C8**), confirming that the particles induced localized effects. However, training may also modulate immune cell populations at the spleen. Analysis of splenic cell populations between nanoparticles and other free formulations revealed a slight but non-significant increase in the percent of macrophages in mice trained with nanoparticles. We observed no changes in other cell types like neutrophils which were upregulated in mice trained with 1 mg free β-glucan (**Figure C9**). These results were inconclusive

but indicated that the nanoparticles might exert some localized effects at the injection site, and further study of the localized effects of controlled release is warranted.

To explore if the dosing regimen would alter the activity and cellular makeup at the site of action in nanoparticle-induced training at earlier time points (day 7), mice were trained with either two doses of 0.5 mg spaced four days apart or a single dose of 1 mg of nanoparticles. In this case, both groups would ultimately release an equivalent amount of β-glucan. Yet, the distributions would differ, resulting, theoretically, in different cellular compositions in the injection site and altered training responses. After a standard training injection of either 0.5 mg of nanoparticles at intervals of 4 days or 1 mg of nanoparticles, we collected cells from the peritoneal cavity, spleen, and bone marrow. Cells were challenged with LPS ex-vivo, and cytokines released into the supernatant were analyzed.[32,33,34] We observed a single dose of 1 mg nanoparticles resulted in better training in peritoneal macrophages. (**Figure 4.3 H**) However, two doses of 0.5 mg of nanoparticles resulted in better-trained immunity effects in splenic macrophages (**Figure 4.3 I**). No significant differences were observed in bone marrow-derived macrophages (BMDMs) harvested from nanoparticle trained mice, confirming that the site of action was restricted to the peritoneal cavity and spleen at earlier time points (**Figure C10**). These results indicate that the dosing regimen of nanoparticles could provide more spatial control over the site of training at earlier time points. Taken together, these results indicate that the training with nanoparticles occurs mainly within the local tissue but can be altered via dosing and distribution. Future therapeutic approaches might take that timing and dose into consideration. However, further experiments are needed to evaluate the extent of local vs. systemic training thoroughly.

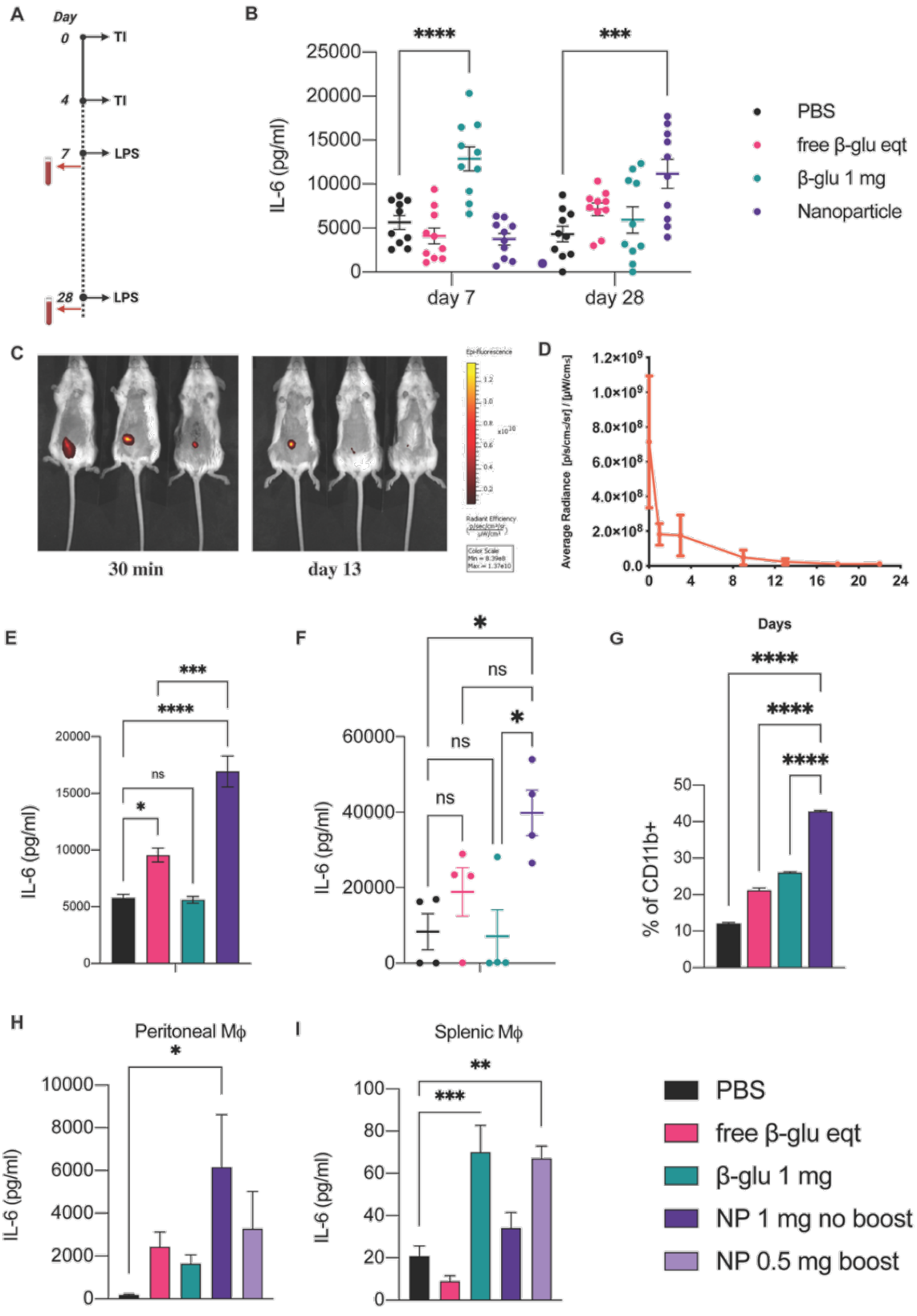

Figure 4.3: *in vivo* trained immunity

Figure 4.3 continued
A) *in vivo* trained immunity schematic. Training materials were administered on day 0 and day four, and separate sets of mice were challenged 7 or 28 days later. Systemic cytokines were measured 1 h after the LPS challenge
B) Systemic IL-6 levels 1 h after LPS challenge on day 7 and day 28 with mice trained with PBS (black), the free equivalent amount of β-glucan (pink), 1 mg of β-glucan (green) or nanoparticles (purple), n=10, significance compared with PBS (untrained) group.
C) *in vivo* biodistribution assay of NIR-labelled PLGA nanoparticles encapsulating β-glucan at 30 min and 13 days measured by IVIS.
D) PLGA degradation profile *in vivo* measured by fluorescence intensity over time.
E) Analysis of trained immunity phenotype in peritoneal macrophages isolated from mice 28 days after training. Training was administered on day 0 and day 4 with PBS (black), the equivalent amount of β-glucan (pink), 1 mg of β-glucan (green), or nanoparticles (purple). After 28 days, peritoneal macrophages were harvested and challenged ex-vivo with LPS (10 ng/mL), and IL-6 levels were quantified.
F) Analysis of the effect of adoptive transfer of peritoneal macrophages from trained mice in conferring trained immunity phenotype in naïve mice. Training was administered on day 0 and day 4 with PBS (black), the equivalent amount of β-glucan (pink), 1 mg of β-glucan (green), or nanoparticles (purple). After 28 days, peritoneal macrophages were harvested and cultured for 1 day. 1 million peritoneal macrophages per group were adoptively transferred (i.p) to naïve mice. After 24 h, these mice were challenged with LPS, and serum cytokines were analyzed 3 h post-challenge.
G) Analysis of percentage of SPMs in the peritoneal cavity after LPS challenge after 7 days of training. Training was administered on day 0 and day 4 with PBS (black), the equivalent amount of β-glucan (pink), 1 mg of β-glucan (green), or nanoparticles (purple). After one week, mice were challenged with LPS, and peritoneal cells were harvested 2 h later. The percentage of small peritoneal macrophages (SPMs) (CD11b+ F4/80-) was analyzed by flow cytometry, n=5, significance compared with PBS (untrained) group.
H) Analysis of trained immunity phenotype in peritoneal macrophages after 7 days. Training was administered on day 0 and day 4 with PBS (black), the equivalent amount of β-glucan (pink), 1 mg of β-glucan (green), 1 mg only on day 0 (purple) or 0.5 mg nanoparticles on both day 0 and day 4 (lilac). Peritoneal macrophages were harvested on day 7 and challenged ex-vivo with LPS. Cell supernatants were analyzed for inflammatory cytokines – IL-6, n=5, significance compared with PBS (untrained) group.
I) Analysis of trained immunity phenotype in splenic macrophages after 7 days. Training was administered on day 0 and day 4 with PBS (black), the equivalent amount of β-glucan (pink), 1 mg of β-glucan (green), 1 mg only on day 0 (purple), or 0.5 mg nanoparticles on both day 0 and day 4 (lilac). Splenic macrophages were harvested and challenged ex-vivo with LPS. Cell supernatants were analyzed for inflammatory cytokines- IL-6. n=5, significance compared with PBS (untrained) group.
$*P < 0.05$, $**P < 0.01$, and $***P < 0.001$. n.s., not significant.

4.3.4 Tumor challenge

Trained immunity has been proposed and demonstrated to be useful in both infectious diseases and immune therapy. In initial experiments, we explored how altering the temporal persistence of trained immunity could be applied to cancer immuno-therapy owing to the potential to generate a long-lived response. Generating durable responses against tumor growth is an oft-cited goal to sustain therapeutic effects. We tested to see if nanoparticle-trained mice would provide greater resistance to a tumor challenge owing to its sustained release. Using a similar setup to previous experiments, mice were injected intra-peritoneally, either with nanoparticles containing β-glucan, an equivalent amount of unencapsulated free β-glucan, or a standard training dose of β-glucan at 1 mg. In this experiment, injections were given twice, 4 days apart, indicated as day 0 and day 4. Mice were challenged with B16.F10 tumors three weeks (day 21) after the training. Tumors take about a week to form a visible mass (day 28) which we had previously measured to be the time by which nanoparticles elicited complete release of encapsulated β-glucan (**Figure 4.4a**). Measuring tumor volume, we observed that the nanoparticle trained mice significantly resisted tumor growth compared to the free β-glucan trained groups (**Figure 4.4b**). Looking for a mechanism, analysis of the tumor-infiltrating innate immune cells at the end of the experiment revealed increased neutrophils and macrophages in the tumor microenvironment, confirming that the anti-tumor effects in nanoparticle trained mice were due to changes in the tumor microenvironment[35] (**Figure 4.4c, d, e, Figure C11**). In previous work, β-glucan was shown to skew TAMs into an inflammatory M1 phenotype and train neutrophils to improve tumor resistance.[36,37,38,39] From this preliminary examination, we conjecture that the nanoparticles may sustain this same result for a more extended period, resulting in the observed phenotype. Additionally, spleen weights corresponded with tumor size as well – splenomegaly was observed for both the PBS and 1 mg

free β-glucan groups (**Figure C12**). Beyond this model, we also tested the anti-tumor effects of the nanoparticles in an EG7.OVA tumor model. We observed similar effects with nanoparticle-trained mice exhibiting the highest tumor resistance. (**Figure C13**) These results suggest that sustained-release training platforms could potentially be combined with existing anti-cancer therapies, including checkpoint blockade, to prolong protection as they provide an alternate method to influence the tumor micro-environment.[40]

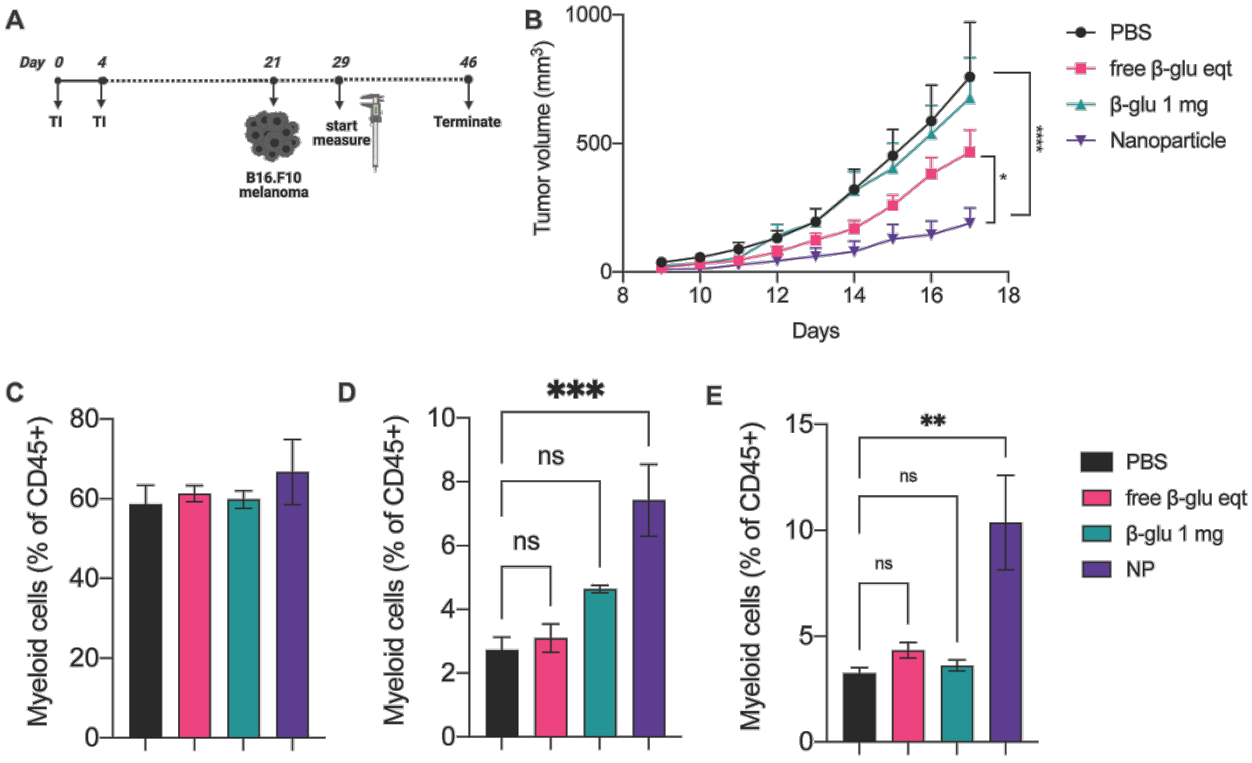

Figure 4.4: Tumor challenge

A) Experimental scheme for B16.F10 tumor challenge. (created with BioRender.com)
B) Mice were trained on day 0 and day 4 with the indicated training materials- PBS (black bars), the free equivalent amount of β -glucan (pink bars), 1 mg β -glucan (green), or PLGA nanoparticles encapsulating β -glucan (purple bars). Mice were then challenged subcutaneously with B16.F10 tumor cells. Tumor volume was recorded after the tumors were palpable – day 29 onwards, n=5.
C) Tumors were excised at the end of the experiment on day 46, and the percentage of myeloid cells (Cd45+ Cd11b+) was analyzed using flow cytometry, n=5.
D) Tumors were excised at the end of the experiment on day 46, and the percentage of neutrophils (Cd45+ Cd11b+Ly6g+) was analyzed using flow cytometry, n=5, significance compared to the PBS group.

Figure 4.4 continued
E) Tumors were excised at the end of the experiment on day 46, and the percentage of macrophages (Cd45+ Cd11b+Ly6g-F4/80+) was analyzed using flow cytometry n=5, significance compared to the PBS group.
*$P < 0.05$, **$P < 0.01$, and ***$P < 0.001$. n.s., not significant.

4.3.5 Modulating the kinetics of TI using different molecular weight PLGA nanoparticles encapsulating β-glucan

One of the well-established properties of PLGA is its control over the release kinetics of encapsulated cargo.[20] Increasing the molecular weight of PLGA decreases diffusion of the encapsulated cargo, thereby prolonging the duration of release and vice versa.[40,22,21] We hypothesized that this property might be uniquely suited to improve temporal control of trained immunity. Additionally, PLGA end groups can also affect release kinetics- carboxylic acid end groups degrade faster than those with ester end groups. To test this hypothesis, we encapsulated β-glucan using two different molecular weight PLGA polymers of molecular weights ranging from 7kDa-17kDa and 35kDa-55kDa. We also used PLGA with two different end groups- acid terminated and ester terminated. For simplicity, the formulations are hereby categorized as low acid/ester and high acid/ester, respectively. SEM characterization revealed a spherical morphology for all the PLGA nanoparticles. Encapsulation efficiency was in the range of 72-41% for all the synthesized nanoparticles (**Figure C14, C Table 1**). *In vitro* release data confirmed that nanoparticles composed of smaller molecular weight PLGA degraded faster than higher molecular weight PLGA nanoparticles. (**Figure 4.5 A**) Because our experiment was solely focused on the temporal control of the training and not on inducing a specific magnitude of training, we proceeded with this level of control over loading and release.

To study the kinetics of training, we tested the different molecular weight nanoparticles in an *in vivo* model with a time-course analysis of serum cytokines following an LPS challenge (**Figure 4.5 B**). Mice were trained as previously described with the various molecular weight nanoparticles and challenged with LPS at increasing time points- 7, 21, 25, or 30 days after the first training. We observed peak systemic IL-6 responses at day 7 for both the acid and ester terminated low molecular weight nanoparticles. By day 21, the high molecular weight acid terminated group demonstrated significantly higher systemic IL-6 levels after LPS challenge. However, the high molecular weight ester terminated group peaked at day 25 (**Figure 4.5 C**) suggesting that controlled release could be achieved by modulating both molecular weight as well as polymer end groups used. Continued analysis through day 30 confirmed the absence of sustained inflammatory responses (**Figure C15**). These results further supported our hypothesis that fine-tuning the properties of sustained-release platforms can be used for precise temporal control over the duration of trained immunity. These results suggest that with different formulations, it is possible to partially control the timing of training and lengthen or shorten the window over which higher innate responses are induced via training. Controlled training is an important step to preventing potential over-inflammatory or chronic-inflammatory responses which might cause adverse reactions.

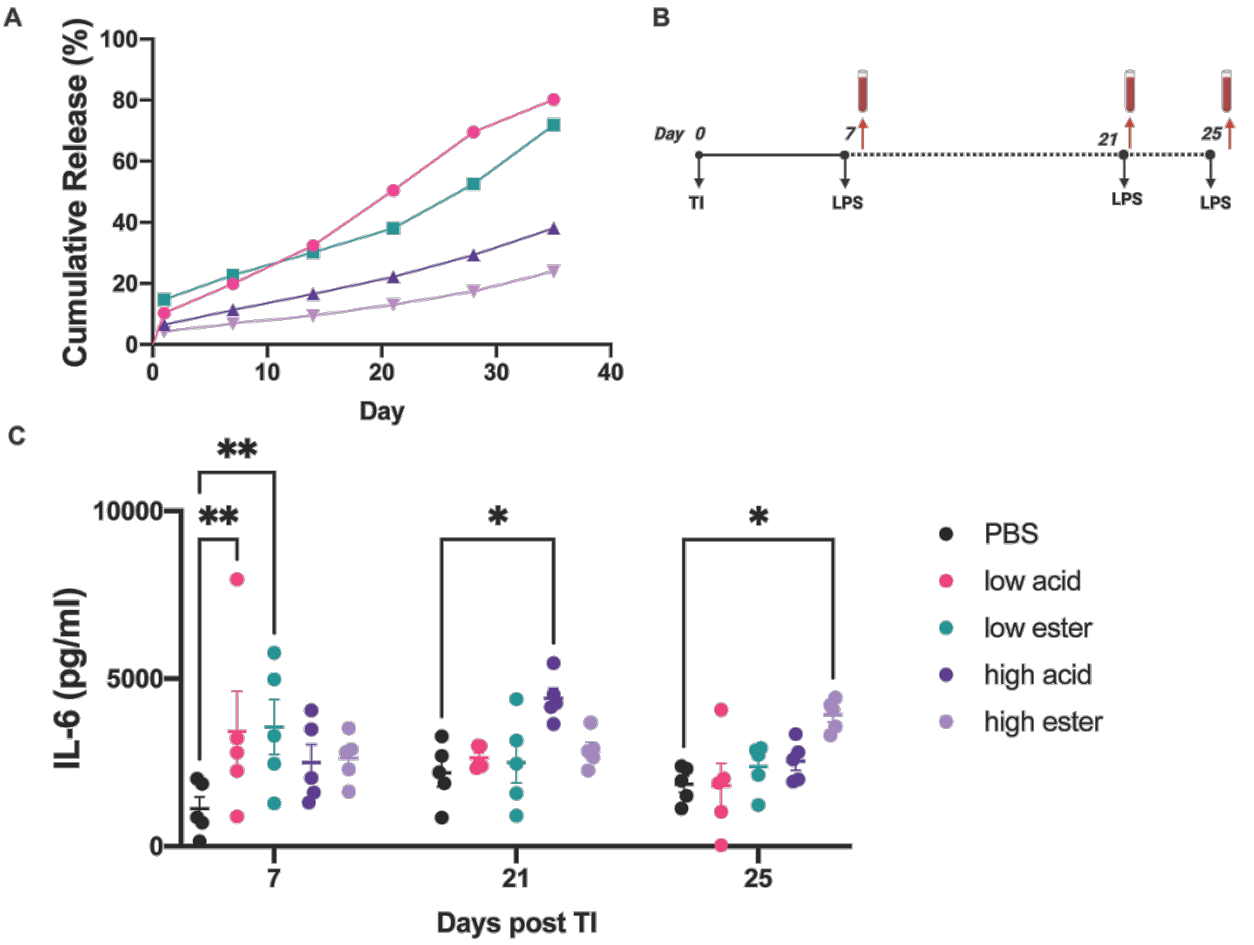

Figure 4.5: Modulating PLGA properties for temporal control of trained immunity

A) 7 day *in vitro* release profile of low molecular weight ester-terminated PLGA nanoparticles (green), high molecular weight acid-terminated nanoparticles (purple), or high molecular weight ester-terminated nanoparticles (lilac) at pH 7.4.
B) *in vivo* experimental protocol. (created with BioRender.com)
C) Mice were trained with either PBS (black) low molecular weight acid-terminated PLGA nanoparticles (pink), low molecular weight ester-terminated PLGA nanoparticles (green), high molecular weight acid-terminated nanoparticles (purple), or high molecular weight ester-terminated nanoparticles (lilac) on day 0. Different sets of mice (n=5) were challenged with LPS on the indicated days (7, 21, or 25), and systemic cytokines were quantified. Significance compared with PBS group.

4.4 Conclusion

Trained immunity improves the innate immune response to pathogenic challenge and tumor burden. However, current methods only provide transient approaches to induce training due to the short lifespan of the trained cells. While methods to direct training at the bone-marrow level ensure long-term effects, this approach suffers from the potential disadvantage of inducing long-term adverse inflammatory responses. Precise control of timing and dosage of innate immune cell activation may provide a method to improve training duration while managing unwanted adverse reactions due to prolonged activation. We report on a nanoparticle-based sustained delivery platform for temporal control over training. Controlled release of training material, β-glucan, resulted in both more sustained and higher training than a comparable injection of standard-dose β-glucan or an equivalent amount of β-glucan to that in the particle. We observed that particle training proceeded through similar pathways and mechanisms as free β-glucan training with the potential difference that some kinetic elements are altered. These results indicate that the enhanced training effect resulted mainly from the altered timing of the release. We further studied the pharmaco-kinetics by examining the release in animals using IVIS imaging, concluding that sustained-release occurred for at least the first 14 days. This altered and improved training resulted in differences in the location of training and the degree of trained cells in the peritoneal cavity and spleen, demonstrating that control of cell training can be achieved through material programming. To demonstrate the potential of temporal control for trained immunity, we also demonstrated that training-induced by nanoparticles improved tumor resistance in mice than those trained with free β-glucan. Finally, to show the potential of this technology for future application, we showed that different training windows could be achieved with different molecular weights of nanoparticle formulation PLGA. This novel nanoparticle-based delivery platform provides

reduced bulk inflammation and effective temporal control of trained immunity. We present this work as its potential for biomaterials and formulations methods employed in drug delivery to modulate and improve trained immune responses. Improving trained immunity offers the potential to develop novel therapeutics that can work independently and in conjunction with current immune-therapies to enhance therapeutic outcomes.

4.5 Materials and Methods

HEK mTLR4, B16F10 and EG7.OVA cells were obtained from InvivoGen. All cell culture reagents were obtained from Thermo Fisher Scientific. mTLR4 cells were cultured in DMEM supplemented with 10% FBS and selective antibiotics. Cells were maintained at 37°C and 5% CO2. C57Bl/6J mice were obtained from Jackson Laboratories and acclimatized for 1 week prior to experimentation. All animal experiments were conducted with approval from the University of Chicago Institutional Animal Care and Use Committee. All statistical analyses were performed using GraphPad Prism.

Formulation of nanoparticles

β-glucan was purchased from Sigma (G5011). The payload was added in 200 μL to 2 mL of 100 mg/mL of PLGA in methylene chloride. The mixture was ultrasonicated at 40% amplitude for 3 minutes (30 seconds stirring following 30 seconds of rest). After ultra-sonification, a determined amount of 5% (w/v) PVA solution was added to the primary w/o emulsion and ultrasonicated for 60 seconds to produce the w/o/w double emulsion. The w/o/w emulsion was poured into 200 μL of chilled 1% (w/v) PVA and stirred at room temperature for 6 hours. The microspheres were centrifuged at 4000 rpm for 40 minutes and the pellet were washed three times with ultrapure deionized water and then lyophilized.

Characterization of nanoparticles

For SEM imaging, nanoparticles were first sputter coated with 12 nm of Pt/Pd using Sputter Coater - Cressington 208HR. SEM images were taken with Carl Zeiss Merlin SEM at 3.0 kV. Particles were immersed in PBS at 1 mg/mL concentration for DLS measurements. Measurements were taken with 10 acquisitions with 5 seconds for each acquisition.

in vitro Release

A graham vials containing 20 mg of β-glucan nanoparticles were treated with 0.5 mL of pH 7.45 PBS buffer. The vials were gently stirred at 90 rpm at 37 ºC. The particle solution was collected by centrifuging the vials at 4000 rpm for five minutes and stored at -20 ºC. The β-glucan concentration was determined by using a total carbohydrate assay kit (Millipore Sigma).

BMDM harvest and culture

Bone marrow derived macrophages (BMDMs) were harvested from the femurs of 6-week old C57BL/6 mice (Jackson Laboratory). BMDMs were cultured in primary medium: RPMI 1640 (Life Technologies), 10% heat inactivated fetal bovine serum (HIFBS) 2 mM L-glutamine (Life Technologies), antibiotic antimycotic (1×) (Life Technologies) and 10 % MCSF (mycoplasma free L929 supernatant) for 5 days at 37 ºC and 5% CO_2. The cells were then released with 5 mM EDTA in PBS, counted and plated at desired densities.

In vitro training assays

BMDMs were plated at a density of 100,000 cells/well in flat bottom 96-well plates (Corning) at a final volume of 200 mL) and rested for a few hours to adhere at 37 ºC and 5% CO_2. After the cells were adherent, training material was added at desired concentration and incubated for 24 h.

(Nanoparticle concentration used was 100 μg/mL unless otherwise stated) Then cells were washed and rested for 3 days. On day 4, BMDMs were washed again and primed with 25 ng/mL IFN-γ (BD Biosciences) for 24 hr. On day 5, a final wash was performed, and cells were stimulated with 10 ng/mL standard Escherichia coli LPS (serotype O55:B5; Invivogen). Cell supernatant was collected after 24 h to measure IL-6 and TNF-α levels using ELISA (BioLegend) according to manufacturer's instructions.

For inhibition studies, BMDMs were pre-incubated for 30 min with inhibitors before stimulating with training materials and were left in the media during the 24 h training period.[24] For epigenetic pathway analysis, cells were pre-treated with 500 μM 5′-deoxy-5′-(methylthio)adenosine (MTA), 6 μM pargyline and 50 μM (-)-epigallocatechin-3-gallate (EGCG) (all from Sigma Aldrich). For metabolic pathway analysis, cells were pre-treated with 100 nM rapamycin (Invivogen), 10 μM Wortmannin, 30 μM Metformin and 1 mM 2' deoxyglucose (all from Sigma). For testing different pathways contributing to endocytosis, cells were pre-treated with 5 μM Filipin (Sigma), 100 μM Dynasore (Abcam) and 3 μM chlorpromazine hydrochloride (Sigma).

To quantify uptake, β-glucan was labelled with fluorescein isothiocyanate (FITC) using a previously described protocol.[41] BMDMs were treated with an equivalent amount of free FITC-labelled β-glucan or 100 μg/mL nanoparticles encapsulating FITC-labelled β-glucan for 24 h. Then, media was removed and cells were released by gentle scraping and the cells were analyzed by flow cytometry (NovoCyte Benchtop Flow Cytometer).

After *in vitro* training assay, the cells were incubated in 100 μL PBS and 10 μL of cell counting kit-8 (CCK-8) solution was added to each well and incubated at 37 ºC. Absorbance was measure at 540 nM using Multiskan FC plate reader (Thermo Scientific).

HEK mTLR4 cells were passaged and plated in a 96 well plate at 100,000 cells/well in 180 μL DMEM containing 10% HI-FBS and selective antibiotics. The cells were stimulated with the synthesized nanoparticles for 24 h at 37 °C and 5% CO_2. TLR4 binding was measured by a QUANTI-Blue (Invivogen) assay and the absorbance was measured at 620 nm using a Multiskan FC plate reader (Thermo Scientific).

In-vivo training assay

Mice were trained intra-peritoneally either once or twice on days -7 and/or day -4 with indicated amount of nanoparticles, equivalent amount of free β-glucan or 1 mg free β-glucan. Sterile PBS was always used as a control. After training, different set of mice were challenged intra-peritoneally with 5 mg LPS (serotype O55:B5; Invivogen) at desired time points and serum was collected after 1 h or 3 h. None of the mice received repeated LPS challenges. Serum cytokines were analyzed using Legendplex Mouse Inflammation Panel (BioLegend) according to the manufacturer's protocol. 2 h after LPS challenge, mice were euthanized and peritoneal cells were harvested by lavage. Cells were flow cytometry analysis was performed to determine the percentage of small peritoneal macrophages. All antibodies were purchased from BioLegend or BD Biosciences. Anti-mouse phycoerythrin (PE) CD11b, APC- MHC2, Pe/Cy7-F4/80, Brilliant violet 570- Ly6G, APC/fire 750-CD11c, Alexa fluor 700- Ly6C, APC- NK1, PE-cd115, PerCP/Cy5.5- cd19, Alexa flour 488- CD3, Brilliant violet 788- MHC2, Brilliant violet 711 CD8a, Brilliant violet 650- F4/80, BUV 395 CD45R/B220. In other experiments, spleens and peritoneal exudate cells were isolated prior to LPS challenge. Spleens were homogenized, and cells were filtered through a 70 μm strainer. Red blood cells were lysed by incubating with ACK Lysing Buffer for 5 min at 25 °C. Cells were plated in petri dishes for 2 h and washed to remove non-adherent cells. Peritoneal cells were harvested by lavage according to previously described

protocol.[42] Briefly, the skin was peeled off and clamped, followed by injection of 5 mL PBS containing 3% heat- inactivated fetal bovine serum (HIFBS) into the peritoneal cavity. The peritoneal content was then collected and centrifuged (400 g for 10 min). Peritoneal cells were plated in petri dishes for 2 h and washed to remove non-adherent cells. Peritoneal and splenic macrophages (0.1 million cells) were plated in a 96-well plate and allowed to adhere for 2 h before being challenged with LPS.

Training was administered on day 0 and day 4 with the desired material. After 28 days, mice were euthanized and cells were harvested by peritoneal lavage. The peritoneal macrophages were split for two sets of experiments. In one set, 100,000 cells were plated in 96 well flat bottom plates in a final volume of 200 mL. These cells were allowed to adhere for 3 h and then challenged with LPS (10 ng/mL). Supernatant was collected after 24 h and IL-6 levels were quantified. In a second set of experiments, 1 million peritoneal macrophages per group was adoptively transferred (ip) to naïve mice. After 24 h, these mice were challenged with LPS (5 mg/mouse) and serum cytokines were analyzed 3 h post challenge using Legendplex Mouse Inflammation Panel (BioLegend).

To determine the biodistribution, nanoparticles were synthesized using NIR-labelled PLGA (Poly(lactide-co-glycolide)-Flamma Fluor near-IR, Millipore Sigma). Fluorescence intensity was measured using Xenogen IVIS 200 Imaging System at F stop=2, 1 second Exposure, Ex= 570 nm, and Em= 620 nm.

Tumor Challenge

Mice were anesthetized and shaved of hair from their right-side using clippers. Following grooming, the mice were injected with 200,000 B16F10 melanoma cells or 1 million EG7OVA cells in 50 μL of PBS subcutaneously. For B16.F10 tumor model, mice were first trained with

indicated materials and rested for three weeks. After three weeks, all the animals were challenged with B16.F10 tumor. For EG7.OVA tumor model, mice were trained first and were vaccinated with CpG (50 μg) and OVA (100 μg) a week later. Tumor cells were injected two weeks after vaccination. Tumor progression was monitored and measured with a caliper, recording the width, length and height of the tumor every other day throughout the experiment. Mice with tumor sizes exceeding 20 mm along any direction was sacrificed.

Statistical Analysis

All values are expressed as mean ± SEM. Data were analyzed by one- or two-way analysis of variance (ANOVA) for comparison of multiple groups using the GraphPad Prism 9 software. P values less than 0.05 were considered statistically significant.

4.6 References

1. Kawai, T. & Akira, S. The role of pattern-recognition receptors in innate immunity: update on Toll-like receptors. *Nature Immunology* **11**, 373–384 (2010).

2. Netea, M. G. *et al.* Trained immunity: A program of innate immune memory in health and disease. *Science* **352**, (2016).

3. Netea, M. G. *et al.* Defining trained immunity and its role in health and disease. *Nature Reviews Immunology* **20**, 375–388 (2020).

4. Aaby, P. *et al.* Randomized trial of BCG vaccination at birth to low-birth-weight children: beneficial nonspecific effects in the neonatal period? *J Infect Dis* **204**, 245–252 (2011).

5. Lund, N. *et al.* The Effect of Oral Polio Vaccine at Birth on Infant Mortality: A Randomized Trial. *Clin Infect Dis* **61**, 1504–1511 (2015).

6. Aaby, P. *et al.* Non-specific beneficial effect of measles immunisation: analysis of mortality studies from developing countries. *BMJ* **311**, 481–485 (1995).

7. Spencer, J. C., Ganguly, R. & Waldman, R. H. Nonspecific Protection of Mice against Influenza Virus Infection by Local or Systemic Immunization with Bacille Calmette-Guerin. *The Journal of Infectious Diseases* **136**, 171–175 (1977).

8. Butkeviciute, E., Jones, C. E. & Smith, S. G. Heterologous effects of infant BCG vaccination: potential mechanisms of immunity. *Future Microbiol* **13**, 1193–1208 (2018).

9. Ciarlo, E. *et al.* Trained Immunity Confers Broad-Spectrum Protection Against Bacterial Infections. *J Infect Dis* **222**, 1869–1881 (2020).

10. Moorlag, S. J. C. F. M. *et al.* β-Glucan Induces Protective Trained Immunity against Mycobacterium tuberculosis Infection: A Key Role for IL-1. *Cell Reports* **31**, 107634 (2020).

11. Vetvicka, V. & Vetvickova, J. Glucan supplementation enhances the immune response against an influenza challenge in mice. *Ann Transl Med* **3**, (2015).

12. Muramatsu, D. *et al.* β-Glucan Derived from Aureobasidium pullulans Is Effective for the Prevention of Influenza in Mice. *PLOS ONE* **7**, e41399 (2012).

13. Garcia-Valtanen, P., Guzman-Genuino, R. M., Williams, D. L., Hayball, J. D. & Diener, K. R. Evaluation of trained immunity by β-1, 3 (d)-glucan on murine monocytes in vitro and duration of response in vivo. *Immunology & Cell Biology* **95**, 601–610 (2017).

14. Leent, M. M. T. van *et al.* A modular approach toward producing nanotherapeutics targeting the innate immune system. *Science Advances* **7**, eabe7853 (2021).

15. Braza, M. S. *et al.* Inhibiting inflammation with myeloid cell-specific nanobiologics promotes organ transplant acceptance. *Immunity* **49**, 819-828.e6 (2018).

16. Priem, B. *et al.* Trained Immunity-Promoting Nanobiologic Therapy Suppresses Tumor Growth and Potentiates Checkpoint Inhibition. *Cell* **183**, 786-801.e19 (2020).

17. Mulder, W. J. M., Ochando, J., Joosten, L. A. B., Fayad, Z. A. & Netea, M. G. Therapeutic targeting of trained immunity. *Nat Rev Drug Discov* **18**, 553–566 (2019).

18. Hines, D. J. & Kaplan, D. L. Poly (lactic-co-glycolic acid) controlled release systems: experimental and modeling insights. *Crit Rev Ther Drug Carrier Syst* **30**, 257–276 (2013).

19. Kamaly, N., Yameen, B., Wu, J. & Farokhzad, O. C. Degradable Controlled-Release Polymers and Polymeric Nanoparticles: Mechanisms of Controlling Drug Release. *Chem Rev* **116**, 2602–2663 (2016).

20. Lu, X. *et al.* Engineered PLGA microparticles for long-term, pulsatile release of STING agonist for cancer immunotherapy. *Science Translational Medicine* **12**, (2020).

21. Bailey, B. A., Ochyl, L. J., Schwendeman, S. P. & Moon, J. J. Toward a Single-Dose Vaccination Strategy with Self-Encapsulating PLGA Microspheres. *Advanced Healthcare Materials* **6**, 1601418 (2017).

22. Nakagawa, T. *et al.* Changes in content of triterpenoids and polysaccharides in Ganoderma lingzhi at different growth stages. *J Nat Med* **72**, 734–744 (2018).

23. Saz-Leal, P. *et al.* Targeting SHIP-1 in Myeloid Cells Enhances Trained Immunity and Boosts Response to Infection. *Cell Reports* **25**, 1118–1126 (2018).

24. Fanucchi, S., Domínguez-Andrés, J., Joosten, L. A. B., Netea, M. G. & Mhlanga, M. M. The Intersection of Epigenetics and Metabolism in Trained Immunity. *Immunity* **54**, 32–43 (2021).

25. Quintin, J. *et al.* Candida albicans Infection Affords Protection against Reinfection via Functional Reprogramming of Monocytes. *Cell Host Microbe* **12**, (2012).

26. Arts, R. J. W., Joosten, L. A. B. & Netea, M. G. Immunometabolic circuits in trained immunity. *Seminars in Immunology* **28**, 425–430 (2016).

27. Cheng, S.-C. *et al.* mTOR/HIF1α-mediated aerobic glycolysis as metabolic basis for trained immunity. *Science* **345**, 1250684 (2014).

28. Guo, P. *et al.* Nanoparticle elasticity directs tumor uptake. *Nature Communications* **9**, 130 (2018).

29. Quinn, S. M. *et al.* Anti-inflammatory Trained Immunity Mediated by Helminth Products Attenuates the Induction of T Cell-Mediated Autoimmune Disease. *Front. Immunol.* **10**, (2019).

30. Jeljeli, M. *et al.* Trained immunity modulates inflammation-induced fibrosis. *Nature Communications* **10**, 5670 (2019).

31. Mitroulis, I. *et al.* Modulation of Myelopoiesis Progenitors Is an Integral Component of Trained Immunity. *Cell* **172**, 147-161.e12 (2018).

32. Chen, J. *et al.* In situ cancer vaccination using lipidoid nanoparticles. *Science Advances* **7**, eabf1244 (2021).

33. de Graaff, P. *et al.* Curdlan, zymosan and a yeast-derived β-glucan reshape tumor-associated macrophages into producers of inflammatory chemo-attractants. *Cancer Immunol Immunother* (2020) doi:10.1007/s00262-020-02707-4.

34. Liu, M. *et al.* Dectin-1 Activation by a Natural Product β-Glucan Converts Immunosuppressive Macrophages into an M1-like Phenotype. *J Immunol* **195**, 5055–5065 (2015).

35. Kalafati, L. *et al.* Innate Immune Training of Granulopoiesis Promotes Anti-tumor Activity. *Cell* **183**, 771-785.e12 (2020).

36. Ning, Y. *et al.* β-glucan restores tumor-educated dendritic cell maturation to enhance antitumor immune responses. *Int J Cancer* **138**, 2713–2723 (2016).

37. Maldonado, R. A. *et al.* Polymeric synthetic nanoparticles for the induction of antigen-specific immunological tolerance. *PNAS* **112**, E156–E165 (2015).

38. Essa, D., Kondiah, P. P. D., Choonara, Y. E. & Pillay, V. The Design of Poly(lactide-co-glycolide) Nanocarriers for Medical Applications. *Frontiers in Bioengineering and Biotechnology* **8**, (2020).

39. Lee, P. W. & Pokorski, J. K. PLGA Devices: Production and Applications for Sustained Protein Delivery. *Wiley Interdiscip Rev Nanomed Nanobiotechnol* **10**, e1516 (2018).

40. Thomas, C., Rawat, A., Hope-Weeks, L. & Ahsan, F. Aerosolized PLA and PLGA Nanoparticles Enhance Humoral, Mucosal and Cytokine Responses to Hepatitis B Vaccine. *Mol. Pharmaceutics* **8**, 405–415 (2011).

41. Yu, M. *et al.* Specifically targeted delivery of protein to phagocytic macrophages. *Int J Nanomedicine* **10**, 1743–1757 (2015).

42. Santecchia, I. *et al.* Innate immune memory through TLR2 and NOD2 contributes to the control of Leptospira interrogans infection. *PLOS Pathogens* **15**, e1007811 (2019).

5. Effect of β-glucan induced trained immunity on antibody response

5.1 Summary

Trained immunity induced by β-glucan confers disease resistance against bacterial, fungal, and viral infections. It does so by epigenetically and metabolically rewiring innate immune cells like macrophages and neutrophils. The trained cells can produce higher pro-inflammatory cytokines when exposed to a pathogen in the future. Cytokines from innate immune cells that function as antigen-presenting cells polarize T-cell responses, so trained immunity can potentially modulate adaptive immunity. However, the effect of trained immunity on subsequent vaccinations to improve antibody levels has not yet been reported. We show that intraperitoneal β-glucan training in mice increases co-stimulatory marker expression in splenic macrophages. We also observed increased antibody levels to vaccines containing a model antigen OVA and a TLR 2 or TLR 4 agonist administered a week after training. This is the first report showing the utility of trained immunity as a novel tool to boost the effects of vaccination and can be potentially used to improve vaccines using TLR2 and TLR 4 agonists in their formulations such as Cervarix and MMR.

5.2 Introduction

The immune system consists of innate and adaptive arms. The innate immune system forms the first line of defense and recognizes molecular patterns on pathogens employing pattern recognition receptors (PRRs) present on them.[1] Activation of PRRs on innate immune cells generates an immune response designed to clear the infection.[2] In the meantime, antigen-presenting cells like macrophages and dendritic cells drain to the lymph nodes to activate T-cells and initiate an adaptive immune response.[3] This generates memory T and B-cells that provide long-lasting immunity from the pathogen. Apart from the adaptive immune memory, innate immune cells are also known to possess non-specific memory against certain whole cells vaccines and fungal cell

component- β-glucan.[4] This process, called trained immunity, improves host defense against various bacterial, fungal, and viral infections in both mice and humans.[5,6,7]

A variety of stimuli activate different PRRs to induce trained immunity. For example, the bacillus Calmette-Guerin (BCG) vaccine induces training by activating nucleotide-binding oligomerization domain-2 (NOD 2) receptor.[8,9] In contrast, fungal cell wall component- β-glucan activates cell surface receptor Dectin-1. While different PRRs can initiate trained immunity, they converge on similar downstream effects—namely epigenetic and metabolic rewiring of innate immune cells. Chromatin remodeling enables increased histone methylations on genes coding for pro-inflammatory cytokines.[10] Additionally, the trained cell switches from oxidative phosphorylation to aerobic glycolysis to facilitate its energy needs.[11] During this shift, metabolites such as acetyl-CoA and succinate further modulate the epigenetic landscape.

β-glucan induced trained immunity modulates innate immune cells such as macrophages which are important antigen-presenting cells (APCs).[12] Trained immunity is associated with increased production of pro-inflammatory cytokines like IL-6, TNF-α, and IL-1.[13] Training also increases the expression of co-stimulatory markers, such as CD80, CD86, and CD40, on APCs.[14] Both these signals are essential in activating and polarizing T-cells. Therefore, it has been hypothesized that trained immunity can improve adaptive immune responses.[15] However, there have been no reports demonstrating the effects of training on T-cell activation and antibody production.

We provide preliminary evidence that β-glucan increases co-stimulatory marker expression and antigen presentation in an *in-vitro* trained immunity model in BMDMs. We also observed that splenic macrophages expressed higher co-stimulatory markers CD86, CD40, and MHCII seven days after training with β-glucan. To test if the systemic effects of trained immunity improve

antibody levels in mice, we used a vaccination model with model antigen OVA with Pam_3CSK_4 (TLR 2 agonist) or monophosphoryl lipid A (MPLA) (TLR-4 agonist). We observed that intraperitoneally administered training one week before subcutaneous vaccination improved antibody levels in mice. This strategy of inducing trained immunity a week before vaccination offers a novel approach to boost adaptive immune responses to childhood vaccines like MMR or existing vaccines using TLR 2 or TLR 4 as adjuvants.

5.3 Results and discussion

5.3.1 *in-vitro* training assay

We first tested if β-glucan training in an *in-vitro* model improved the expression of costimulatory molecules such as CD86 and CD40 on BMDMs. In this experiment, 3 million BMDMs were trained with either PBS (untrained) or 100 μg/mL of β-glucan for 24 h in a 12 well plate in a total volume of 2 mL. Then the cells were washed and the media was replaced. Cells were harvested after a resting period of 4 days and analyzed for cell surface markers- CD86 and CD40 by flow cytometry. A separate set of cells were stimulated with Pam_3CSK_4 (TLR 2 agonist) and analyzed 18 h later for cell surface marker expression. We observed significantly higher expression of both costimulatory molecules suggesting that β-glucan training *in-vitro* can improve antigen-presentation. (**Figure 5.1a** and **Figure 5.1b**).

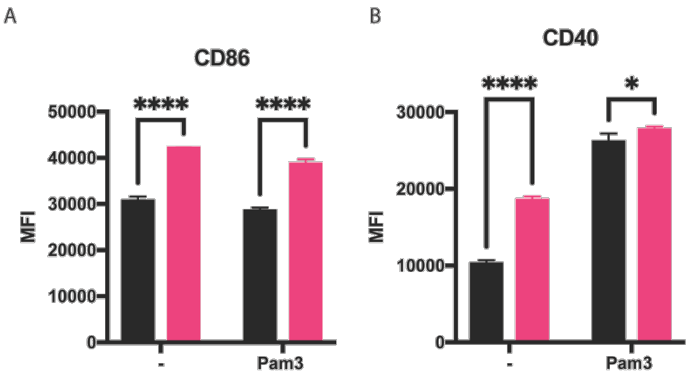

Figure 5.1: *in-vitro* training assay with β-glucan to analyze costimulatory marker expression

BMDMs were trained with PBS (black bar) or 100 mg/mL of β-glucan (pink bars) for 24 h. Cells were then washed and rested for four days. Cells were released from the plate on day 5 and analyzed for expression of A) CD86 or B) CD40 by flow cytometry.
n=3; *$P < 0.05$, **$P < 0.01$, and ***$P < 0.001$. n.s., not significant.

5.3.2 *in-vivo* training assay

Encouraged by this result, we turned to an *in-vivo* model of training. The training effects of intra peritoneally injected β-glucan have been reported to occur at three key locations- the peritoneal cavity, spleen and bone marrow.[16] To check the biodistribution of intra peritoneally administered β-glucan, we labelled β-glucan with a fluorophore (Alexa fluor 647) and measured fluorescence using IVIS. We observed that the β-glucan distributed systemically in mice after just 30 min of administration (**Figure D1**). Since we were interested in distinguishing adjuvanticity with training, we first determined if β-glucan training induced changes in splenic macrophages. To do this, we trained mice with either PBS or 1 mg of β-glucan. We isolated the splenic macrophages after 7 days and analyzed the expression of costimulatory markers- CD40, CD86 and MHCII. We observed significantly higher increase in all three markers in splenic macrophages from β-glucan trained mice. (**Figure 5.2A**) Additionally, we stimulated these macrophages with Pam_3CSK_4 ex vivo and measured the resulting cytokines produced. We observed significantly higher IL-6, TNF-

α and MCP-1 following challenge in splenic macrophages from β-glucan trained mice. (**Figure 5.2B**)

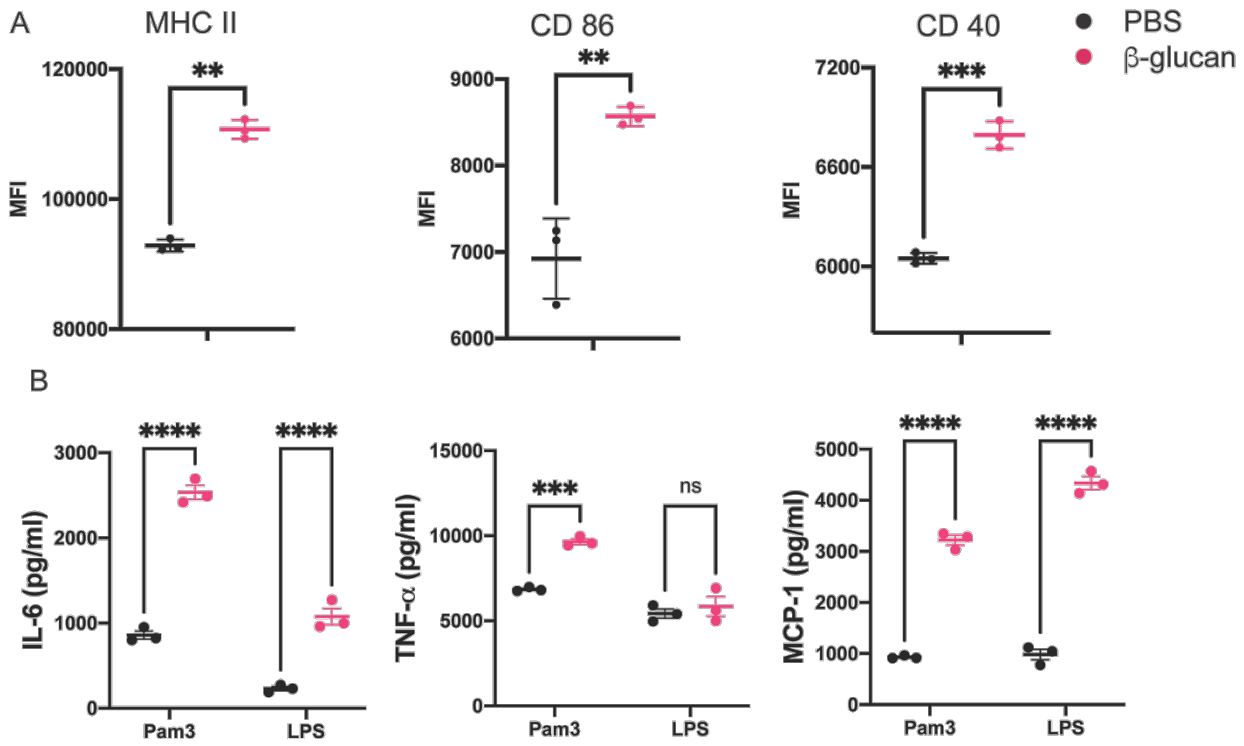

Figure 5.2: Analysis of splenic macrophages following trained immunity

Mice were trained with either PBS (black) or 1 mg of β-glucan (pink) intraperitoneally. 7 days later, splenic macrophages were harvested. A) Flow cytometry was used to analyze expression of MHC II, CD86 and CD40. B) 100,000 splenic macrophages were plated in 96 well plates and stimulated with Pam3 (10 ng/mL) or LPS (10 ng/mL) in a total volume of 200 mL. Cytokines were analyzed after 20 h using cytokine bead array (CBA).
n=3; *$P < 0.05$, **$P < 0.01$, and ***$P < 0.001$. n.s., not significant.

5.3.3 TI in vaccination

To test if mice demonstrated improved antigen presentation, we performed a vaccination experiment. In this experiment, mice were either untrained (PBS control) or intra peritoneally administered with 1 mg of β-glucan. We let the mice rest for 1 week to ensure all of the training material was dispersed and did not contribute towards adjuvanticity. 1 week post training, we

vaccinated mice with model antigen OVA combined with an agonist subcutaneously near the spleen. A different route was chosen for the vaccination experiment to clearly differentiate between training and adjuvant effects of β-glucan. We performed a preliminary screen to determine the adjuvant that would work best with the training model considering possible synergistic interactions. In this screen, we utilized Pam_3CSK_4 (TLR1/2 agonist), MPLA (TLR4 agonist), R848 (TLR7/8 agonist) and CpG (TLR 9 agonist). OVA was administered at 100 μg per mouse and adjuvant concentrations were determined based on literature precedent. Vaccinated mice received a boost 2 weeks later and serum cytokines were analyzed 2 weeks after boost. We observed significantly higher anti-OVA IgG levels in β-glucan trained mice that were vaccinated with MPLA and Pam_3CSK_4. No difference was observed with the other adjuvants tested. This observation was in agreement with prior literature citing increased synergies between Dectin-1 and TLR2 and TLR 4 mediated immune activation.[17] Taken together, these results suggest that β-glucan training can be used to improve antibody levels when used in combination with the appropriate agonist/antigen combinations. (**Figure 5.3**)

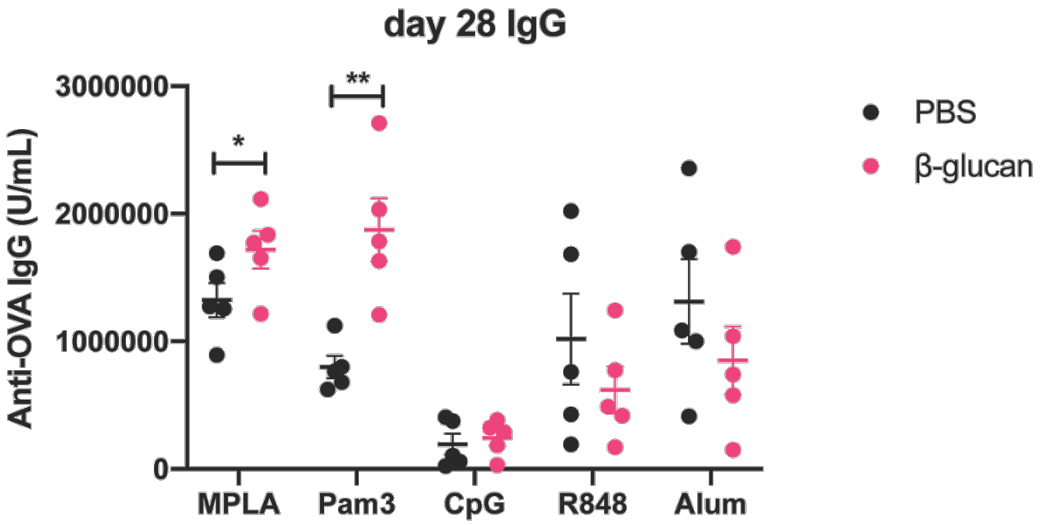

Figure 5.3: Effect of β-glucan induced trained immunity on antibody levels

Figure 5.3 continued
Mice were trained with PBS (black) or β-glucan (pink) intraperitoneally. 1 week later, mice received vaccination containing OVA with an adjuvant of choice. Mice were boosted 2 weeks later and serum cytokines analyzed for antibody levels 2 weeks post boost.

5.4 Conclusion

Innate immune cells shape adaptive responses through cytokines and costimulatory molecule expression. Trained immunity induces epigenetic and metabolic reprogramming of innate immune cells, including DCs and macrophages, facilitating higher inflammatory cytokines production following a secondary pathogenic challenge. These cytokines mainly include IL-1, IL-6, and TNF-α that can polarize and differentiate naive CD4-T cells. BCG and adenovirus increase the expression of costimulatory markers- MHC2, CD40, and CD80 in macrophages.[13,18] BCG vaccine has also been shown to induce heterologous TH1/TH17 activation in humans.[19] These key signals play essential roles in polarizing T-cell responses. However, these effects are not yet fully understood. Here, we report the enhanced antibody responses generated as a result of training mice with β-glucan a week ahead of vaccination.

β-glucan training improved antigen-presentation in BMDMs *in-vitro* as well as splenic macrophages *in-vivo*. Splenic macrophages also exhibited elevated inflammatory cytokines - IL-6, TNF-α and MCP-1 following ex-vivo challenge with Pam_3CSK_4, characteristic of a training response. Finally, we show that β-glucan training 1 week before vaccination improves antibody levels to a model antigen OVA. This method is most effective for vaccines containing TLR2 and TLR4 as adjuvants due to synergy with Dectin-1 signaling

This is the first report to demonstrate the potential use of β-glucan as a prophylactic to boost responses to vaccines. This method can be utilized to improve childhood vaccines like MMR that contain TLR 2 agonists. Cervarix and Shingrix are two other commercial vaccines that utilize

TLR4 as adjuvants in their formulation and could potentially benefit from combining with training ahead of vaccination. This work is also promising in designing novel materials that target training in addition to conventional signaling pathways. Microparticulate β-glucan conjugated with a model antigen OVA has already been demonstrated to improve antigen presentation and CD4 T cell proliferation.[21,22] Alternatively, skin patches or nasal sprays can be designed to deliver β-glucan prior to vaccination to boost antibody levels.

5.5 Materials and Methods

In-vitro training assay

BMDMs were plated at a density of 3*10^6 cells/well in flat bottom 12-well plates (Corning) at a final volume of 2 mL) and rested for a few hours to adhere at 37 ºC and 5% CO_2. After the cells were adherent, training material was added at desired concentration and incubated for 24 h. Then cells were washed and rested for 3 days. On day 4, BMDMs were released and stained with blocking antibody (CD16/32) for 10 min. The cells were then stained with anti-mouse FITC-CD86, PE-CD40 or APC-MHC II and analyzed using flow cytometry.

In-vivo training assay

Mice were trained intra-peritoneally once with 1 mg free β-glucan or sterile PBS (control). After 7 days, spleens were harvested. Spleens were homogenized, and cells were filtered through a 70 μm strainer. Red blood cells were lysed by incubating with ACK Lysing Buffer for 5 min at 25 °C. Cells were plated in petri dishes for 2 h and washed to remove non-adherent cells. 3 million cells per spleen were analyzed for expression of surface markers. Splenic macrophages were first stained with blocking antibody (CD16/32) for 10 min. The cells were then stained with anti-mouse FITC-CD86, PE-CD40 or APC-MHC II for 30 min in the dark at 4 deg C and analyzed using flow

cytometry. Alternatively, splenic macrophages were plated at a density of 100,000 cells/well and challenged ex-vivo with $PamCSK_4$ (10 ng/mL) or LPS (10 ng/mL) for 18 h. Cell supernatant was collected and analyzed using Legendplex Mouse Inflammation Panel (BioLegend).

Vaccination experiment

Mice were lightly anesthetized with isoflurane and injected intra-peritoneally once with 1 mg free β-glucan or sterile PBS (control). After 7 days, mice received vaccination subcutaneously (near spleen) containing OVA (100 μg) with an adjuvant of choice at the following concentrations: MPLA and Pam_3CSK_4 at 10 μg/mouse, CpG and R848 at 50 μg/mouse or Alum (1:1 with antigen OVA). Mice received a boost two weeks later. Blood was collected at time points indicated in 0.2 ml of heparin-coated collection tubes (VWR Scientific) for plasma or uncoated tubes for serum. Plasma was isolated via centrifugation (2000*g*, 5 min). Serum was isolated by allowing blood to clot for 15 to 30 min at RT and centrifuging (2000*g* for 10 min) at 4°C. Serum was analyzed using a quantitative anti-OVA total Ig's ELISA kit (Alpha Diagnostic International) according to the specified protocol. Plates were analyzed using a Multiskan FC plate reader (Thermo Fisher Scientific), and absorbance was measured at 450 nm and 630 nm. Data were analyzed using GraphPad Prism.

5.6 References

1. Medzhitov, R. & Janeway, C. Innate Immunity. *New England Journal of Medicine* **343**, 338–344 (2000).

2. Akira, S., Uematsu, S. & Takeuchi, O. Pathogen Recognition and Innate Immunity. *Cell* **124**, 783–801 (2006).

3. Guermonprez, P., Valladeau, J., Zitvogel, L., Théry, C. & Amigorena, S. Antigen presentation and T cell stimulation by dendritic cells. *Annu Rev Immunol* **20**, 621–667 (2002).

4. Netea, M. G. *et al.* Defining trained immunity and its role in health and disease. *Nat Rev Immunol* **20**, 375–388 (2020).

5. Brandi, P. *et al.* Trained immunity induction by the inactivated mucosal vaccine MV130 protects against experimental viral respiratory infections. *Cell Reports* **38**, 110184 (2022).

6. Ciarlo, E. *et al.* Trained Immunity Confers Broad-Spectrum Protection Against Bacterial Infections. *The Journal of Infectious Diseases* **222**, 1869–1881 (2020).

7. Arts, R. J. W. *et al.* BCG Vaccination Protects against Experimental Viral Infection in Humans through the Induction of Cytokines Associated with Trained Immunity. *Cell Host & Microbe* **23**, 89-100.e5 (2018).

8. Kleinnijenhuis, J. *et al.* Bacille Calmette-Guérin induces NOD2-dependent nonspecific protection from reinfection via epigenetic reprogramming of monocytes. *PNAS* **109**, 17537–17542 (2012).

9. Mourits, V. P., Wijkmans, J. C., Joosten, L. A. & Netea, M. G. Trained immunity as a novel therapeutic strategy. *Current Opinion in Pharmacology* **41**, 52–58 (2018).

10. Fanucchi, S., Domínguez-Andrés, J., Joosten, L. A. B., Netea, M. G. & Mhlanga, M. M. The Intersection of Epigenetics and Metabolism in Trained Immunity. *Immunity* **54**, 32–43 (2021).

11. Arts, R. J. W., Joosten, L. A. B. & Netea, M. G. Immunometabolic circuits in trained immunity. *Seminars in Immunology* **28**, 425–430 (2016).

12. Camilli, G., Tabouret, G. & Quintin, J. The Complexity of Fungal β-Glucan in Health and Disease: Effects on the Mononuclear Phagocyte System. *Frontiers in Immunology* **9**, (2018).

13. Jeljeli, M. *et al.* Trained immunity modulates inflammation-induced fibrosis. *Nat Commun* **10**, 5670 (2019).

14. Quintin, J. *et al.* Candida albicans Infection Affords Protection against Reinfection via Functional Reprogramming of Monocytes. *Cell Host Microbe* **12**, 10.1016/j.chom.2012.06.006 (2012).

15. Murphy, D. M., Mills, K. H. G. & Basdeo, S. A. The Effects of Trained Innate Immunity on T Cell Responses; Clinical Implications and Knowledge Gaps for Future Research. *Frontiers in Immunology* **12**, 3306 (2021).

16. Hong, F. *et al.* Mechanism by Which Orally Administered β-1,3-Glucans Enhance the Tumoricidal Activity of Antitumor Monoclonal Antibodies in Murine Tumor Models. *The Journal of Immunology* **173**, 797–806 (2004).

17. Ferwerda, G., Meyer-Wentrup, F., Kullberg, B.-J., Netea, M. G. & Adema, G. J. Dectin-1 synergizes with TLR2 and TLR4 for cytokine production in human primary monocytes and macrophages. *Cell Microbiol* **10**, 2058–2066 (2008).

18. Yao, Y. *et al.* Induction of Autonomous Memory Alveolar Macrophages Requires T Cell Help and Is Critical to Trained Immunity. *Cell* **175**, 1634-1650.e17 (2018).

19. Kleinnijenhuis, J. *et al.* Long-Lasting Effects of BCG Vaccination on Both Heterologous Th1/Th17 Responses and Innate Trained Immunity. *J Innate Immun* **6**, 152–158 (2014).

20. Kleinnijenhuis, J. *et al.* Long-Lasting Effects of BCG Vaccination on Both Heterologous Th1/Th17 Responses and Innate Trained Immunity. *Journal of Innate Immunity* **6**, 152 (2014).

21. Berner, V. K., duPre, S. A., Redelman, D. & Hunter, K. W. Microparticulate β-glucan vaccine conjugates phagocytized by dendritic cells activate both naïve CD4 and CD8 T cells in vitro. *Cellular Immunology* **298**, 104–114 (2015).

22. Carter, R. W., Thompson, C., Reid, D. M., Wong, S. Y. C. & Tough, D. F. Preferential Induction of CD4+ T Cell Responses through In Vivo Targeting of Antigen to Dendritic Cell-Associated C-Type Lectin-1. *The Journal of Immunology* **177**, 2276–2284 (2006).

Appendix A: Chapter 2

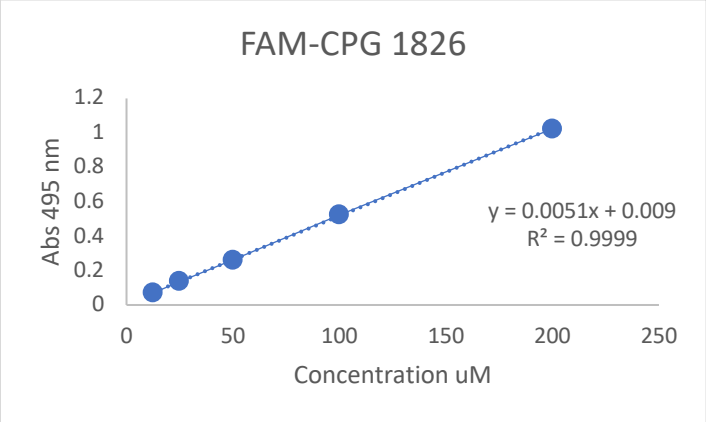

Figure A1. Quantification of CpG dimers

Standard curve to quantify CPG dimers relative to FAM absorbance at 495 nm

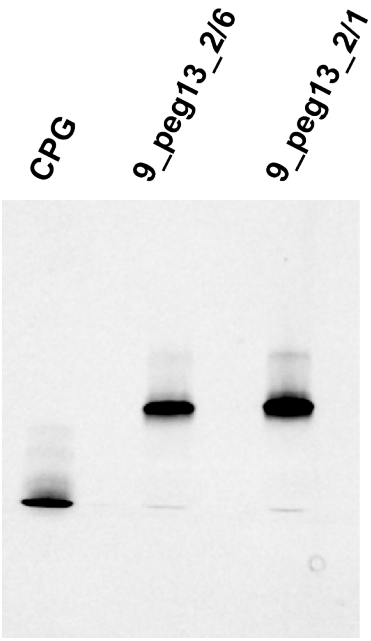

Figure A2. Gel electrophoresis of CpG dimers

Gel electrophoresis of FAM labeled CpG_1826, and FAM labeled Pam_PEG $_{13}$ _CpG compounds visualized by 6 fluorescein amidite tag (495 nm laser excitation).

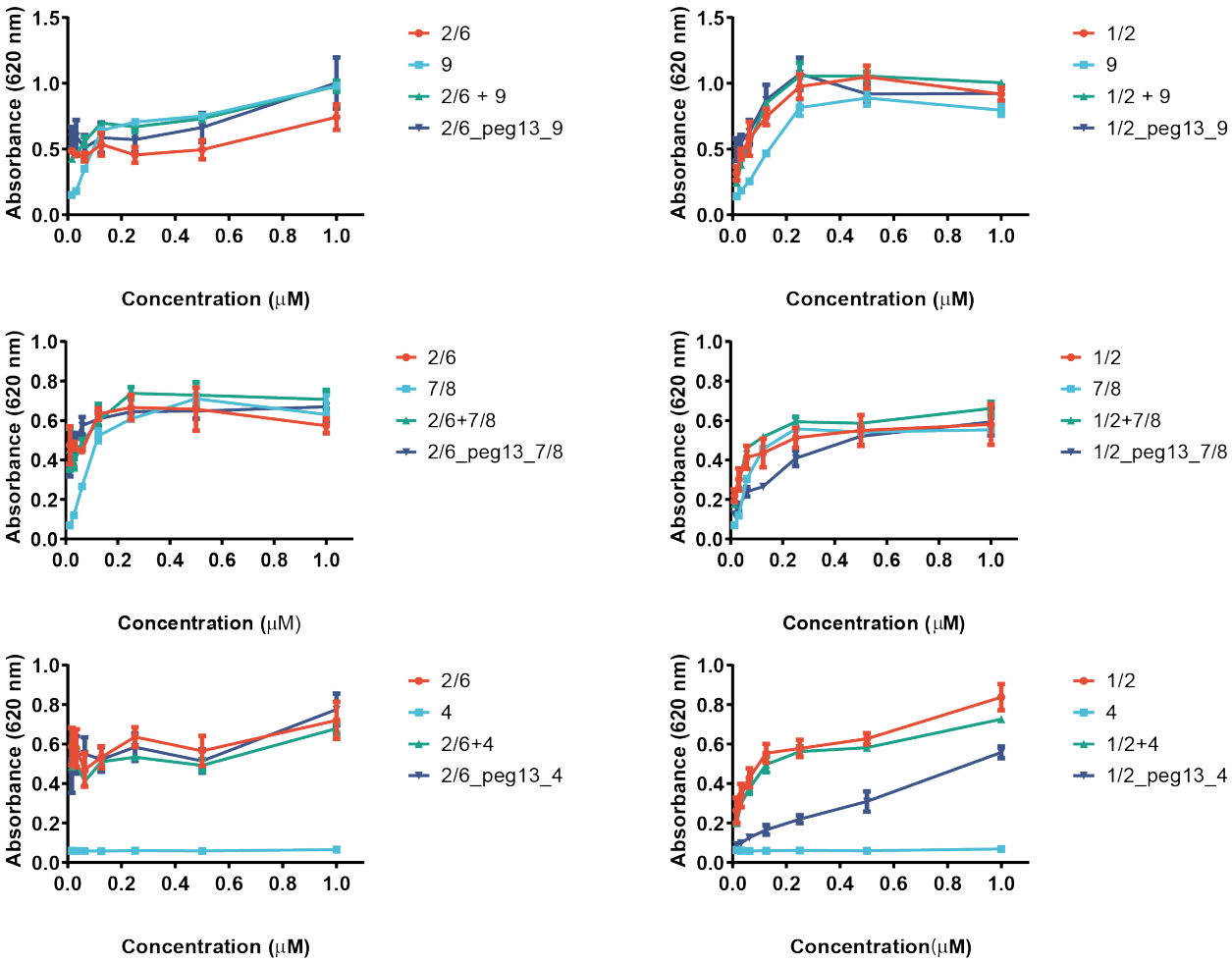

Figure A3: RAW-blue activity of dimers

Concentration scan of Pam2CSK4 (2/6), Pam3CSK4 (2/1), CpG_1826 (9) indole (4) and imidazoquinoline (7/8), corresponding equimolar mixtures and linked agonists measured by RAW-Blue activation after 24 h incubation at 37 °C.

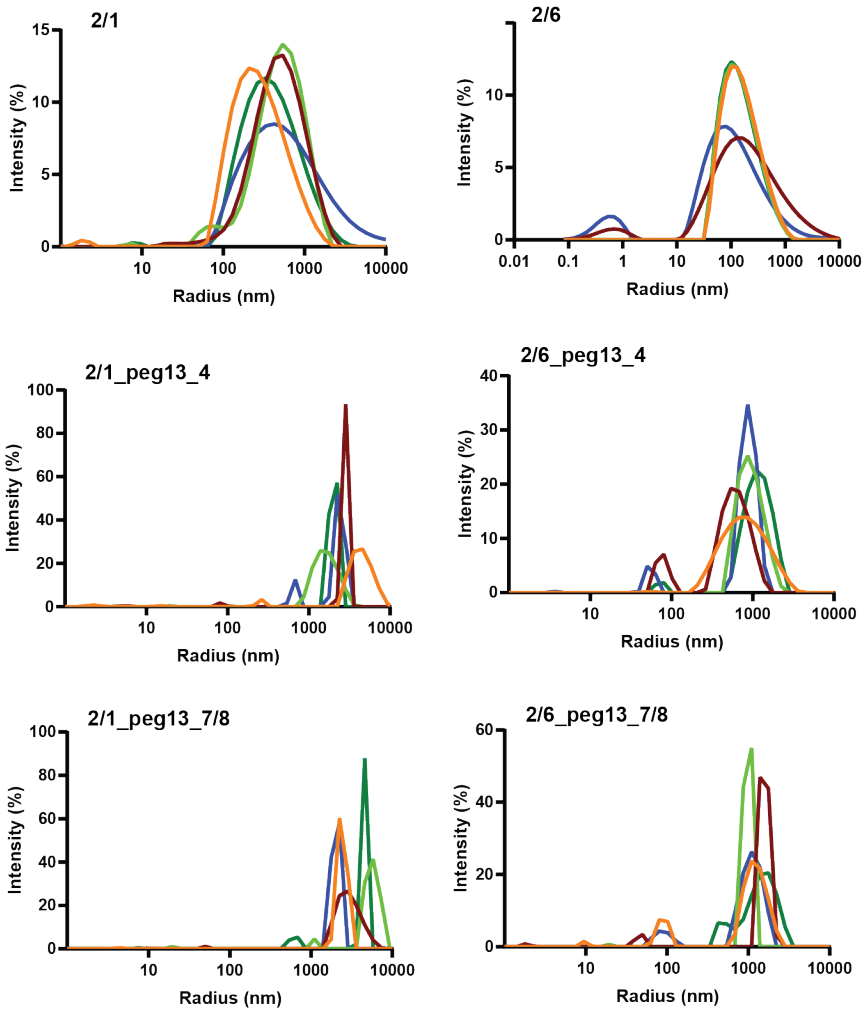

Figure A4: DLS data of dimers

Intensity vs particle size of lipopeptide and lipopeptide derive dimers measured by dynamic light scattering (DLS). Samples measured at 250 nM in PBS

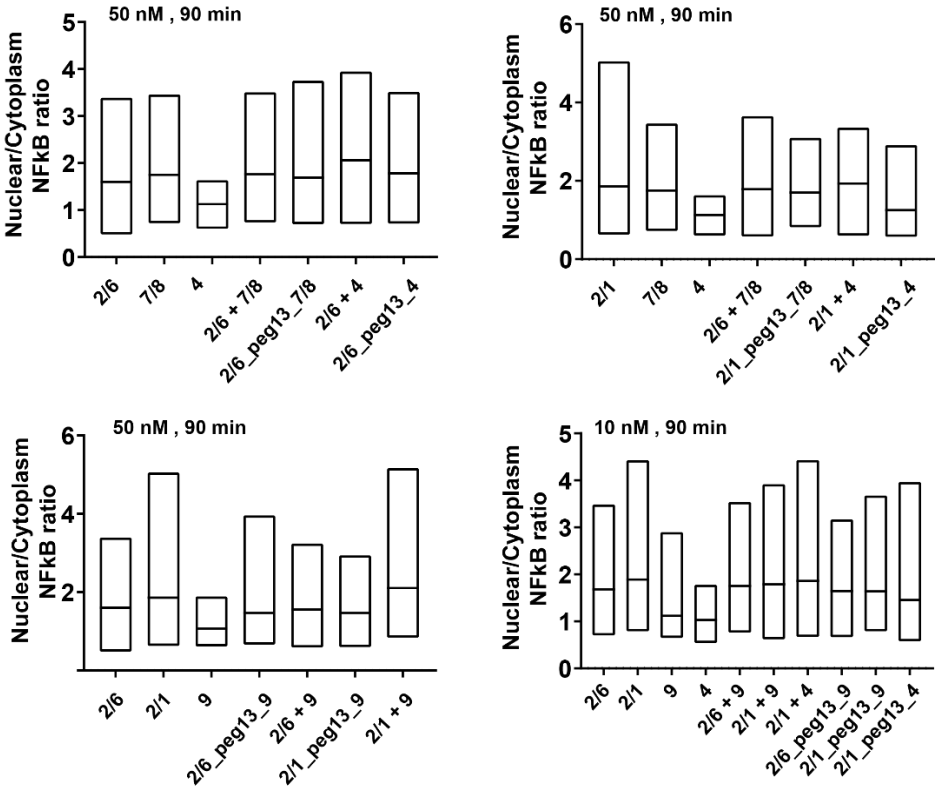

Figure A5. Nuclear/cytoplasm NFκB ratio of dimers

Box graph showing distribution of single cells based on the nuclear/cytoplasm NFκB ratio. Line representing mean.

Appendix B: Chapter 3

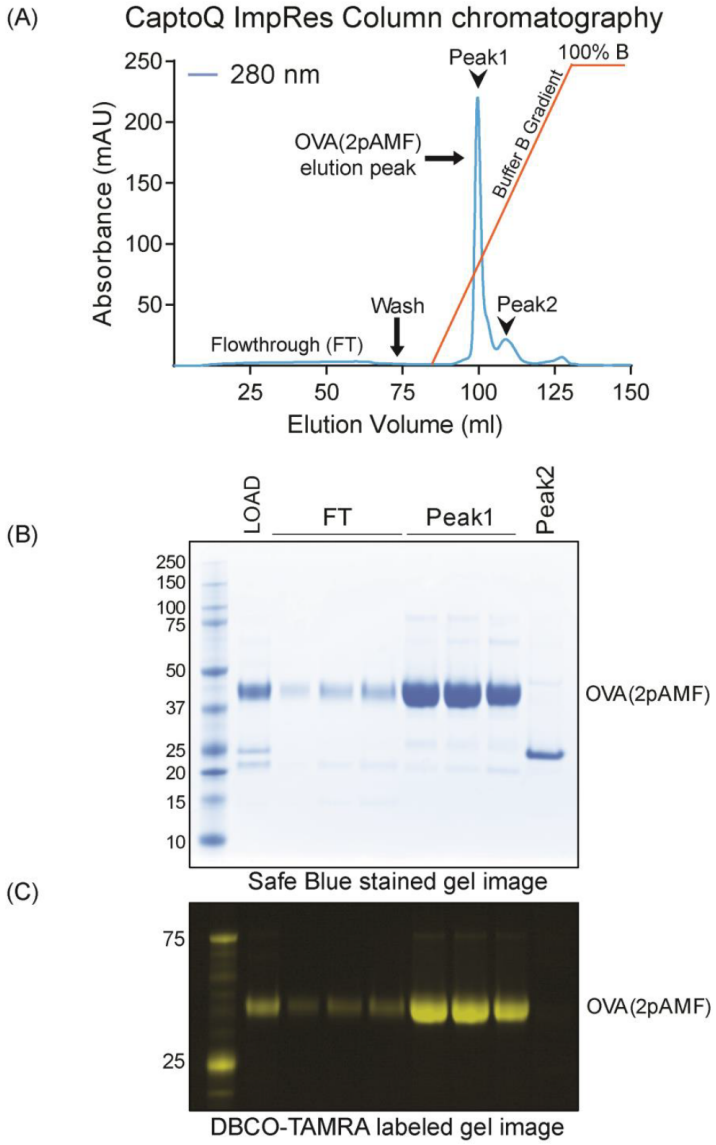

Figure B1: Purification of OVA-2pAMF.

(A) Anion exchange chromatogram showing the final step of purification followed by (B) safe-blue stained and (C) DBCO-TAMRA labeled SDS-PAGE analysis of the FT and elution fractions.

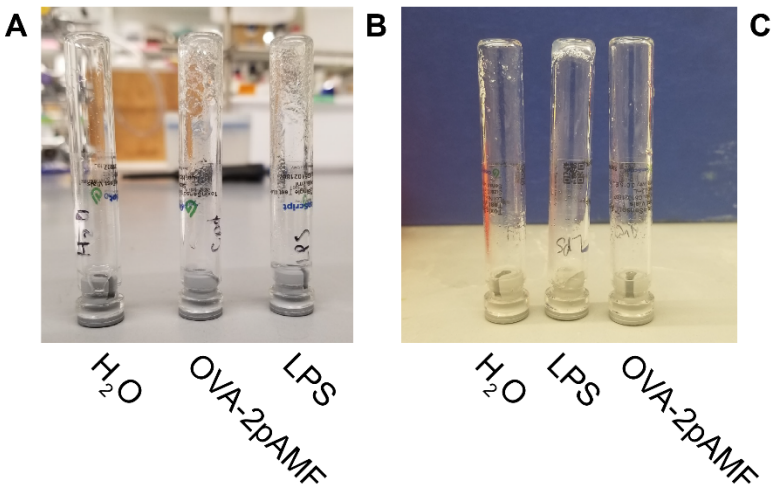

C

Pre-Endotoxin	2.08 mg
Post-Endotoxin	1.63 mg
Recovery	78% recovered

Figure B2: LAL Assay results

A) before and B) after endotoxin was removed from OVA-2pAMF using three Triton X-114 washes. Absence of clotting indicates endotoxin decontamination < 1.5 EU/mL. C) BCA Assays conducted before and after endotoxin decontamination reveal 78% recovery after three washes.

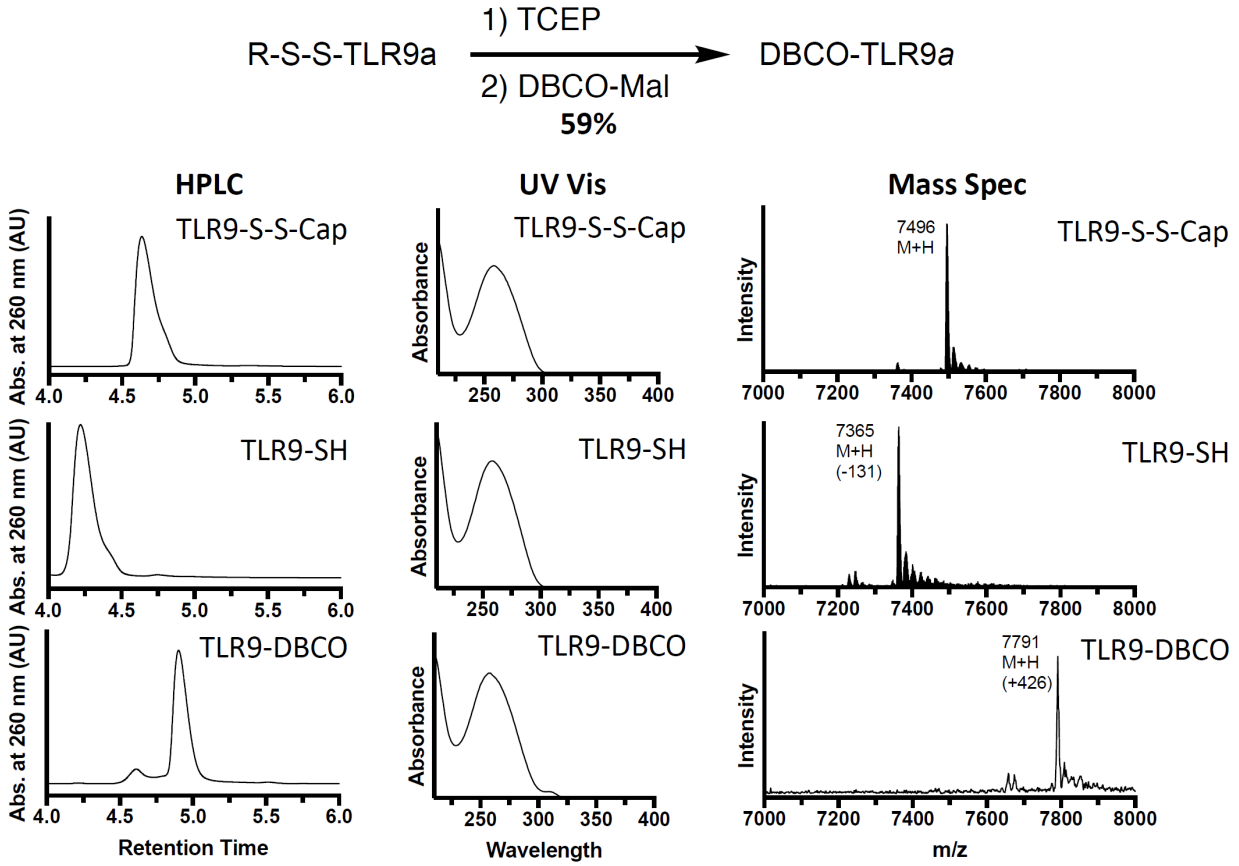

Figure B3: Functionalization and characterization of CpG.

Figure B3 continued
Capped CpG samples (R = -$(CH_2)_6$-OH) were treated first with TCEP to release the free thiol. The free thiol was subsequently reacted with DBCO-Maleimide to obtain an alkyne-modified derivative. Samples were characterized by HPLC, UV-VIS, and Q-TOF ESI-MS at each characterization step as shown to validate that the modifications were successful.

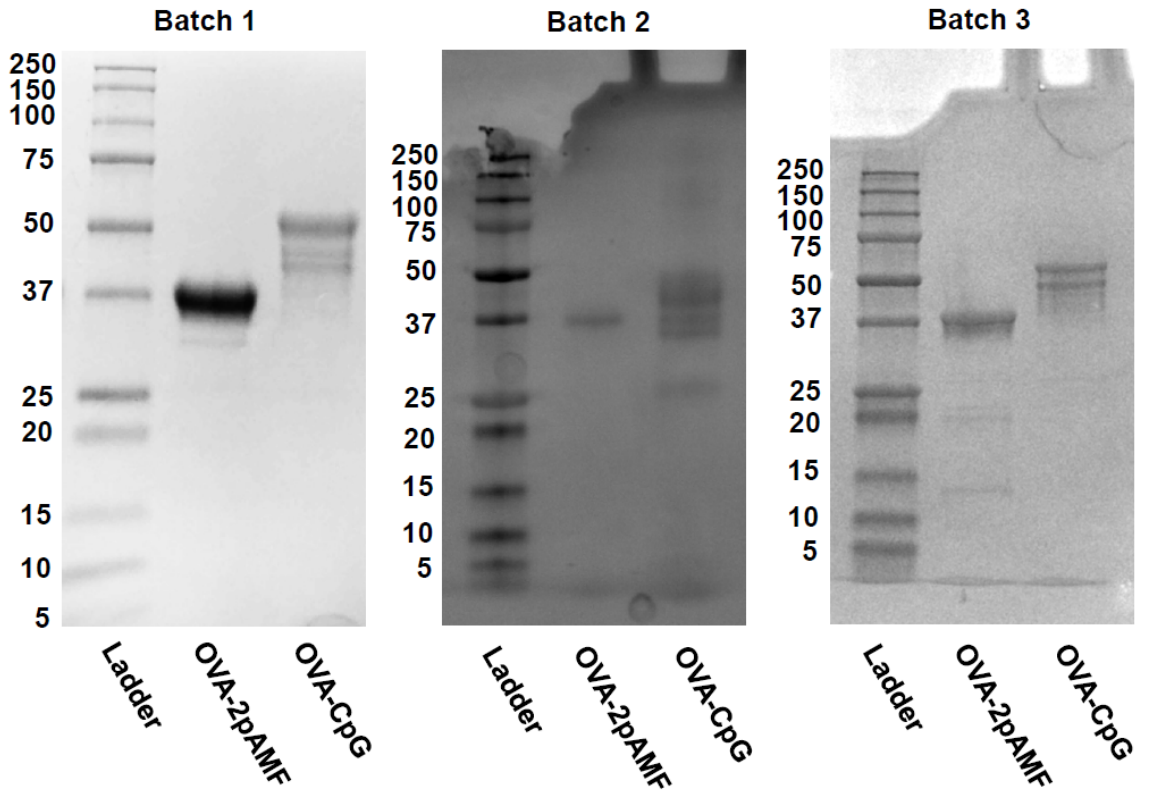

2 CpG/OVA	52%
1 CpG/OVA	39%
0 CpG/OVA	10%
Avg CpG/OVA	1.5

2 CpG/OVA	42%
1 CpG/OVA	33%
0 CpG/OVA	25%
Avg CpG/OVA	1.2

2 CpG/OVA	40%
1 CpG/OVA	49%
0 CpG/OVA	11%
Avg CpG/OVA	1.3

Figure B4: Full gels and densitometry of OVA-CpG conjugates.

Gels were stained using One-Step Blue Protein Gel Stain, and densitometry was conducted using ImageJ to obtain the CpG content per OVA.

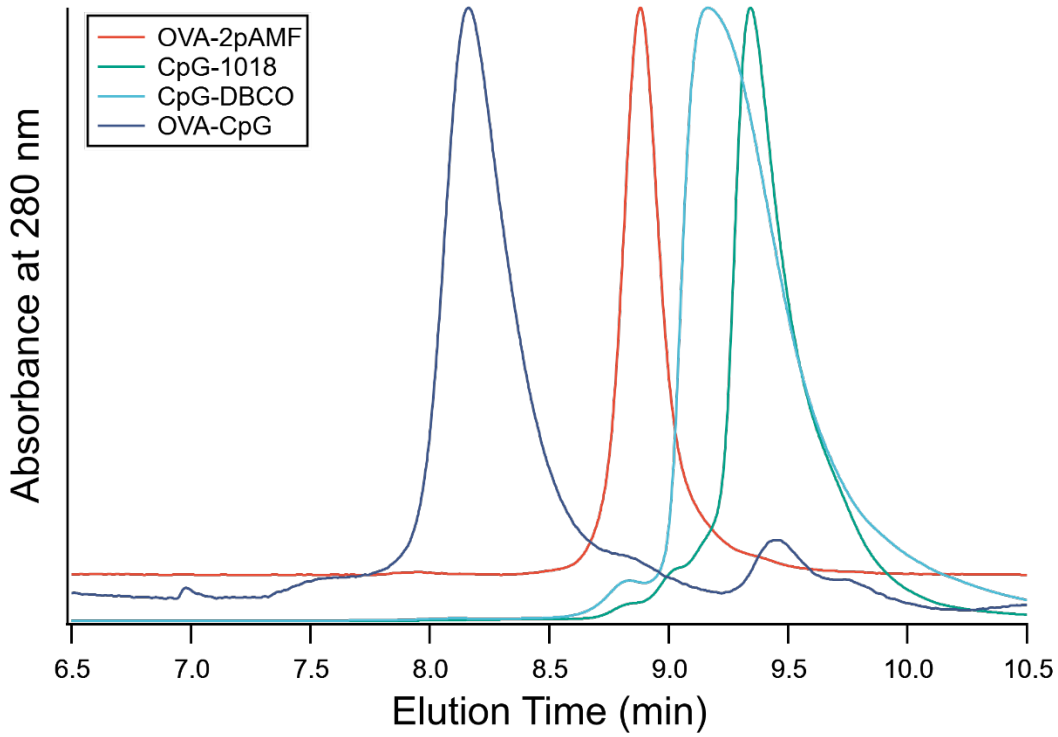

Figure B5: Size exclusion HPLC of OVA-CpG

Size exclusion HPLC of OVA-CpG and component species reveals sufficient removal of CpG-DBCO and absence of high molecular weight aggregates in the OVA-CpG sample. Samples were eluted using 100 mM pH 6.8 phosphate buffer on a Yarra SEC-2000 300Å column and monitored at 280 nm. It should be noted that OVA-$(CpG)_2$ and OVA-$(CpG)_1$ elute as a single fraction at 8.1 min, which was verified by collecting the fractions and submitting them to SDS-PAGE gel chromatography (not shown).

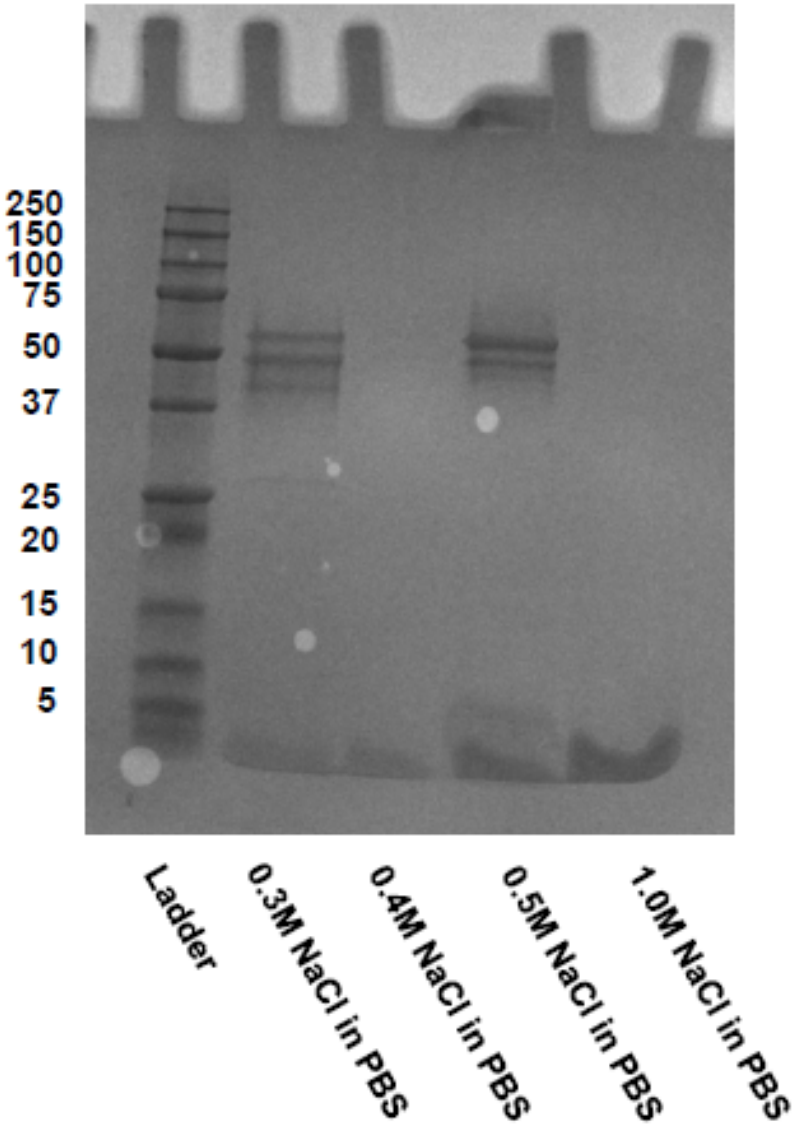

Figure B6: Anion exchange chromatography of OVA-CpG

Anion exchange chromatography of OVA-CpG was attempted to isolate OVA-CpG fractions with different loading of CpG, and SDS-PAGE gel chromatography was used to indicate the purification of fractions containing 0, 1, or 2 CpG/OVA. A band containing 1+2 CpG/OVA eluted at a concentration of 0.5 M NaCl in PBS.

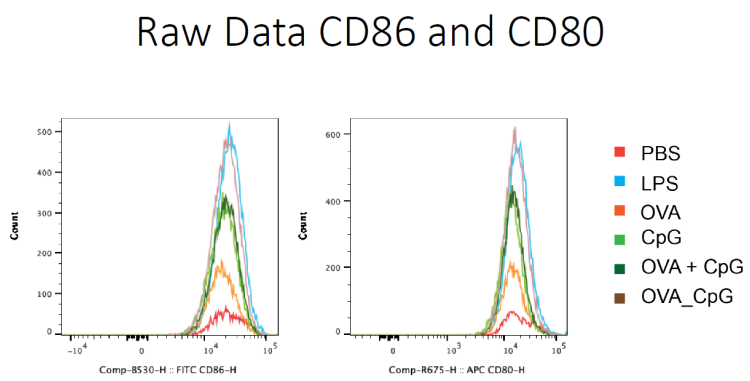

Figure B7: CD86 and CD80 expression levels of OVA-CPG

Fluorescent intensity plots of CD86 (left) and CD80 (right) expression after DC2.4 cells were incubated for 20 h with 50 µg/mL OVA-CpG or unlinked controls, stained, and analyzed using flow cytometry.

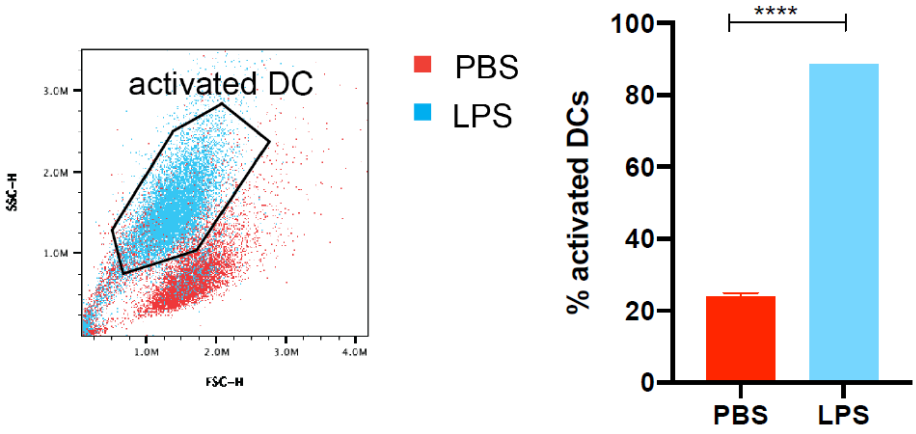

Figure B8: Gating strategy for activated DC2.4 cells

Plot of FSC-H against SSC-H showing gating used in Figure 3.3F and demonstrating enhanced granularity in the activated DC2.4 cell population after treatment with 100 ng/mL LPS relative to PBS.

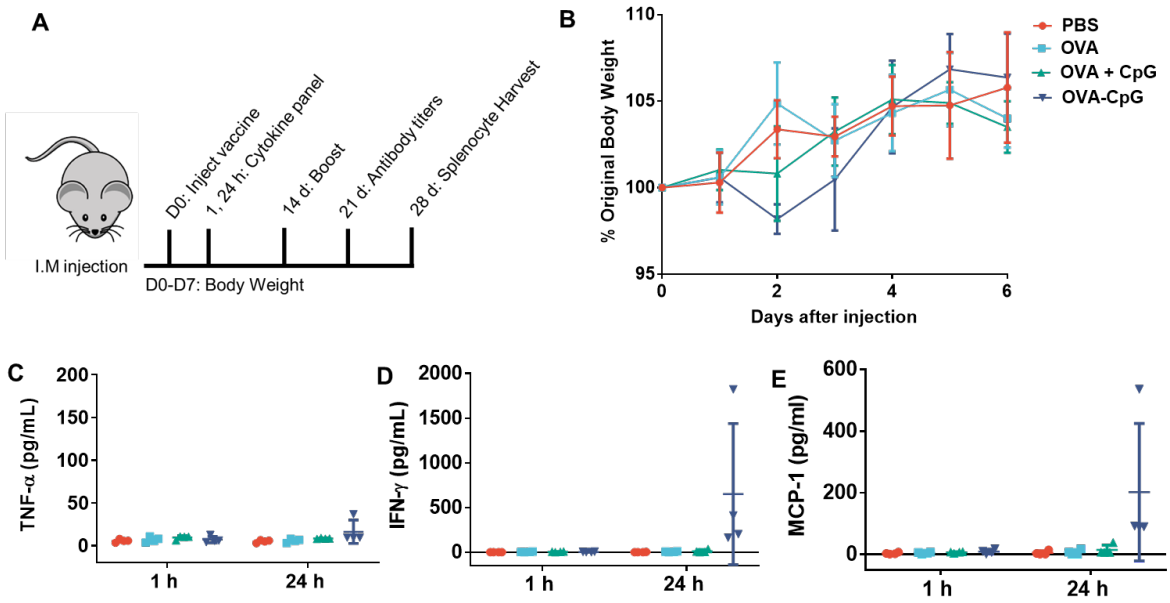

Figure B9: Body weight and inflammatory cytokine data for OVA-CPG conjugate

Acute inflammatory response to injection of OVA-CpG after the vaccination schedule for the first *in-vivo* experiment using 1 nmol of OVA-CpG (batch 1) or unlinked controls as defined in (A). B) No significant changes in body weight were observed after injection. C) No significant changes in TNF-α secretion was observed 1 or 24 h after injection. After 24 h, significant D) IFN-γ and E) MCP-1 production was observed.

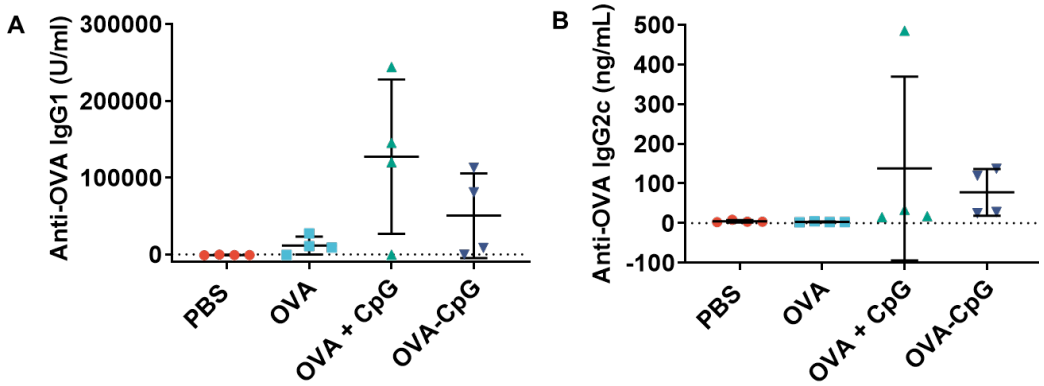

Figure B10: Antibody levels after vaccination with OVA-CpG conjugates

Mice were vaccinated according to the schedule in Figure S6A, and serum was collected after 21 d for ELISAs. No differences in A) IgG1 or B) IgG2c specific anti-OVA titers were observed 21 d after injection

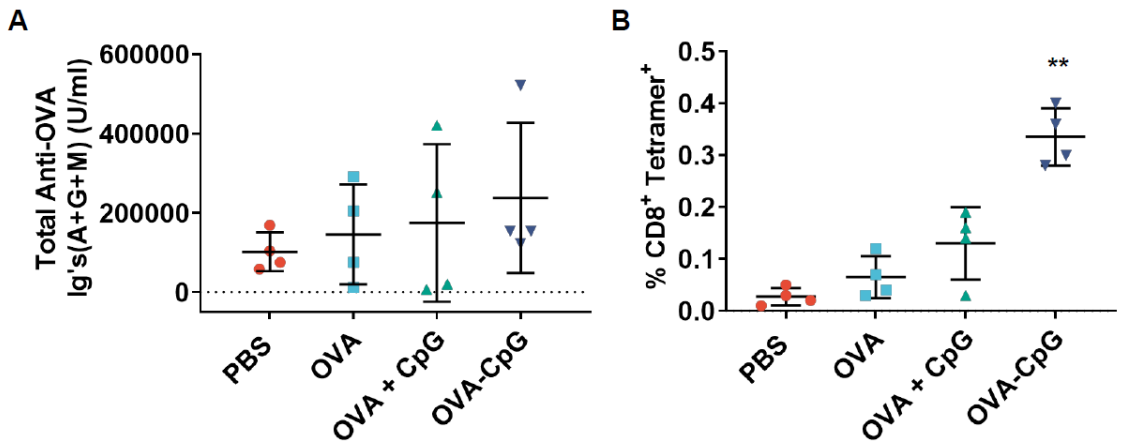

Figure B11: *in-vivo* antibody levels and CD8+-T cell tetramers

Mice were vaccinated according to the schedule in Figure S6A, and serum was collected after 21 d for ELISAs. Mice were sacrificed after 28 d and T cells were harvested for tetramer staining. A) No differences in total anti-OVA Ig(G+A+M) titers were observed 21 d after injection. B) OVA-CpG induced significant increase (**, $p < 0.01$) relative to OVA + CpG in splenic antigen-specific T-cell production 21 d after injection. Statistics were conducted using student's t-test to evaluate OVA-CpG relative to OVA + CpG.

Appendix C: Chapter 4

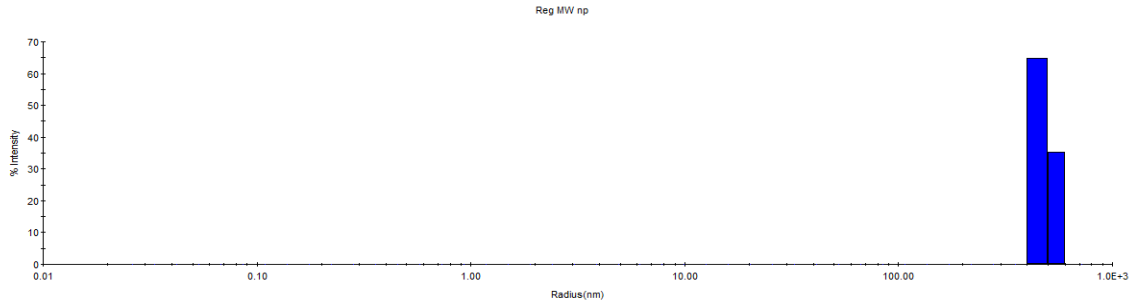

Figure C1: Dynamic light scattering (DLS) for synthesized nanoparticles

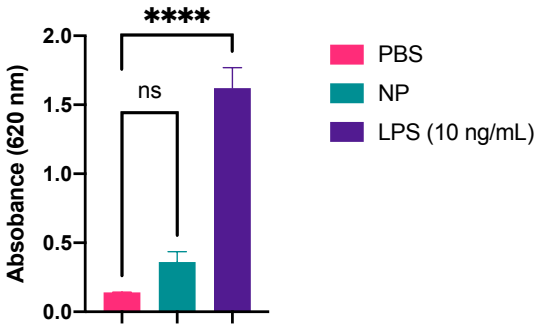

Figure C2: HEKmTLR4 assay for synthesized nanoparticles confirming no endotoxin.

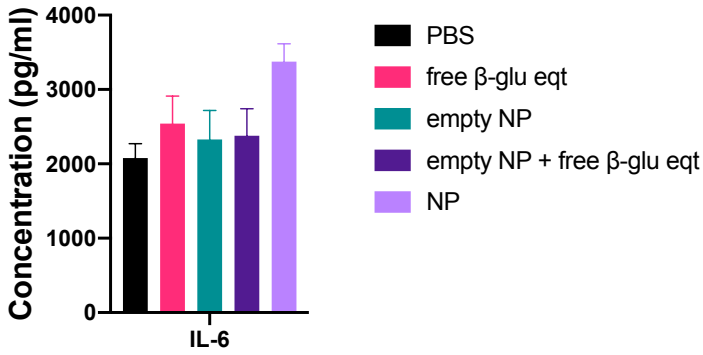

Figure C3: in-vitro TI assay

Figure C3 continued

BMDMs were trained for 24 h with indicated materials (untrained or PBS (black bars), equivalent amount of free β-glucan (pink bars), empty or unencapsulated nanoparticles (green bars), mixture of empty nanoparticles and equivalent amount of free β-glucan (purple bars) or nanoparticles (lilac bars)) and rested for 5 days. On day 6, trained cells were challenged with 10 ng/mL of LPS and IL-6 and TNF-α levels from the supernatant were quantified using ELISA.

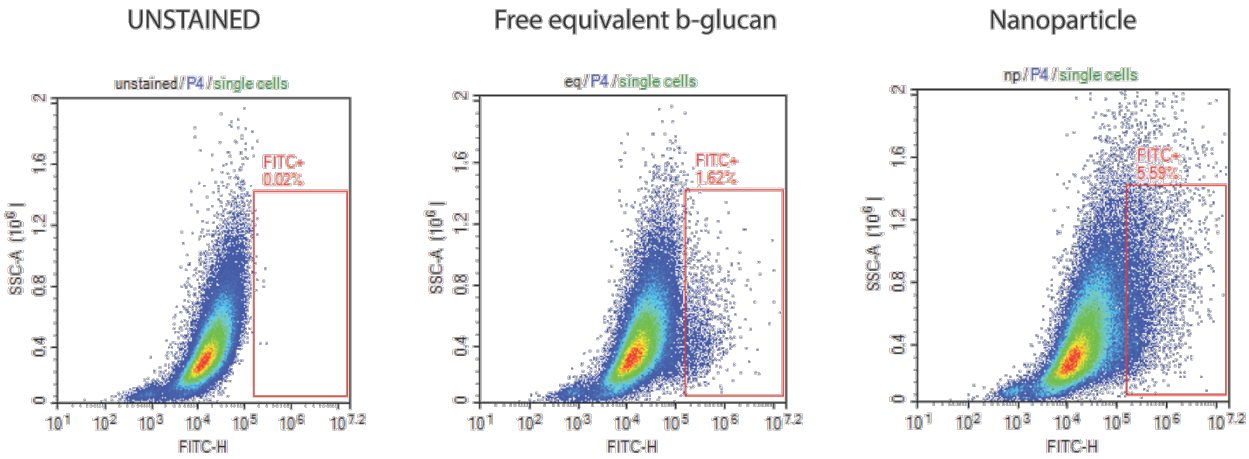

Figure C4: Gating strategy for measuring uptake of nanoparticles

Uptake of free Fitc-labelled β-glucan and Fitc-labelled β-glucan encapsulated in nanoparticles by flow cytometry- representative plots shown. (n=3)

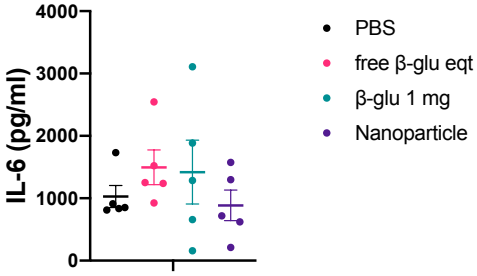

Figure C5: Day 35 serum cytokines

Day 35 serum cytokines for mice trained with indicated materials (PBS (black), equivalent amount of free β-glucan (pink), free 1 mg β-glucan (green) or nanoparticles (purple)) 1 h after challenge with LPS. No significant changes in cytokines were observed after LPS challenge 35 days post training.

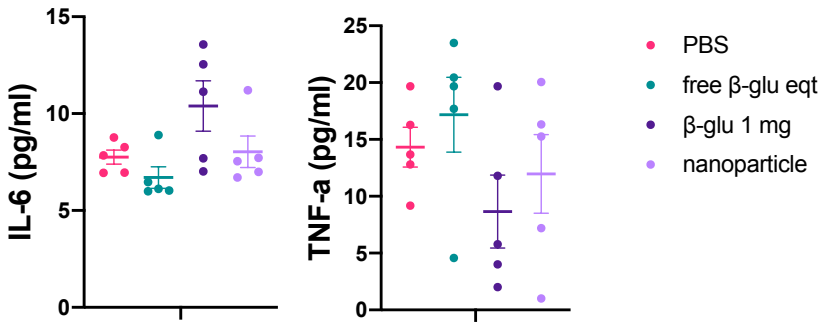

Figure C6: Ruling out innate immune priming for nanoparticles *in-vivo*

Mice that were trained with indicated materials (PBS (pink), equivalent amount of free β-glucan (green), free 1 mg β-glucan (purple) or nanoparticles (lilac)) and serum cytokines were analyzed prior to LPS challenge on day 27. No significant changes in cytokines were observed in any of the groups before LPS challenge.

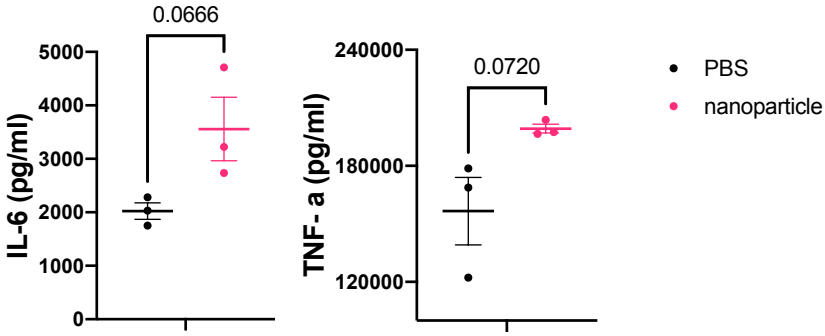

Figure C7: in-vivo TI assay with NIR labelled PLGA nanoparticles

Mice were trained with either PBS (black) or NIR labelled PLGA encapsulating β-glucan (pink). *in-vivo* degradation profile was recorded until 21 days later. The mice were then challenged with LPS and serum cytokines were quantified 3 h later.

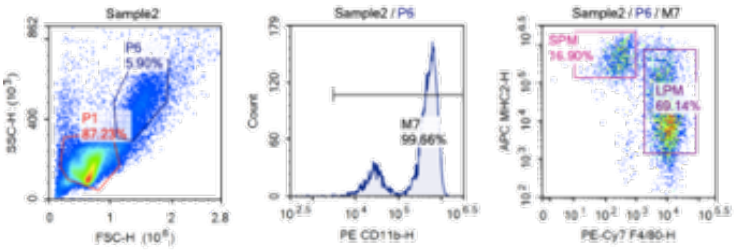

Figure C8: Gating strategy for small peritoneal macrophages (SPM)

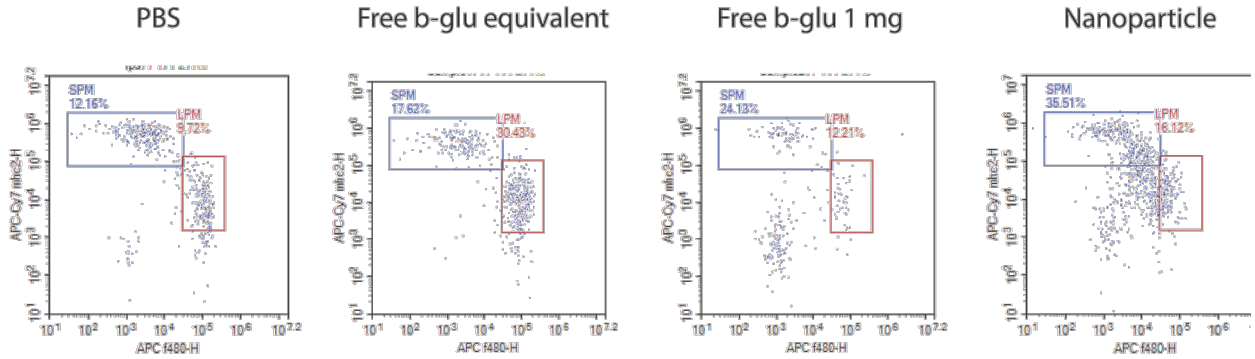

Representative flow cytometry plots for % SPMs in different groups tested (n=5)

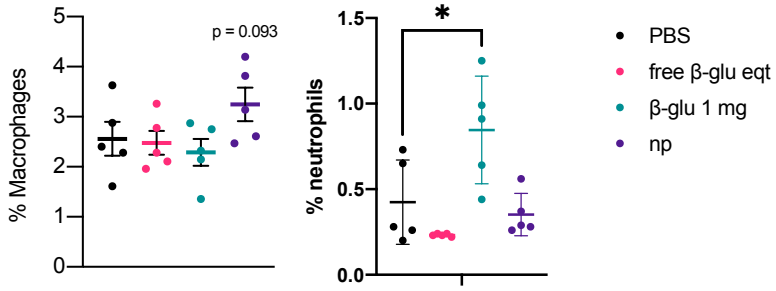

Figure C9: Percentage of splenic macrophages and neutrophils after training

Mice were trained with indicated materials (PBS (black), equivalent amount of free β-glucan (pink), free 1 mg β-glucan (green) or nanoparticles (purple)) and challenged with LPS 7 days later. Spleens were harvested and analyzed. Splenic macrophages ($CD45^{+}B220^{-}CD11b^{+}F4/80^{+}$)

Figure C9 continued

were higher in nanoparticle trained mice whereas neutrophils ($CD45^{+}B220^{-}CD11b^{+}Ly6G^{+}$) were higher in the conventional 1 mg β-glucan trained mice.

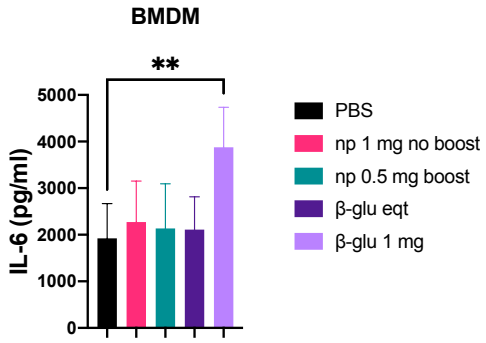

Figure C10: ex-vivo challenge of BMDMs after training

Mice were trained with indicated materials (PBS (black bars), 1 mg of nanoparticles on day 0 only (pink bars), 0.5 mg of nanoparticles on both day 0 and day 4 (green bars), equivalent amount of free β-glucan (purple), free 1 mg β-glucan (lilac). After 7 days, bone marrow was harvested and differentiated into BMDMs. 6 days after culture, cells were re plated at a density of 100,000 cells/ well and were challenged ex-vivo with LPS (10 ng/mL) and cytokines were quantified. Only mice trained with 1 mg of free β-glucan showed increased IL-6 levels confirming that nanoparticles did not act at the bone marrow.

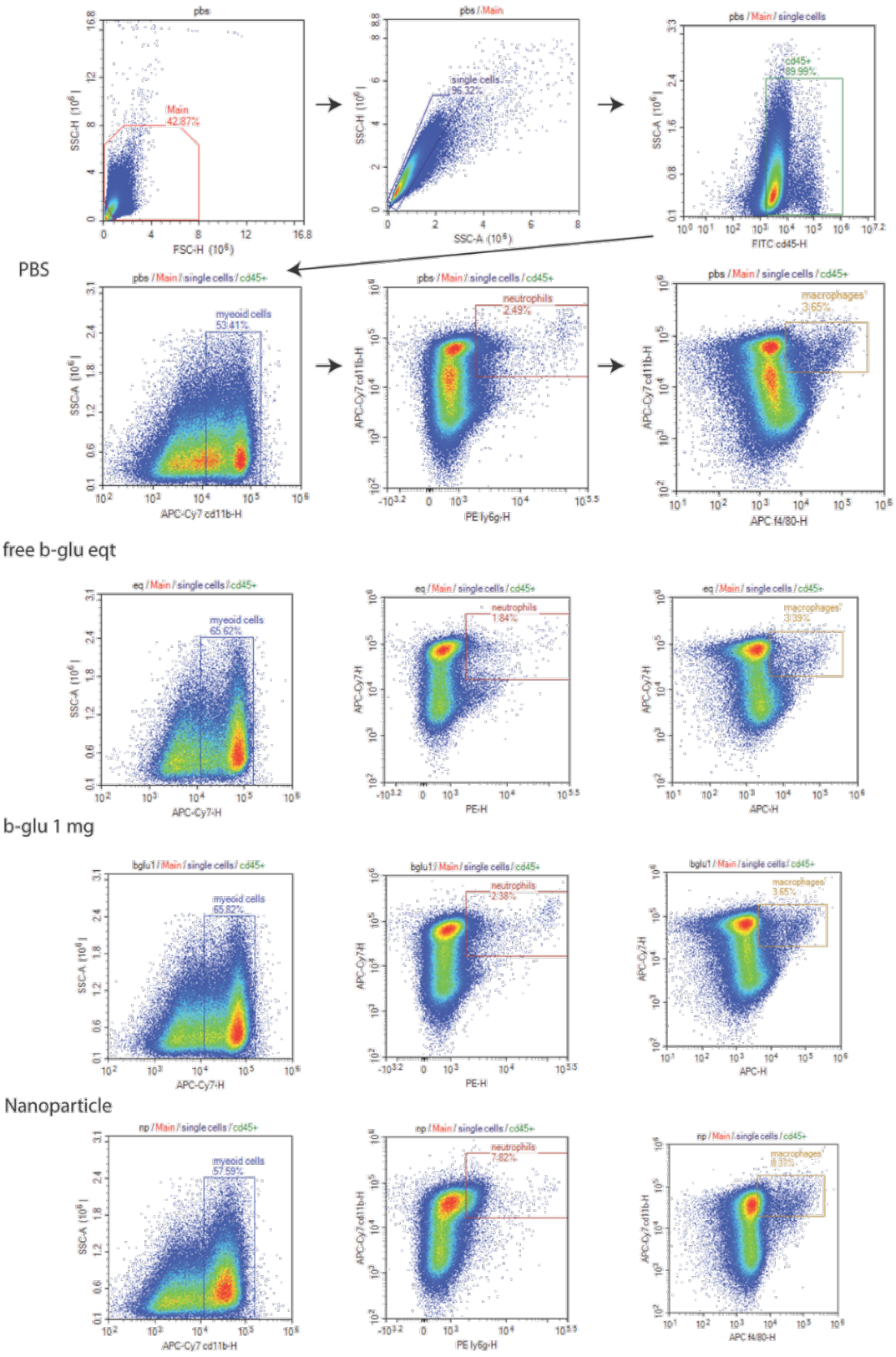

Figure C11: Tumor microenvironment analysis

Figure C11 continued

At day 46, tumors were excised and single cell suspensions were prepared. Gating strategy for tumor associated macrophages ($CD45^+CD11b^+F4/80^+$) and tumor associated neutrophils ($CD45^+CD11b^+Ly6G^+$) and representative flow cytometry plots for % TAMs and % TANs in tumor micro-environment in the groups tested (n=5).

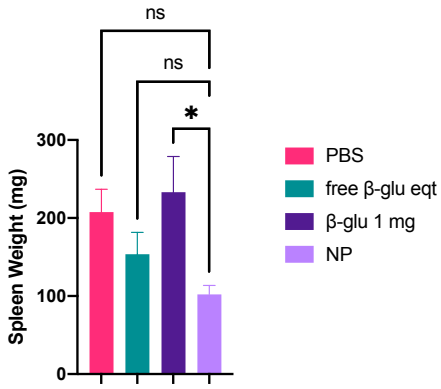

Figure C12: Spleen weight on day 46 after tumor challenge

Mice were trained with indicated materials (PBS (pink), equivalent amount of free β-glucan (green), free 1 mg β-glucan (purple) or nanoparticles (lilac)) and were challenged with B16.F10 tumors after 3 weeks. Mice were sacrificed at day 46 and spleen weights were measured. Splenomegaly was observed for all groups except nanoparticle trained mice.

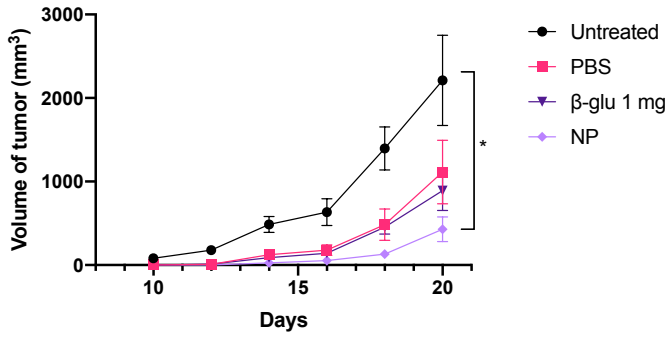

Figure C13: EG7.OVA tumor challenge.

Mice were trained with indicated materials- PBS (black and pink), 1 mg of free β-glucan (purple) or 0.5 mg nanoparticles (lilac). One week after training, all groups except untreated (black)

Figure C13 continued

received CpG/OVA vaccination and were then challenged with EG7.OVA tumor after 2 weeks. Tumor growth was measured and quantified.

Figure C14: SEM and DLS data for synthesized nanoparticles

C14a through C14e appear on the following pages.

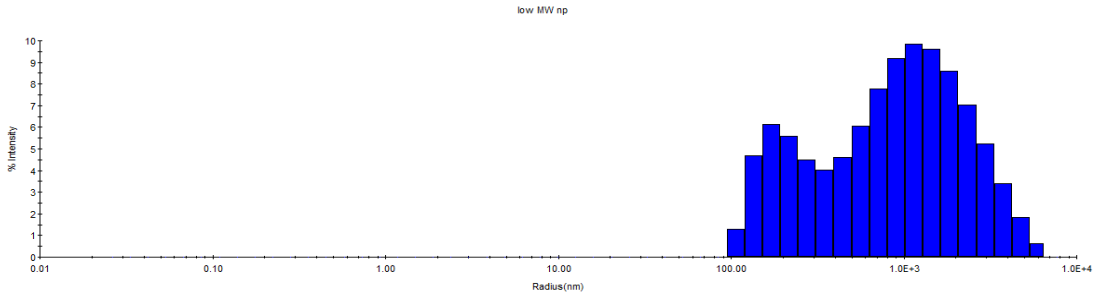

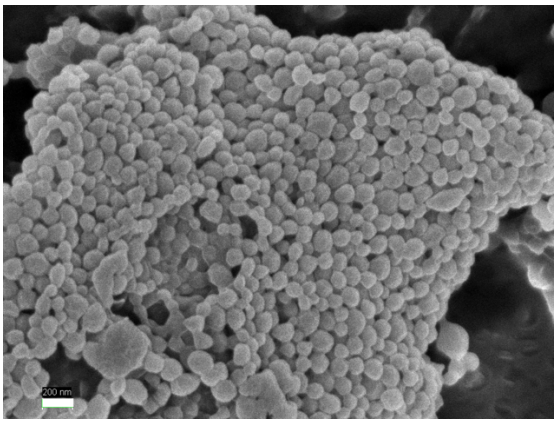

Figure C14a: DLS and SEM data for low molecular weight acid-terminated nanoparticles

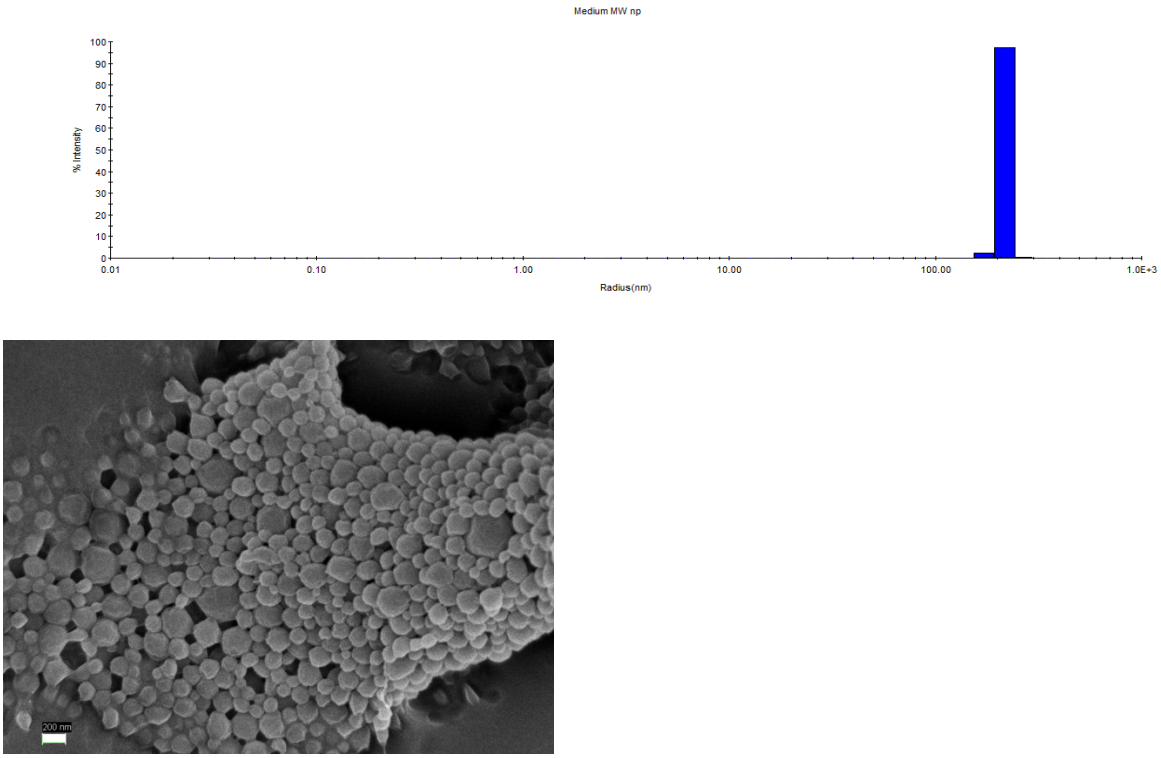

Figure C14b: DLS and SEM data for medium molecular weight ester-terminated nanoparticles (NIR-PLGA nanoparticles used for imaging)

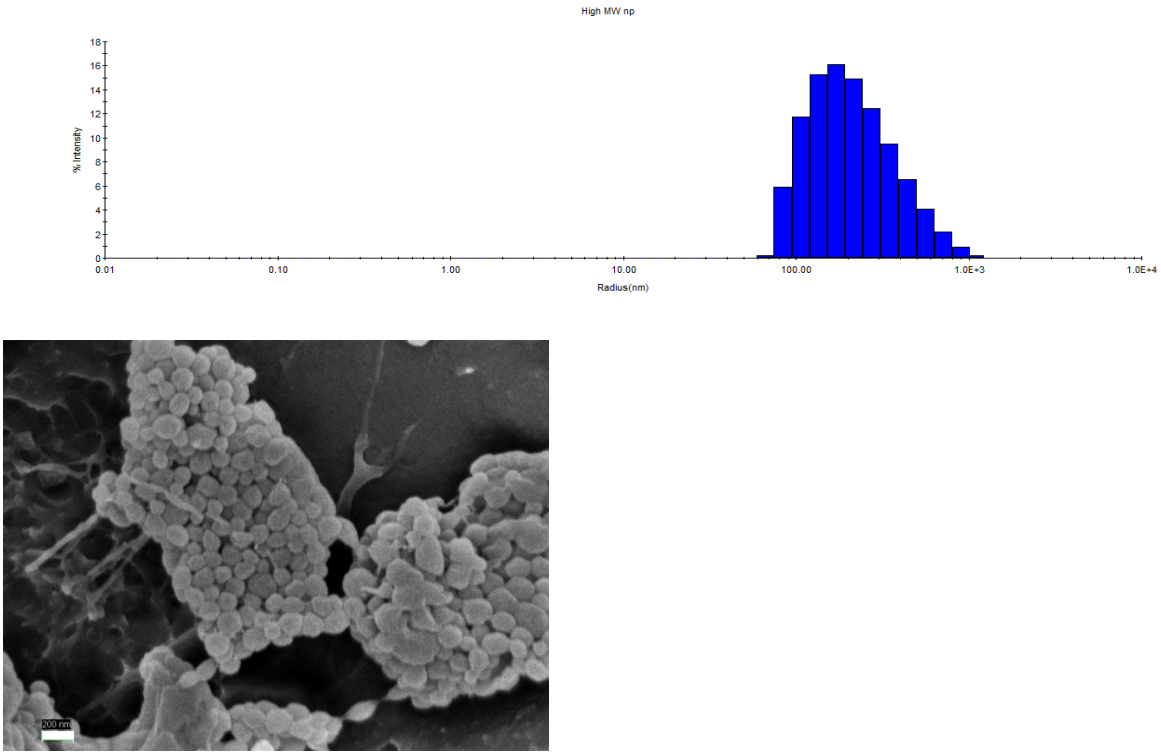

Figure C14c: DLS and SEM data for high molecular weight acid-terminated nanoparticles

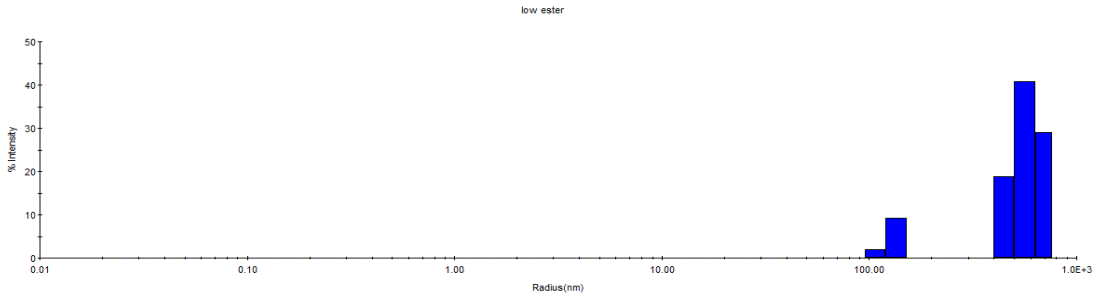

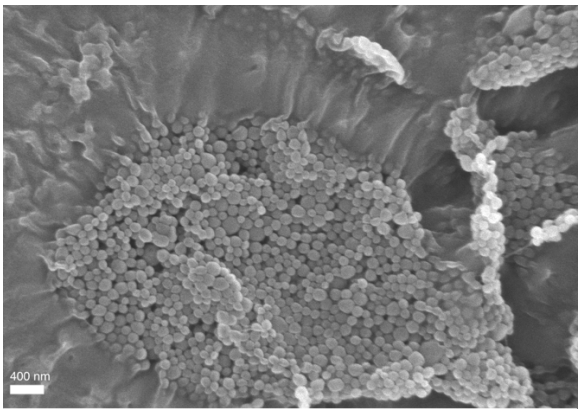

Figure C14d: DLS and SEM data for low molecular weight ester-terminated nanoparticles

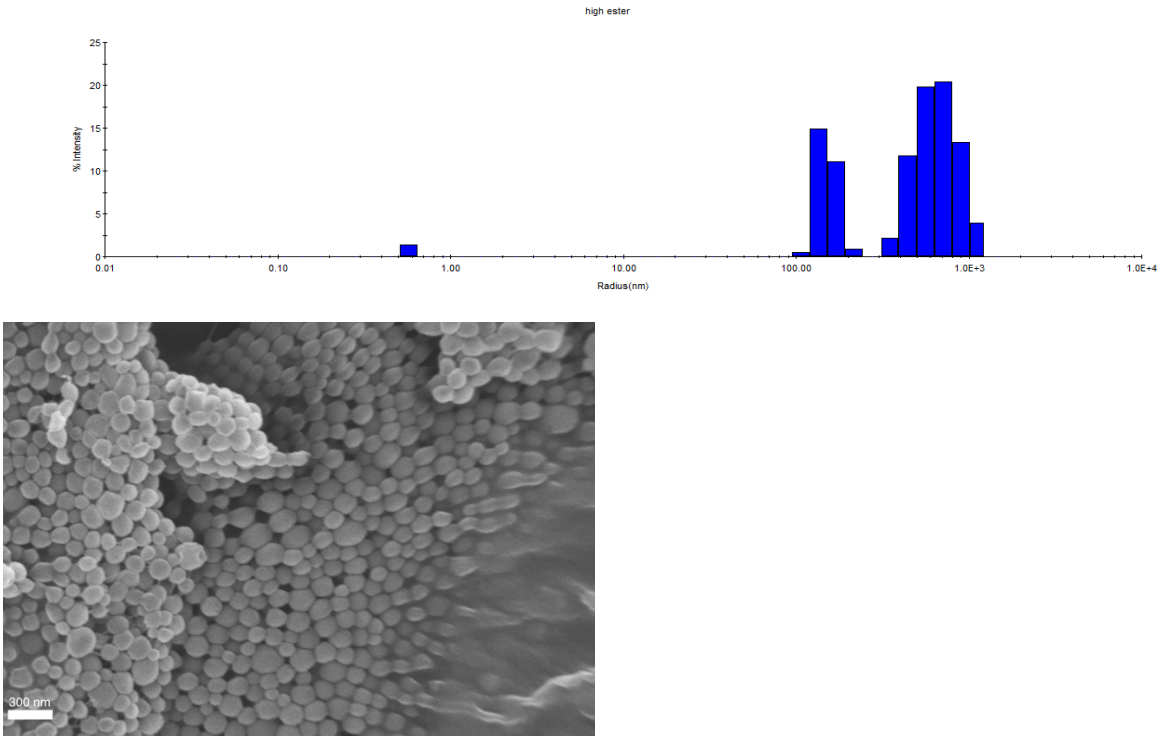

Figure C14e: DLS and SEM data for high molecular weight ester-terminated nanoparticles

Table C1: Characterization data for synthesized nanoparticles

Nanoparticle	Scale	Recovered (mg)	Loading (mg β-glucan/mg of particle)	SEM radius [nm]	DLS radius [nm]	encapsulation efficiency (%)
Regular ester	200	140	52.4	67.2	487.9	73.4
Low acid	100	44	41.0	66.8	687	72.4
Medium ester	100	57	56.4	100	217	63.8
High acid	100	43	24.1	104	245	41.3
Low ester	100	50	43.1	137	468	63.3
High ester	100	66	120	130	413	55.6

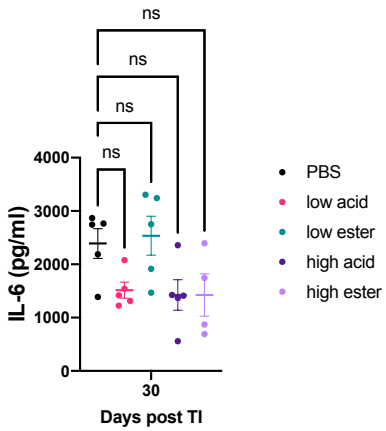

Figure C15: IL-6 levels from in-vivo TI assay on day 30

Mice were trained once on day 0 with the desired training materials – PBS (black), low molecular weight acid terminated nanoparticles (pink), low molecular weight ester-terminated nanoparticles (green), high molecular weight acid terminated nanoparticles (purple) or low molecular weight ester-terminated nanoparticles (lilac). Different set of mice were challenged with LPS at different time points- IL-6 levels from serum of mice challenged on day 30 showed no difference from untrained mice.

Appendix D: Chapter 5

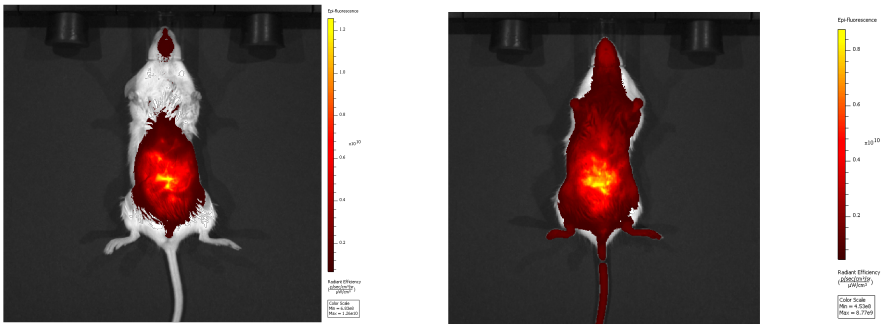

Figure D1: In-vivo biodistriubution of AF647-labelled β-glucan

Mice were injected with AF647-labelled β-glucan (ip) and imaged immediately after and after 30 min using IVIS.